MECHANISM OF BLAST TRAUMA-INDUCED HETEROTOPIC OSSIFICATION: ROLE OF MUSCLE TRAUMA

by

La Li

BA, Peking University Health Science Center, 2010

MS, Peking University Health Science Center, 2013

Submitted to the Graduate Faculty of

School of Medicine in partial fulfillment

of the requirements for the degree of

Doctor of Philosophy

University of Pittsburgh

2019

UNIVERSITY OF PITTSBURGH

SCHOOL OF MEDICINE

This dissertation was presented

by

La Li

It was defended on

September 30, 2019

and approved by

Wendy M. Mars, Associate Professor, Department of Pathology

Harry C. Blair, Professor, Department of Pathology

Bryan N. Brown, Assistant Professor, Department of Bioengineering

Nam Vo, Associate Professor, Department of Orthopaedic Surgery

Fabrisia Ambrosio, Associate Professor, Department of Physical Medicine and Rehabilitation

Dissertation Director:

Rocky S. Tuan, Distinguished Professor, Department of Orthopaedic Surgery

MECHANISM OF BLAST TRAUMA-INDUCED HETEROTOPIC OSSIFICATION: ROLE OF MUSCLE TRAUMA

La Li, PhD

University of Pittsburgh, 2019

Heterotopic ossification (HO) is a pathological condition of abnormal bone formation in soft tissue. HO causes pain and restricts range of motion, greatly impairing functional mobility of the patient. Blast trauma-induced HO, in particular, has the highest incidence, and is the single most significant obstacle for combat-injured military personnel to return to active duty. Despite the clinical importance, the underlying mechanism of HO is poorly understood and effective treatment options are lacking.

This study aims to explore the cellular and molecular mechanism of blast trauma-induced HO. Using a live animal blast trauma model, we firstly showed that muscle trauma resulting from blast wave exposure is associated with HO formation. We then investigated the role of muscle injury in HO pathogenesis and showed that bone morphogenetic protein-7 (BMP-7) expression was highly upregulated following muscle injury. Inhibition of BMP-7 activity *in vitro* suppressed the osteogenesis-promoting effect of culture medium conditioned by injured muscle tissue on muscle-derived stromal cells (MDSCs), and *in vivo* reduced the volume of HO. These results indicate that BMP-7 is a key osteoinductive factor in injured muscle that facilitates HO formation.

Next, we sought to identify additional factors that could contribute to the pathogenesis of blast trauma-induced HO. We investigated the impact of glucocorticoids on HO formation since excessive endogenous glucocorticoid production due to stress is found in severe trauma patients. Our results showed that dexamethasone treatment together with cardiotoxin (CTX)-induced muscle injury led to a significant amount of dystrophic calcification (DC) in muscle. This effect was likely related to decreased circulating transforming growth factor-beta 1 (TGF-β1) level, as supplementation of recombinant TGF-β1 markedly rescued this phenomenon.

Lastly, we investigated the involvement of muscle tissue death in HO pathogenesis. We observed that implantation of devitalized muscle tissue together with muscle injury induced by CTX injection caused DC formation, accompanied by a systemic effect of lowered circulating TGF-β1 level.

Taken together, these results strongly suggest that a two-hit mechanism of blast trauma-induced HO, namely muscle injury-induced BMP-7 upregulation combined with pathological condition-induced downregulation of circulating TGF-β1 level, is an important causative mechanism of DC/HO formation.

TABLE OF CONTENTS

LIST OF TABLES

LIST OF FIGURES

PREFACE

Acknowledgments

My first and foremost thanks go to my mentor Dr. Rocky S Tuan. Thank you for providing such a good platform for me to explore my scientific interest, and thank you for your support and encouragement in every critical moment during my PhD life. I have learned from you not only how to do good science but also how to be a good person. My second thanks should go to my awesome thesis committee. Your collective expertise have provided invaluable insights that have guided me through the entire journey of finding the answers towards the scientific question, and your critiques have always pointed to the most important aspects that need to be fixed in order to reach the goal. A special thanks I would like to give to my committee chair, Dr. Wendy Mars, who is also my PhD program director. She runs the Cellular and Molecular Pathology Program so well that I learned equally important thing from my peer students through our internal meetings and seminars.

I am not going to forget mentioning my teachers and friends in lab. They are the people that are around every moment to answer my question and listen to my complaints. Specifically, I would like to thank Dr. Peter Alexander who brought this blast trauma idea into the lab and helped me develop this project from the very beginning. I would also like to thank Dr. Hang Lin and Dr. Bing Wang, whom I consulted most often in the lab since there is no language barriers. Dr. Yangzi Jiang and Dr. He Shen, for giving me scientific instructions while we are dining and

shopping. Dr. Jian Tan and Dr. Jihee Sohn, my bench neighbors, who comforted me and cheered me up when I ran into problems. Alyssa, for helping me with all kinds of animal issues. Dr. Patrick Maher and Dr. Peter Mittwede, for being on the same HO team with me. And thanks to all Tsinghua and Xiangya scholars who have made my life more colorful.

My parents also deserve acknowledgement. I am very lucky that my parents have provided me with everything so that I could stay focused on my study. I am confident that I will have the chance to go even further with their continued support.

ABBREVIATIONS

ACVR1	Activin A Receptor type I
ALK2	activin receptor-like kinase-2
ALP	alkaline phosphatase
BMP	bone morphogenetic protein
BSP-1	bone sialoprotein I
caALK2	constitutive active activin receptor-like kinase-2
CM	conditioned medium
CNS	central nervous system
CSF	cerebrospinal fluid
CT	computed tomography
CTL CM	CM derived from control muscle tissue
CTX	cardiotoxin
CTX CM	CM derived from CTX-injured muscle tissue
DAPI	4′,6-diamidino-2-phenylindole
DC	dystrophic calcification
DEX	dexamethasone
ECSIT	Evolutionarily Conserved Signaling Intermediate in Toll Pathway

EDTA	ethylenediaminetetraacetic acid
ELISA	enzyme-linked immunosorbent assay
EndMT	endothelial-to-mesenchymal transition
FAPs	fibro/adipogenic progenitors
FlEx	flip-excision
FOP	fibrodysplasia ossificans progressiva
GAPDH	glyceraldehyde-3-phosphate dehydrogenase
GM	growth medium
GS	glycine-serine
H&E	Hematoxylin and Eosin
HA	hydroxyapatite
HIF-1α	hypoxia inducible factor-1α
HO	heterotopic ossification
IACUC	Institutional Animal Care and Use Committee
IHC	immunohistochemistry
MDSCs	muscle-derived stromal cells
MPCs	mesenchymal progenitor cells
MSCs	mesenchymal stem cells
Nfatc1	nuclear factor associated T-cell 1
NHO	neurogenic HO
NK1r	neurokinin 1 receptor
NSAIDs	nonsteroidal anti-inflammatory drugs
OCN	osteocalcin

OSM	Oncostatin M
OSX	osterix
PAI-1	plasminogen activator inhibitor-1
PDGFRα	platelet-derived growth factor receptor α
PLG	plasmin
POH	progressive osseous heteroplasia
Prx-1	paired related homeobox 1
qRT-PCR	quantitative real-time reverse-transcription polymerase chain reaction
Runx2	runt-related transcription factor 2
SCI	spinal cord injury
Scx	Scleraxis
SP	substance P
TBI	traumatic brain injury
TGF-β	transforming growth factor-beta
THA	total hip arthroplasty
TLR	toll-like receptor

1.0 INTRODUCTION

Heterotopic ossification (HO) is a pathological condition of abnormal bone formation in soft tissue [1]. Due to the mechanical effect of hard tissue inside soft tissue, HO usually causes pain and restricted range of motion [2]. HO can be generally divided into two broad categories: hereditary and acquired HO. Hereditary HO, also known as fibrodysplasia ossificans progressiva (FOP), is a rare autosomal dominant disease resulting from Activin A Receptor type I (*ACVR1*) gene mutation [3]. Acquired HO typically follows central nervous system (CNS) injury or direct musculoskeletal trauma [4]. However, the mechanism underlying the acquired HO is still unclear. Blast trauma-induced HO in particular, has the highest incidence among all types of HO. It has been shown to be the single most significant obstacle for combat-injured military personnel to return to active duty [5]. The goal of this study is to explore the cellular and molecular mechanism of blast trauma-induced HO.

Chalmers et al. proposed that three factors were required to induce HO: (1) osteogenic precursor cells, (2) osteoinductive agents, and (3) an osteoconductive environment [6]. Since Urist's landmark discovery of bone induction in skeletal muscle tissue by demineralized bone matrix [7], it is generally believed that skeletal muscle itself is a conductive environment for osteogenesis and that resident progenitor cells in skeletal muscle are capable of differentiating into osteoblast to form bone. However, little is known about the naturally occurring osteoinductive agents following trauma. Bone morphogenetic proteins (BMPs) have been the

most popular focus among the osteoinductive agents since their identification as the biologically active component(s) responsible for the osteoinductive capacity of demineralized bone matrix [8]. Previous investigations also suggest that the BMP signaling is normally active in muscle and is indispensable for muscle regeneration following injury [9, 10]. In this study, we have sought to explore if dysregulated BMP signaling is responsible for HO formation following muscle trauma, and what are the other factors that may work in concert with BMP signaling to cause aberrant osteogenesis.

The introduction of the thesis will provide a review of the emerging findings regarding distinct types of HO to summarize the current understanding of HO mechanisms. In the experimental sections, focus will be first directed towards blast trauma-induced HO; specifically, we have shown in a live animal blast trauma model that muscle trauma resulted from blast wave exposure is associated with HO formation. The next part presents our findings on how muscle injury promotes HO formation in general. However, as muscle injury alone cannot cause HO, our next studies are concerned with investigating additional factors/pathological conditions that may contribute to the pathogenesis of blast trauma-induced HO.

1.1 GENETIC HO

The most common form of hereditary HO is FOP. Progressive osseous heteroplasia (POH) is excluded from this review given that it progresses from deep layers of skin to skeletal muscle thus might be different from typical HO [11].

1.1.1 Clinical observations

FOP is a life threatening disease and has an incidence of 1 in 2 million individuals [12]. Patients were born normal only with congenital malformation of the great toes. The extraskeletal ossification begins in childhood following flare-ups (painful soft tissue swelling), initiated by mild bodily trauma, such as childhood immunizations or play-related falls [12]. Progressive HO firstly forms around the trunk in affected patients (Figure 1), and then proceeds to the whole body [4]. Ectopic bone eventually spans the joints, which renders movements impossible. Most patients die of thoracic insufficiency syndrome at the age of around forty [12].

Figure 1. Three-dimensional reconstructed computed tomography (CT) scan of the back of a twelve-year old FOP patient. Reprinted from reference [12]

FOP is caused by a point mutation in the *ACVR1* gene, which results in an amino acid change in codon 206 (R206H) in the glycine-serine (GS) activation domain of a BMP type I receptor, activin receptor-like kinase-2 (ALK2) [3]. The consequence of this R206H mutation is constitutive activation of BMP signaling, although the exact mechanism concerning how this

mutation perturbs BMP signaling is not totally clear. It is thought to be due to the altered binding of an inhibitory protein FKBP12 to GS domain that leads to constitutive activation of ALK2 [3].

1.1.2 Animal models

To simulate human FOP condition, several transgenic mouse models incorporating *ACVR1* gene mutation have been developed. The first constitutive active activin receptor-like kinase-2 (caALK2) over-expression mouse model was developed with an artificial ligand-independent Q207D amino acid substitution at GS activation domain in ALK2 driven by a strong CAG promoter [13]. Further study has shown that induction of caALK2 expression by intramuscular injection of Cre-expressing adenovirus is sufficient to induce endochondral HO that phenocopies key aspects of human FOP, while global postnatal expression of caALK does not lead to HO [14]. Conditionally expressing caALK2 driven by nuclear factor associated T-cell 1 (Nfatc1) gene predisposes mouse to HO as early as P4 without antecedent injury, where HO happens most prominently in distal joints [15].

The second more relevant transgenic mouse model was developed with the R206H mutation as it is identical to the *ACVR1* gene mutation in human FOP [16]. Chimeric *ACVR1* R206H knock-in mice exhibited malformed digits and postnatal extraskeletal bone formation, recapitulating the phenotype of human disease [16]. However, *ACVR1* R206H constitutive knock-in mice exhibited F1 generation lethality, which limits its utility in experimental studies [17]. Conditional *ACVR1* R206H knock-in mice was then developed with a FlEx (flip-excision) system to allow *ACVR1* R206H expression under control of the endogenous promoter [18]. Upon tamoxifen induction, the transgenic mice can develop HO in common ossification sites as they are in FOP patients without antecedent injury [18]. This study further showed that R206H driven

HO is a ligand-dependent process since BMP and activin ligand blockers (ACVR2A-Fc and ACVR2B-Fc) largely prevented HO from happening in these transgenic mice [18].

Based on the mechanism of FOP pathogenesis, BMP protein muscle implantation models and BMP over-expression transgenic mouse models have also been developed [19, 20]. Although non-physiological, these models still faithfully recapitulate the histological sequelae of HO development, i.e., tissue inflammation stage, fibroproliferation stage, chondrogenic stage, and osteogenic stage.

1.1.3 Cellular and molecular mechanisms

Based on the existing animal models, cellular and molecular mechanism leading to HO formation has been extensively studied. Earliest studies performed on BMP protein implantation model and BMP over-expression transgenic mouse model have identified that Tie-2 promoter driven Cre can label the majority of HO forming cells [19, 21]. Tie-2 is a receptor kinase for agiopoietin and is ubiquitously expressed in endothelial cells [22]. However, Tie-2 labeled cells are not necessarily endothelial cells given that Tie-2 positive cell population is distinct from VE-Cadherin labeled endothelium [19], and injury dependent endothelial marker expression has also been observed in mesenchymal cells [23]. In these studies, Tie-2 lineage cells have been shown to be a population of fibro/adipogenic progenitors (FAPs) residing in the skeletal muscle interstitium [17]. They are multipotent mesenchymal progenitor cells which are positive for PDGFRα and Sca-1 surface makers [24]. They also have been shown to constitute a fraction of Scleraxis and Mx1 population [25, 26]. Therefore, targeting caALK2 to a Scleraxis and Mx1 promoter driven Cre also largely mimics the effect of targeting it to Tie-2 promoter driven Cre [27].

In addition to the genetic aspect of the disease etiology, other interesting phenomena have been observed in FOP animal models as well as in *ex vivo* study of FOP patient samples, which shed light on the pathogenesis of FOP. First is that antecedent injury facilitates HO formation in mice either harboring caALK2 gene mutation or in mice with BMP-4 over-expression [16, 28]. Anti-inflammatory drug treatment and depletion of inflammatory cells typically inhibit HO formation in FOP animal models [14, 28, 29]. These findings indicate that tissue trauma/inflammation as the inducing event is required for HO development [30]. Recent study has examined proinflammatory and monocyte/macrophage changes in humans with FOP, and shown that there is a proinflammatory state caused by abnormal ALK2 [31]. Another study has demonstrated that FOP connective tissue progenitor cells respond to inflammatory signals through toll-like receptor (TLR), and ECSIT (Evolutionarily Conserved Signaling Intermediate in Toll Pathway) links TLR to BMP signaling [32]. This may suggest a possible link between the innate immune system and dysregulated BMP signaling in tissue progenitor cells. The second unexpected finding is that Activin A, usually acting as BMP signaling pathway inhibitory ligand, can activate caALK2 and its downstream Smad1/5 signaling pathway [18, 33]. Systemic inhibition of Activin A by its neutralizing antibody completely prevented spontaneous and injury-induced HO development in *ACVR1* R206H knock-in mice, indicating a pivotal role of Activin ligand in inducing HO in FOP [18, 27]. Given that Activin plays a key role in the immune system, Activin could also mediate the cross-talk between Toll-like signaling pathway and BMP signaling pathway [34]. Other signaling pathways that are involved in the immune system, such as mTOR signaling [35], TGF-β signaling [36], hypoxia inducible factor-1α (HIF-1α) signaling [37, 38] and retinoid signaling [39-41], have also been reported to affect HO

formation. However, the inter-relationship between these signaling pathways and BMP signaling pathway remains to be further explored.

1.2 NEUROGENIC HO

Neurogenic HO (NHO) is defined as HO following spinal cord injury (SCI) and traumatic brain injury (TBI) [42].

1.2.1 Clinical observations

The incidence for NHO following CNS injury has been reported to be 1 in 5 patients [43]. Ectopic bone formation begins within 2 months after neurologic injury and usually forms around large joints (Figure 2) [44]. It has also been reported that many patients with head injury have accelerated fracture healing, which has been considered as a variant of NHO [45]. In some circumstances, injury to peripheral nerve could also compromise CNS integrity [46]. It is still unclear whether HO in elbow and hip joint is the result of damage to ulnar nerve and sciatic nerve. Risk factors for neurogenic HO include: artificial ventilation, immobilization, and muscular spasticity [42]. Specifically, artificial ventilation alters blood homeostasis of electrolytes and acid-base balance, both of which will affect osteogenesis [45]. Immobilization and muscular spasticity have been suggested as a cause of increased risk of muscle tears from active or passive movement [47]. Current prophylaxis and treatment for NHO include: nonsteroidal anti-inflammatory drugs (NSAIDs), bisphosphonates, radiation therapy and surgery [48].

Figure 2. X-ray image of HO formed around the knee joint of a patient with paraplegia. Reprinted from reference [44], License Number 4685550963219

The etiology of NHO is incompletely understood. Central hypothesis for the pathogenesis of NHO is the release of osteogenic humoral factors following the breakdown of blood-brain barrier [49]. *In vitro* studies support this notion by demonstrating that the cerebrospinal fluid (CSF) and serum from patients with severe TBI have an osteoinductive effect and are able to stimulate cell proliferation [50-52]. Neuroinflammation has also been implicated in NHO [53]. Neuroinflammation refers to a process in which CNS injury triggers inflammatory reactions in peripheral tissue through the release of substances from the peripheral terminals of peptidergic, sensory nerve fibers [54]. Indeed, the neural-inflammatory factor substance P (SP) has been found dramatically increased in NHO lesions [55] and in the plasma of NHO patients [56]. In addition, conditioned medium derived from activated CD14+ monocytes/macrophages isolated

from NHO lesion strongly stimulated the mineralization of muscle-derived stromal cells (MDSCs) isolated from the same place [57].

1.2.2 Animal models

The first and only mouse model of NHO was developed by a combined thoracic spinal cord transection and local muscular trauma [56]. NHO developed in the muscle injury site; mineralization was evident on CT scans as early as 3 days after injury [56]. The development of NHO was independent of paraplegia associated with SCI since non-paralyzed front limb also developed HO following local muscular trauma [56]. Further research done by the same group showed that peripheral denervation increased HO volume on the original model, and peripheral denervation alone without SCI could also induce HO in about 50% of mice with local muscular injury [58].

1.2.3 Cellular and molecular mechanisms

In the above mentioned mouse NHO model, the research group tested several cell lineages derived from muscle tissue and showed that muscle satellite cells (D45-Ter119-CD31-Sca1-CD34+), interstitial cells (CD45-Ter119-CD31-Sca1+CD34+) and muscle progenitor cells (CD45-Ter119-CD31-Sca1-CD34-) could all mineralize *in vitro* to the same extent as mesenchymal progenitor cells derived from bone marrow [56]. They also showed that muscle interstitial cells underwent osteoblastic differentiation in response to plasma derived NHO mice without additional osteogenic stimuli, suggesting that progenitor cells in the muscle could be the cell source for NHO [56]. Other studies speculate that progenitor cells that reside in

endoneurium of peripheral sensory nerves give rise to NHO given that many cells positive for osterix, an osteogenic marker gene, can be found in nerve during bone formation process [59-61]. Furthermore, depletion of macrophages by clodronate-loaded liposomes reduced the size of NHO by 90%, indicating the participation of inflammatory cells in NHO as well [56].

Recently, Oncostatin M (OSM) has been found to be the coupling factor linking macrophages with MDSCs, which is indispensable for NHO development [57]. Data supporting this notion are as follows. OSM level significantly increased in plasma of NHO patients compared to healthy controls. Treatment with OSM neutralizing antibody greatly reduced the osteogenesis stimulating effect of conditioned medium derived from activated CD14+ monocytes/macrophages isolated from NHO lesion. Mice that are deficient for OSM receptor had significantly reduced HO volume compared to WT control after SCI and local muscular trauma. However, since depletion of OSM receptor did not achieve the same effect with depletion of macrophages, other factors linking macrophages with MDSCs should also exist and have yet to be explored.

Several earlier studies also indicate that SP is indispensable for BMP-induced HO formation [55], and SP delivery could induce HO with up-regulated BMP-2 expression in mouse tendon [62]. SP acts on mast cells via binding to neurokinin 1 receptor (NK1r), which induces mast cell degranulation and release of numerous pro-inflammatory factors [60]. Studies showed that in animals lacking functional sensory neurons or in null mutation of SP gene animals, BMP-induced HO was dramatically inhibited [55, 60]. Inhibition of mast cell degranulation or in mast cell deficient mouse line, HO was dramatically reduced as well [55, 60]. In summary, these data collectively suggest that there is a potent neuro-inflammatory circuit contributing to BMP-induced HO formation.

1.3 TRAUMATIC HO

The following part will review the literature of traumatic HO with special focus on blast trauma-induced HO.

1.3.1 Clinical observations

Traumatic HO is typically considered as HO triggered solely by injury, most often following extensive soft tissue injury [63]. The rate for HO happening following distal humerus fractures is about 8.6%, elbow fractures about 5.5-18.8% [64]. The rate can reach to 90% following acetabular fractures and total hip arthroplasty (THA) (Figure 3) [65]. The severity of post-THA HO is assessed using the Brooker classification system [66]. Radiographic HO may be apparent 2 weeks after surgery and reaches fully mature around 3 months [67]. Sex, surgical approach, and implant type have large effects on HO incidence [68]. HO happening subsequent to thermal injury ranges from 0.2% to 4%, with elbow being the most affected site [69]. The risk factors for developing HO after burn injury include: greater burn size, greater burn depth, longer period of immobilization [69]. Current prophylaxis for traumatic HO include radiation therapy and NSAIDs treatment [70]. However, the treatments and preventive measures are contingent upon the severity of the trauma. Use of bisphosphonates can prevent mineralization and is advantageous for treating bone loss caused by metabolic changes following burn injury [71].

Figure 3. X-ray image of HO following THA surgery. Reprinted from reference [44], License Number 4685550963219

The highest rate of HO happens in combat-related blast injuries, the prevalence of which is reported to be 64.6% in high-energy wartime extremity wounds during Operation Enduring Freedom and Operation Iraqi Freedom [72]. HO can cause significant pain and functional immobility when it forms adjacent to neurovascular structures and joint structures (Figure 4). HO can be evident on radiographs less than two months after the initial injury, and is not very likely to develop after this two-month period has passed [73]. In these war-wounded patients, TBI, age of less than thirty years, an amputation, and multiple extremity injuries with an Injury Severity Score $\geqslant$16 are regarded as risk factors for HO development [72]. The number of debridement procedures and the longer duration of negative-pressure wound therapy are also positively correlated with HO development, but they are more likely to be an indicator of the severity of

local injury rather than an independent indicator for development of HO [72]. In another cohort of amputees, a final amputation level within the zone of injury and a blast mechanism are considered as risk factors for HO development [73]. Common prophylaxis measures of HO are usually restrictive in blast injury patients, either because of other complications of the patients or logistical barriers that prevent the employment of these treatments [5]. Symptomatic HO can be managed with conservative therapies, such as rest, pain medication, physical therapy, and socket modification for amputees [74]. Fortunately, only 6.7% patients need surgical excision due to persistent symptoms [73].

Figure 4. Radiograph showing severe HO in amputated limb of blast-injured patient. Reprinted from reference [74], License Number 4685560368540

The mechanism for traumatic HO remains unclear. It can be considered as a condition of pathological wound healing [75], which involves both local and systemic inflammatory reactions

[76]. Studies have confirmed that there is a hyper-inflammatory local and systemic response in patients who developed HO compared with those who did not, which is associated with elevated injury severity score, bacterial wound colonization and eventually wound failure [77, 78]. A proposed theory for HO development is that progenitor cells induced by this imbalance in local and systemic factors following traumatic injury undergo osteogenic differentiation to form HO [74, 79]. Our laboratory has previously identified and characterized a population of muscle resident mesenchymal progenitor cells (MPCs) derived from wound debridement of blast trauma-injured patients who later developed HO [80-82]. This cell population is capable of tri-lineage differentiation, a characteristic of adult mesenchymal stem cells (MSCs), expresses MSC lineage markers, and also exhibits trophic properties that are associated with MSCs [83-86]. Davis et al. further showed that this cell population was found in greater number in muscle biopsies of patients with subsequent HO, suggesting its potential role as cell source for HO [87]. At the tissue level, osteogenic maker genes were up-regulated in wounds in which HO developed compared with wounds in which HO did not [88]. Further studies are needed to identify the pro-osteogenic factors in traumatized muscle and to investigate how they interact with muscle progenitor cells to initiate HO formation [34].

1.3.2 Animal models

The most widely studied animal model for traumatic HO is Achilles tenotomy with burn injury model [89]. Specifically, mice received Achilles tenotomy and 30% dorsal surface area burn for 18 seconds with a 60℃ heated metal brand. Mice that underwent Achilles tenotomy alone develop HO in calf muscle through an endochondral ossification process 10 weeks post trauma [90]. Concurrent dorsal burn injury enhanced HO growth in calf muscle and Achilles tenotomy

site [91]. Burn injury also enhanced HO formation in BMP-induced HO model [92]. HO growth and development was attenuated when Achilles tenotomy and burn injury were performed on immunocompromised mice [93].

The first blast trauma HO model was developed by Tannous et al. using real explosive placed inside a water tank [94]. Rats were placed on a platform above the water with a hole only exposing the animal's hind limb to the water column caused by detonation. They showed that 100% of rats subjected to this extremity blast hind limb amputation model developed HO in 4 weeks in the absence of additional exogenous osteogenic stimulus [94]. They further demonstrated that a sand blasting medium could also induce HO, suggesting that the blast mechanism induces HO regardless of the blast medium [95]. The second model of this kind was developed by Polfer et al. using a blast tube capable of producing a blast overpressure at 120 kPa [96]. They showed that blast overpressure plus severe extremity trauma was able to create HO in 100% of the experimental rats in 2 weeks. In this study, they also pointed out that blast overpressure alone was not able to induce HO, but severe extremity trauma alone created HO in about 60% of the experimental animals [96]. In another study, they further introduced bacterial colonization into this model, and found increased HO volume which may due to the chronic soft tissue inflammation [97].

1.3.3 Cellular and molecular mechanisms

Earliest studies performed on Achilles tenotomy model have reported that cells forming traumatic HO are from the paired related homeobox 1 (Prx-1) lineage [37]. Later studies showed that Scleraxis lineage (Scx) cells contributed to each stage of traumatic HO anlagen [26]. It is highly likely that cells from both lineages are PDGFRα and Sca-1 positive multipotent

mesenchymal progenitor cells which constitute a fraction of the Prx-1 and Scx population [25]. It is also possible that endothelial-to-mesenchymal transition (EndMT) to serve as a mechanism to produce the PDGFRα positive cell source to HO lesion [23].

Studies have shown that modulation of Smad1/5/8 phosphorylation with either small molecule inhibitor targeting BMP type I receptor kinase activity or drugs that promote ATP hydrolysis could mitigate traumatic HO formation resulting from Achilles tenotomy [91]. However, unlike genetic HO which is caused by mutation in ALK2 hyperactivity, all BMP type I receptors (ALK2, ALK3, ALK6) are likely involved in traumatic HO pathogenesis, given that knocking out any single receptor cannot inhibit HO formation [75]. Same with genetic HO, mTOR signaling [37, 98], TGF-β signaling [99], and HIF-1α signaling [37] also affects HO formation following Achilles tenotomy.

Molecular and histological analysis of HO progression in blast trauma-induced HO model confirmed its endochondral ossification nature [100]. Therefore, drugs modulating tissue inflammation stage, fibroproliferation stage, chondrogenic stage, and osteogenic stage should all affect HO formation. In line with this, Vancomycin treatment [101], Palovarotene treatment [102, 103], and Rapamycin treatment [104] all could suppress HO formation, probably through a combined effect of modulation of systemic inflammation, progenitor cell proliferation and chondrogenesis.

2.0 DEVELOPMENT OF A NOVEL MOUSE MODEL OF BLAST TRAUMA-INDUCED HO

2.1 INTRODUCTION

Blast injury is a complex type of physical trauma resulting from the exposure to an explosion. The unique injury pattern of blast injury is comprised of primary injury caused by blast wave itself, secondary injury caused by missiles being propelled by the blast force, tertiary injury due to impact with another object, and quaternary injury such as burn injury due to heat dissipated from explosive etc. [105]. Blast injury sets it apart from civilian trauma, given that a polytrauma comprised of soft tissue injury, CNS injury, open fracture, foreign body and bacterial contamination, and burn injury is seldom seen outside the battlefield [106]. This multifaceted injury pattern may account for the highest rate of HO happening following blast trauma, since CNS injury and burn injury have already been shown to increase the chances of HO development. However, given that HO was not a common occurrence in previous wars but had an increased prevalence in modern wars since higher order explosive has been used [74], we postulate that high-energy extremity trauma caused by supersonic blast wave plays a dominant role in driving HO formation.

In this part of the thesis, we report the employment of a blast device to test the direct effect of blast wave exposure on HO pathogenesis. The device was constructed based upon a

previously reported design used to test the effects of blast waves on internal organs [107], which was able to produce a supersonic blast wave comprised only of air. By using this blast device, we have demonstrated that blast wave exposure is sufficient stimulus for induction of HO, and muscle trauma resulted from blast wave exposure is associated with HO formation.

2.2 METHODS

2.2.1 Blast device

A blast device was constructed based on a design described previously (Figure 5) [107]. Briefly, a 3,500 psi compressed nitrogen cylinder was used to charge a 150 mL air storage chamber. Using a solenoid control system, the stored air was allowed to discharge to the blast nozzle. A rupture disc (OSECO, Broken Arrow, OK) at the base of the blast nozzle would burst at 1,850 psi, generating a blast wave emitting from the base of the nozzle. Theoretically, a burst pressure of 1,850 psi at 1 inch above the specimen platform should deliver an estimated 530 m/s blast wave reaching the tissue. The distance between the nozzle and the specimen platform could determine the force of the blast wave.

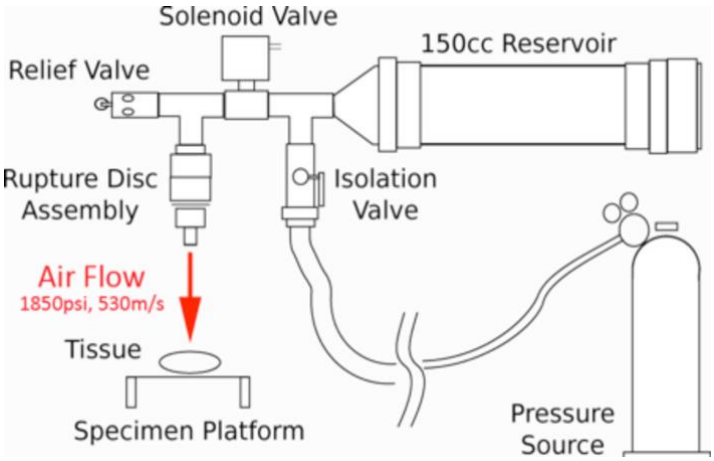

Figure 5. Schematic of the blast device

2.2.2 Blast-amputation procedure

Using an IACUC-approved protocol, 8-12 week old male C57BL/6J mice (Jackson laboratory) were first anesthetized by Isoflurane inhalation. The right hind limb was then removed of hair and was sterilized broadly with Povidone-iodine. The animal was positioned onto the operative field with a protective shield placed over the body, and only the right hind limb was left outside to be exposed to the blast wave (Figure 6). The animal was positioned so that the right hind limb knee was centered below the blast nozzle. Immediately following the blast, an above-knee amputation was performed. In cases of substantial bleeding, handheld thermal cautery was used to obtain hemostasis. Wound was closed in layer. Muscular compartments were closed over the residual limb with 4-0 vicryl sutures. Skin was closed with 4-0 nylon sutures. Prophylactic antibiotics (100 mg/kg ampicilin) were administered one-time at the end of surgery. The animal was allowed to recover under a heat lamp until ambulating about the cage, and received a 3-day course of buprenorphine (0.05 mg/kg administered subcutaneously twice a day) for pain management.

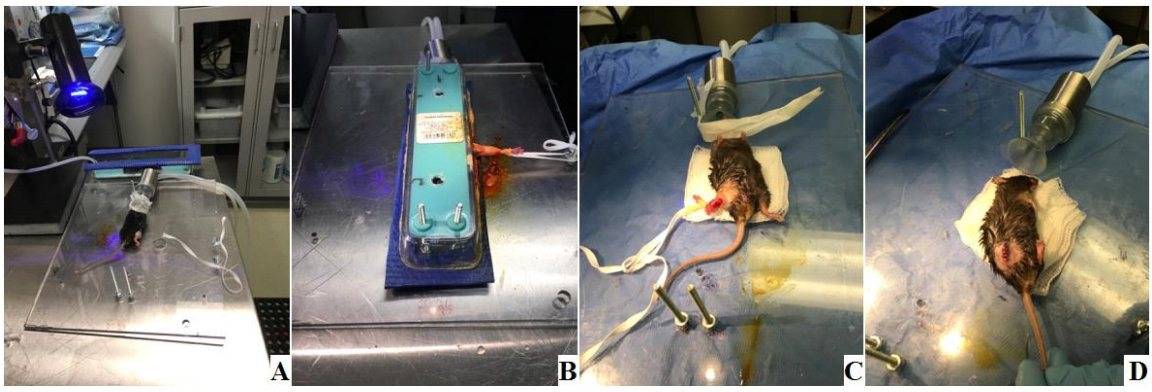

Figure 6. Blast-amputation procedure

(A) Animal was deeply anesthetized. **(B)** The body of animal was protected, only the right hind limb was left outside the shield to be exposed to the blast wave. **(C)** Severe extremity trauma was seen following blast injury. **(D)** Animal underwent above-knee amputation and wound closure.

2.2.3 HO formation assessment

Blast-injured mice were harvested for different time points for microCT and histology analysis of HO formation. A Scanco vivaCT 40 scanner (Brüttisellen, Switzerland) was used for all microCT image acquisition. Scans were acquired at 45 kVp, 88 μA, 300 ms integration time and at an isotropic voxel size of 35 μm. Following micoCT imaging, muscle tissues were isolated from the animal and fixed in methanol overnight. Muscle tissues were then paraffin embedded and sectioned. H&E staining and Alizarin Red staining were performed to visualize tissue structure and calcium deposition.

2.3 RESULTS

2.3.1 Characterization of blast trauma-induced HO

Radiographic evidence of HO formation was observed at 4 weeks post blast injury (Figure 7A). Histology revealed that it was mature bone formation with lamellar bone and bone marrow cavity (Figure 7C&D). Red blood cells were also observed in HO lesion, indicating active hematopoiesis. From serial sections, we found that isolated HO grew inside the muscle fibers and had a size of approximately 300 μm sphere. Interestingly, HO is always located proximal to the amputation site and distant from the femur, which is quite different from periosteal reaction that we have observed adjacent to the fractured femur.

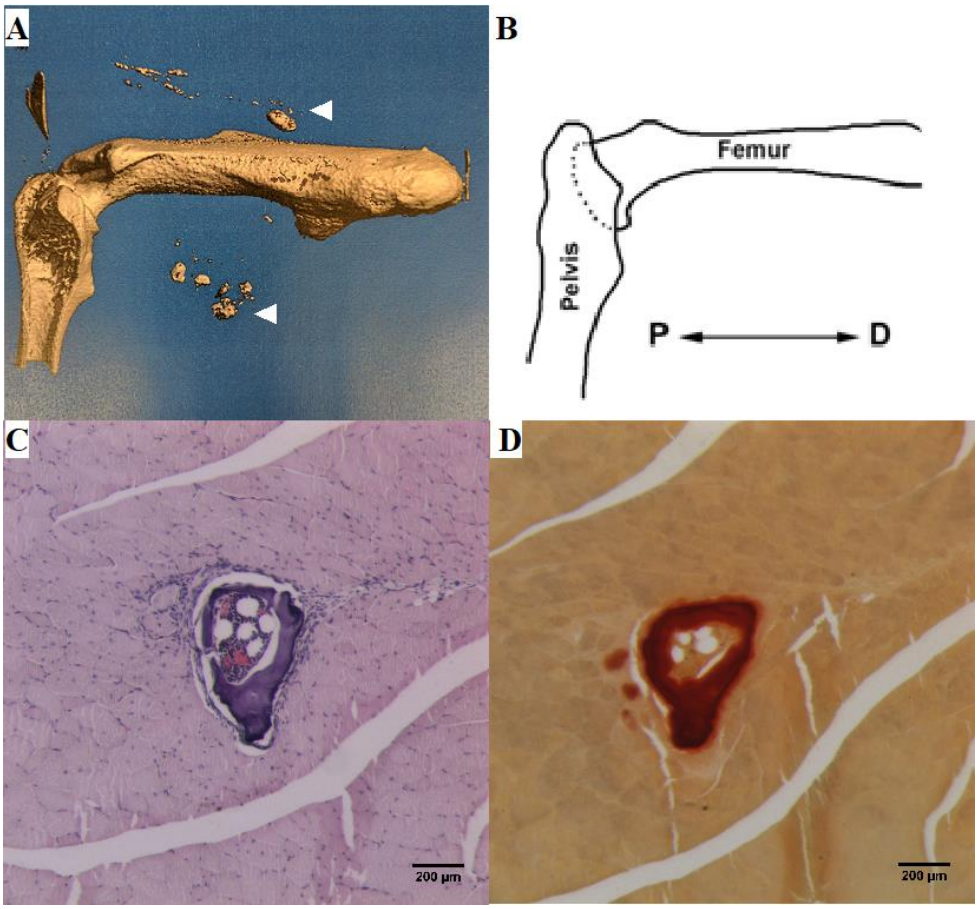

Figure 7. Characterization of blast trauma-induced HO

(A) Representative microCT image showing HO (arrowhead) in muscle. **(B)** Diagram providing orientation for microCT. **(C)** H&E staining showing mature HO in muscle. **(D)** Alizarin Red staining demonstrating calcium deposition. Scale bar = 200 μm

2.3.2 Muscle trauma is associated with HO formation

To determine the time course of HO progression, we harvested muscle tissue 3 days, 7 days, 14 day and 28 days post blast injury. H&E staining revealed that muscle tissue was severely damaged at early time points with inflammatory cell infiltration (Figure 8A&B). In 2 weeks, dystrophic calcification (DC) was found within regenerated muscle fibers (Figure 8C), and mature bone structure was found in 4 weeks (Figure 8D).

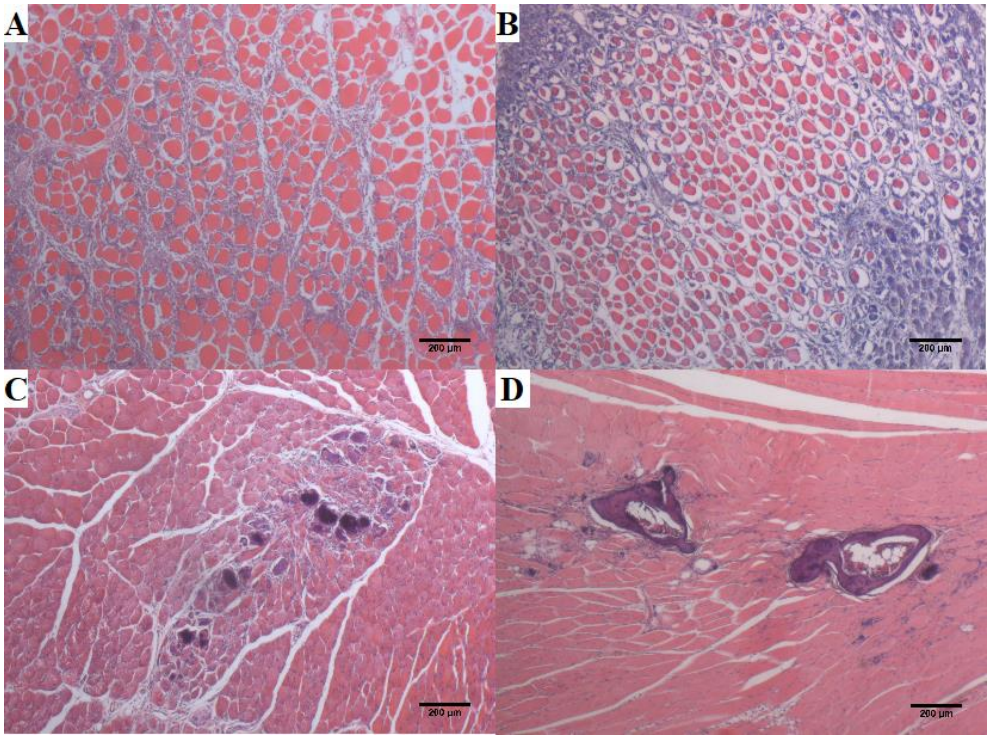

Figure 8. Time course of HO progression

H&E staining illustrating HO progression: **(A)** 3 day post blast injury **(B)** 7 day post injury **(C)** 14 day post injury **(D)** 28 day post injury. Scale bar = 200 μm

2.4 DISCUSSION AND CONCLUSION

In this part of the thesis work, we have successfully developed a novel mouse model of blast trauma-induced HO. We showed mature bone formation in the hind limb muscle 4 weeks following blast wave exposure to the mouse extremity. We demonstrated that HO formation is independent of exposure to heat and chemical residue from the explosive, since we employed a blast device that produces a supersonic blast wave comprised only of air. We largely ruled out the effects of CNS injury, foreign body and bacterial contamination on HO pathogenesis, given that the body of the animal was protected from being exposed to the blast wave and the operation

was performed under aseptic condition. Therefore, we concluded that blast wave exposure is sufficient stimulus for induction of HO in residual limb.

The progression of HO seemed to be through DC directly towards mature lamellar bone formation. Cartilaginous precursor stage typical of endochondral ossification was not as readily evident in HO lesions. Recent study has reported that the transition from calcification to ossification may be stages of a pathologic continuum [108]. In other words, persistent DC in skeletal muscle is sufficient to drive HO formation. This discovery may uncover a potential new paradigm in HO pathogenesis, which seems to bypass the classical fibroproliferative stage and cartilaginous stage of endochondral bone formation. Our data support this postulation by showing that a DC precursor stage may initiate HO formation. We also demonstrated that severe muscular trauma precedes the formation of DC. In the next chapter, role of muscle injury in HO pathogenesis will be further explored to delineate the whole picture of this pathologic condition.

3.0 ROLE OF MUSLCE INJURY IN HO PATHOGENESIS

Chapter 3 is adapted from a published article in Journal of Orthopaedic Translation

Li L., Jiang Y., Lin H., Shen H., Sohn J., Alexander P.G., Tuan R.S.. *Muscle injury promotes heterotopic ossification by stimulating local bone morphogenetic protein-7 production.* J Orthop Translat, 2019. 18:142-153.

3.1 INTRODUCTION

As mentioned above, different types of HO do not utilize identical mechanistic pathways of pathogenesis. However, muscle injury appears to be a unifying feature for all types of HO. In FOP patients, low levels of muscular trauma following childhood immunizations or play-related falls can result in HO [12]. In neurogenic HO, microtrauma to muscles resulting from forced passive movements following a period of immobilization will lead to an increased risk of HO [47]. In traumatic HO, more severe levels of muscular trauma, as in cases of arthroplasty and blast trauma, can lead to an HO incidence of 20% and 64.6%, respectively [72, 109]. Muscle injury usually incurs an inflammatory response, and anti-inflammatory drugs have been used as prophylaxis in HO-susceptible patients [43]. However, the precise mechanism by which muscle injury facilitates HO formation and the mechanistic rationale for the use of anti-inflammatory drugs in the prevention of HO are still largely unknown.

In experimental animal HO models, cardiotoxin (CTX) injection has been commonly used to induce muscle injury and subsequent HO. CTX belongs to the family of snake venom polypeptide toxins that cause depolarization and contraction of muscle fibers [110]. Eventually, CTX causes muscle degeneration through myocyte death, which subsequently elicits a regenerative response thought to be mediated by infiltrating inflammatory cells [111]. CTX has been widely used in a large number of mouse HO models, such as the BMP-4 over-expression HO model [21, 28], constitutively active Activin receptor-like kinase-2 (caALK2) HO model [16, 25, 26, 55], spinal cord injury neurogenic HO model [56], plasminogen deficiency HO model [112], and the burn injury HO model [113]. Similar to human HO conditions, muscle injury seems to be indispensable for HO development in these experimental animal models. However, given the importance of muscle injury in HO pathogenesis, it is striking that few studies have justified the usage of CTX and explained by which mechanisms CTX-induced muscle injury facilitates HO formation.

This study examines the underlying cellular and molecular mechanisms linking muscle injury to HO by using CTX to induce muscle injury in a BMP-2-induced HO mouse model. We hypothesized that soluble, pro-osteogenesis factors present in damaged muscle tissue are able to push muscle-derived stromal cells (MDSCs) towards osteoblastic differentiation to facilitate HO formation. In this study, we sought to identify the osteoinductive factors actively involved in this process, thus providing a general mechanism by which muscle injury facilitates HO formation.

3.2 METHODS

3.2.1 *In vivo* induction of HO

Using a protocol approved by the Institutional Animal Care and Use Committee (IACUC), the calf muscle of the right leg of 8-12 week old male C57BL/6J mice (Jackson laboratory, Bar Harbor, ME, USA) were first injected with 50 μL of 10 μM CTX (Calbiochem, San Diego, CA, USA). One day later, the calf muscles of both legs were injected with 0.5 μg BMP-2 (R&D Systems, Minneapolis, MN, USA) encapsulated in 50 μL photocrosslinked methacrylated 8% (w/v) gelatin hydrogel scaffold developed in our laboratory [114]. Two weeks later, mice were euthanized for imaging by microCT (Scanco Medical vivaCT 40, Brüttisellen, Switzerland) to detect HO formation. Scans were acquired at 45 kVp, 88 μA, 300 ms integration time and at an isotropic voxel size of 35 μm. Bone density was calculated as mg hydroxyapatite (HA)/volume (cubic centimeter, ccm).

A separate group of mice were subcutaneously injected with 1 mg/kg dexamethasone daily (Vedco Inc., Saint Joseph, MO, USA) for seven days following CTX and BMP-2 injection to suppress inflammation. Two weeks later, mice were euthanized for microCT analysis of HO formation.

3.2.2 CTX-injured muscle tissue sample collection

CTX injection alone group was performed as follows. The calf muscles of both legs of C57BL/6J mice were injected with CTX as described above. At different time points, mice were sacrificed and calf muscles from left and right sides were immediately harvested and snap-frozen in liquid

nitrogen for later muscle tissue RNA and protein isolation respectively. Uninjected mice served as Day 0 control.

A separate group of mice were used for muscle tissue derived conditioned medium collection. The calf muscle of the right leg of C57BL/6J mice was injected with CTX as described above. On day 2, mice were sacrificed and the calf muscles of both legs were processed as follows. Briefly, pooled muscle tissue samples (1 g) from either the control left leg or the CTX-injured right leg were cut into 3-mm pieces and cultured in 10 mL growth medium (GM, high-glucose Dulbecco's Modified Eagle's Medium [Gibco, Gaithersburg, MD, USA] supplemented with 20% fetal bovine serum [Gemini Bio Product, West Sacramento, CA, USA] and 1% penicillin/streptomycin [Gibco]). Conditioned medium (CM) was changed and collected every day for three days and stored at -80℃ for later use.

3.2.3 *In vitro* osteogenesis induction with muscle tissue derived conditioned medium

CM derived from CTX-injured muscle tissue (CTX CM) and CM derived from control muscle tissue (CTL CM) were used to culture MDSCs at a dilution of 1:2 in GM for three days. MDSCs were harvested from another cohort of mice according to a previously described protocol [115]. On culture day 3, MDSCs were collected either for quantitative real-time reverse-transcription polymerase chain reaction (qRT-PCR) analysis or Western blot analysis. PCR data and Western blot data were normalized to MDSCs cultured in GM only.

For inhibition of BMP-7 *in vitro*, MDSCs were maintained for three days in GM or muscle tissue derived CM with the supplementation of either 1 μg/mL BMP-7 neutralizing antibody (ab27569, abcam, Cambridge, MA, USA) or 1 μg/mL isotype control antibody (ab171870, abcam). On culture day 3, MDSCs were collected either for measurement of alkaline

phosphatase activity using an Alkaline Phosphatase Assay kit (ab83369, abcam) or phosphorylated Smad1 level using a SMAD1 (pS463/S465) ELISA Kit (ab186036, abcam). For the phosphorylated Smad1 ELISA, protein was extracted 1 hour after the change of day 3 CM.

3.2.4 qRT-PCR analysis

Tissues or cells were lysed in QIAzol Lysis Reagent and isolated using the RNeasy Mini Kit according to the manufacturer's instructions (QIAGEN, Hilden, Germany). RNA was then converted to cDNA using the SuperScript™ IV First-Strand Synthesis System (Invitrogen, Carlsbad, CA, USA). Quantitative real-time PCR was performed with a StepOne Plus Realtime PCR system using PowerUp™ SYBR® Green Master Mix (Applied Biosystems, Foster City, CA, USA). The relative level of gene expression was calculated using the 2-delta delta Ct method. Primer sequences for actin, runt-related transcription factor 2 (*Runx2*), osterix (*OSX*), alkaline phosphatase (*ALP*), bone sialoprotein I (*BSP-1*), *BMPRIA*, *BMPRIB*, and *ACVR1* are listed in Table 1.

3.2.5 Western blot

Total protein from tissues or cells was extracted using lysis buffer provided in the phosphorylated Smad1 ELISA kit. Protein concentration was determined using the bicinchoninic acid assay (ThermoFisher Scientific, Waltham, MA, USA), and equal loads of reduced protein samples were electrophoretically separated on NuPAGE™ 4-12% Bis-Tris Gel (Invitrogen) and then transferred to a PVDF membrane using iBlot Dry Blotting System (Invitrogen). Primary antibodies directed against BMP-2 (ab14933, abcam), BMP-4 (ab39973, abcam), BMP-7

(ab56023, abcam), BMP-9 (ab35088, abcam), glyceraldehyde-3-phosphate dehydrogenase (GAPDH) (CST5174, Cell Signaling Technology, Danvers, MA, USA), total Smad1 (CST6944, Cell Signaling Technology) and phosphorylated Smad1/5 (CST9516, Cell Signaling Technology) were incubated at 4℃ overnight, followed by horseradish peroxidase-conjugated secondary antibody (GE Healthcare Life Sciences, Marlborough, MA, USA) incubation. Western blots were developed using SuperSignal™ West Dura Extended Duration Substrate (ThermoFisher Scientific), and visualized using a FOTO/Analyst1 Fx CCD imaging system (Fotodyne, Hartland, WI, USA).

3.2.6 Histology and immunostaining

Muscle tissues were fixed in methanol and paraffin embedded. For histology, sections (9 μm thick) were collected on Colorfrost Plus microscope slides (ThermoFisher Scientific), rehydrated, and H&E staining was performed according to a routine Harris Hematoxylin and Eosin protocol. Immunohistochemistry (IHC) was performed according to protocols described for the Vectastain Elite ABC Kit (Vector Laboratories, Burlingame, CA, USA). Images were taken using a CKX41 microscope (Olympus, Tokyo, Japan) equipped with a DFC 3200 camera (Leica, Wetzlar, Germany). For immunofluorescence staining, tissue sections were blocked in 10% bovine serum albumin for 20 minutes, then incubated overnight at 4℃ with mixed primary antibodies against BMP-7 (ab56023, abcam) and CD68 (ab53444, abcam). On the second day, sections were incubated with mixed secondary antibodies against rabbit IgG (ab150077, abcam) and rat IgG (ab150158, abcam) at room temperature for 1 hour. After washing, the slides were mounted with 4′,6-diamidino-2-phenylindole (DAPI) containing mounting medium (Vector Laboratories). Slides were viewed using an inverted IX81 microscope (Olympus) equipped with a Retiga EXi

cooled CCD camera (Qimaging, Surrey, BC, Canada) and a MetaMorph software (Molecular Devices, San Jose, CA, USA).

3.2.7 Inhibition of BMP-7 *in vivo*

The calf muscle of the right leg of C57 BL/6J mice was injected with CTX as described above. One day later, the calf muscles of both legs were injected with 0.5 μg BMP-2 (R&D Systems) either with 5 μg BMP-7 neutralizing antibody (ab27569, abcam) or 5 μg isotype control antibody (ab171870, abcam) coencapsulated in 50 μL photocrosslinked methacrylated 8% (w/v) gelatin hydrogel scaffold. Two weeks later, mice were euthanized for imaging by microCT to detect the change in HO volume. Same scan setting was employed as previously described.

3.2.8 Statistical analysis

All data were expressed as mean ± SD. Student's *t*-test was used to make comparisons between two groups, while one way ANOVA followed by the Tukey's multiple comparisons test was used for comparisons of three or more groups. Statistical significance (*) was considered at $p < 0.05$. Statistical analyses were performed using GraphPad Prism 7.0 software (GraphPad Software Inc., LaJolla, CA, USA).

3.3 RESULTS

3.3.1 CTX-induced muscle injury significantly increased HO volume

To determine the role of muscle injury in HO formation, CTX was injected into the calf muscle of the right leg of the animal one day before BMP-2 injection into the calf muscles of both legs. Two weeks later, microCT imaging and analysis showed significantly larger bone volume in the right legs that were co-injected with CTX and BMP-2 (3.458 ± 0.994 mm^3), compared with the left legs that were injected with BMP-2 alone (1.573 ± 0.577 mm^3) (Figure 9A). Histology revealed severe inflammatory cell infiltration into the muscle tissue of the CTX-injured leg, while such infiltration was absent in the group with BMP-2 injection alone (Figure 9B). Bone tissue became evident after two weeks when most of the hydrogel vehicle had been degraded. There were no morphological differences (Supplemental Figure 1) between the bone formed in the different groups and no qualitative differences in bone mineral density (Figure 9A).

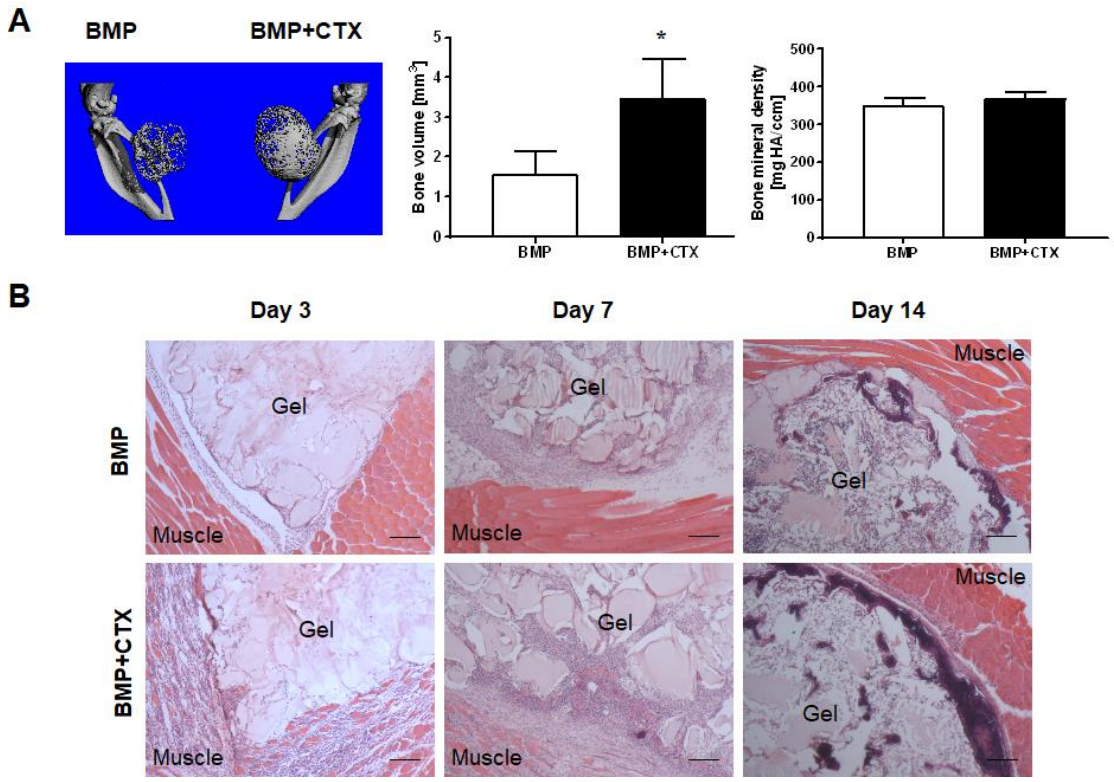

Figure 9. CTX-induced muscle injury significantly increased HO

(A) microCT imaging and analysis. Significantly larger HO volume was observed in the BMP-2/CTX co-injection group (right leg), compared to the group receiving BMP-2 injection alone (left leg) (*, $p < 0.05$; $n = 4$). No significant difference in bone mineral density was found between the two groups. **(B)** H&E staining illustrating the time course of HO progression. Severe inflammatory response in muscle tissue was seen at the early time points in the CTX-injured groups. Scale bar = 200 μm.

3.3.2 CTX-induced muscle injury generated an osteoinductive environment with BMP signaling activation

CTX administration alone was not sufficient for the induction of HO and the inflammatory response was resolved after two weeks (data not shown). However, during this regeneration process, BMP signaling was activated with significantly higher phosphorylated Smad1 level

observed 7 days following muscle injury (Figure 10A). Osteogenic marker genes were also found to be upregulated with the expression of different genes peaking at different time points (Figure 10B), suggesting the generation of a pro-osteogenesis environment with highly coordinated gene regulation following muscle injury.

To explore how this pro-osteogenesis environment could promote HO formation, muscle tissue derived conditioned medium was collected and applied to MDSCs in culture. After exposure to either GM or CM for two days, MDSC cultures were extracted for total protein at various time points after the change of medium on day 3. BMP signaling activation was observed immediately after the application of GM and CM (Figure 10C). However, the phosphorylation of Smad1/5 protein level diminished in GM group quickly but persisted in CM groups for an extended period of time. Phosphorylation of Smad1/5 protein level in CM groups peaked at the 1-hour time point and remained the highest in the CTX CM treatment group thereafter (Figure 10C). Exposure to CTX CM was also found to greatly enhance osteogenic marker gene expression in MDSCs, compared to exposure to CTL CM (Figure 10D). Concomitantly, *BMPRIB* gene expression increased significantly in MDSCs cultured in CTX CM (Figure 10D). Taken together, these results suggested that soluble factor(s) present in injured muscle tissue were able to promote MDSC osteogenesis via BMP signaling pathway.

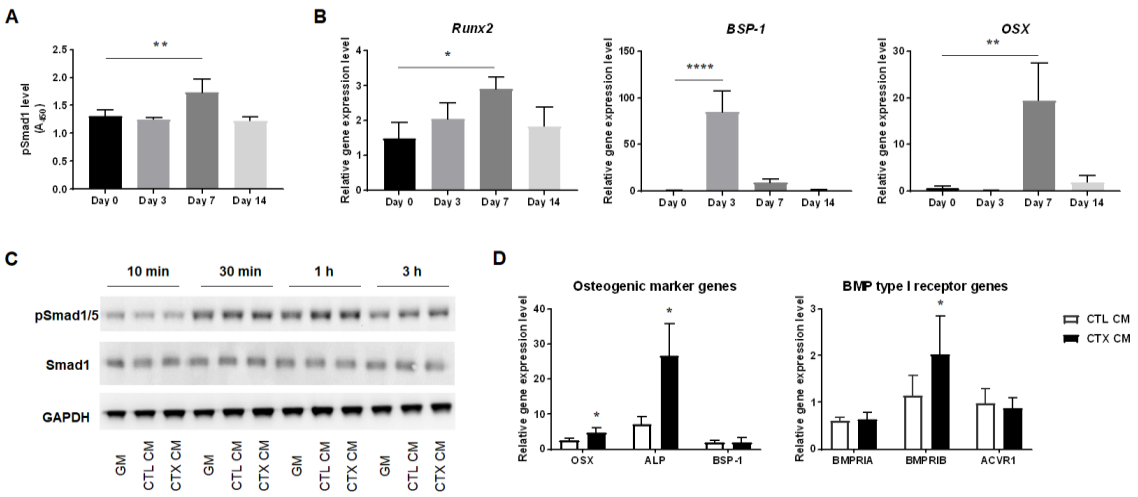

Figure 10. CTX-induced muscle injury generated an osteoinductive environment

(A) Phosphorylated Smad1 level in muscle tissue lysates measured by pSMAD1 ELISA at different time points following CTX injection demonstrated the activation of BMP signaling (**, $p < 0.01$; $n = 3$). **(B)** PCR analysis showed the upregulation of osteogenic marker gene expression in muscle tissue following CTX injection with the expression of different genes peaking at different time points. (*, $p < 0.05$; **, $p < 0.01$; ****, $p < 0.0001$; $n = 3$). Data are normalized to uninjected Day 0 control mice. **(C)** Western blot analysis of phosphorylated Smad1/5 protein and total Smad1 levels revealed the time course of BMP signaling activation in MDSCs cultured in GM and muscle tissue derived CM. **(D)** PCR analysis of osteogenic marker gene and BMP type I receptor gene expression in MDSCs. Significantly higher *OSX*, *ALP*, and *BMPR1B* expression was detected in MDSCs cultured in CTX CM compared to CTL CM (*, $p < 0.05$; $n = 3$). Data are normalized to MDSCs cultured in GM.

3.3.3 BMP-7 level increased in CTX-injured muscle

To identify the soluble factor(s) involved in BMP signaling activation, Western blotting was performed to examine the expression profile of several BMP ligands that have been reported to exhibit significant osteoinductive potential [116]. Among these BMP subtypes, we found that BMP-7 expression changed drastically with substantially increased expression 3 days following muscle injury, whereas BMP-2, BMP-4, BMP-9 expression remained relatively constant during

the muscle regeneration period (Figure 11A). Histology confirmed the expression of BMP-7 on CTX-injured muscle tissue at 48 hours after CTX injury, but not on control uninjured muscle tissue (Figure 11B). Histology also revealed severe inflammatory cell infiltration into the muscle tissue, suggesting the possibility that BMP-7 could be derived from the infiltrating inflammatory cells. Double immunofluorescence staining indeed demonstrated the presence of the macrophage marker, CD68, localized in close proximity to BMP-7 signals (Figure 11C). There were double positive cells as well as single positive cells for either marker in CTX-injured muscle tissue.

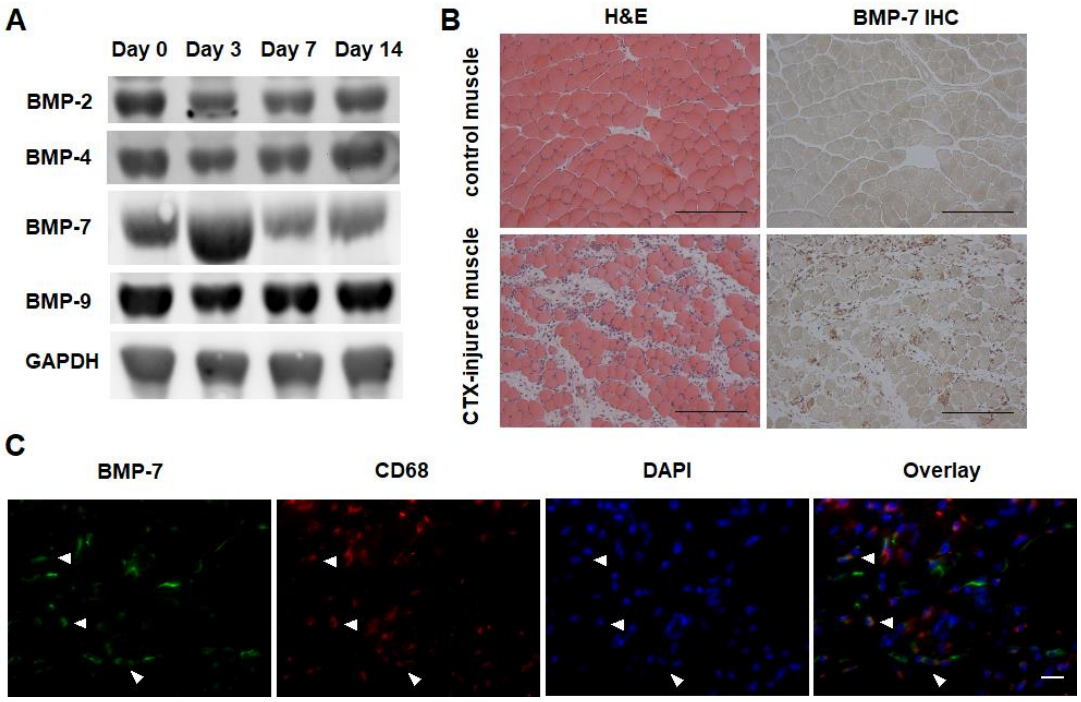

Figure 11. BMP-7 level increased in CTX-injured muscle

(A) Western blot analysis of the expression profile of selected BMP ligands following muscle injury. **(B)** H&E and IHC images showing the presence and distribution of BMP-7 in CTX-injured muscle tissue at 48 hours after CTX injury. Bar = 200 μm. **(C)** Immunofluorescence staining showing the location of BMP-7 (green) in relation to macrophage marker CD68 (red) in CTX-injured muscle tissue. Arrowheads indicate the double positive cells present in CTX-injured muscle tissue. Bar = 20 μm.

3.3.4 Inhibiting BMP-7 activity *in vitro* suppressed the osteogenesis-promoting effect of conditioned medium derived from CTX-injured muscle tissue

To assess the functional involvement of BMP-7, the effect of supplementing BMP-7 neutralizing antibody to muscle tissue CM was tested on the promotion of MDSC osteogenesis, based on ALP activity and phosphorylated Smad1 level. Our results showed that ALP activity increased significantly in MDSCs cultured in CTX CM compared to CTL CM, and that this osteogenesis-promoting effect of CTX CM was significantly inhibited in the presence of BMP-7 neutralizing antibody (Figure 12A). Concomitantly, addition of BMP-7 neutralizing antibody to CM resulted in the reduction of phosphorylated Smad1 to a nearly basal level (Figure 12B), validating the functional involvement of BMP-7 in BMP signaling activation *in vitro*.

3.3.5 Inhibiting BMP-7 activity *in vivo* reduced HO volume

To assess the *in vivo* relevance of the *in vitro* findings, BMP-7 neutralizing antibody was coencapsulated in hydrogel scaffold at the time of BMP-2 injection in the mouse HO model. microCT imaging and analysis at two weeks showed significantly reduced bone volume in both legs of animals receiving BMP-7 neutralizing antibody treatment (left leg: 0.3715 ± 0.1016 mm^3; right leg: 1.642 ± 0.5055 mm^3), compared to animals receiving isotype control antibody treatment (left leg: 1.557 ± 0.4149 mm^3; right leg: 3.875 ± 0.6129 mm^3) (Figure 12C). No qualitative differences in bone mineral density were found between BMP-7 neutralizing antibody and isotype control antibody treatment groups (Figure 12C).

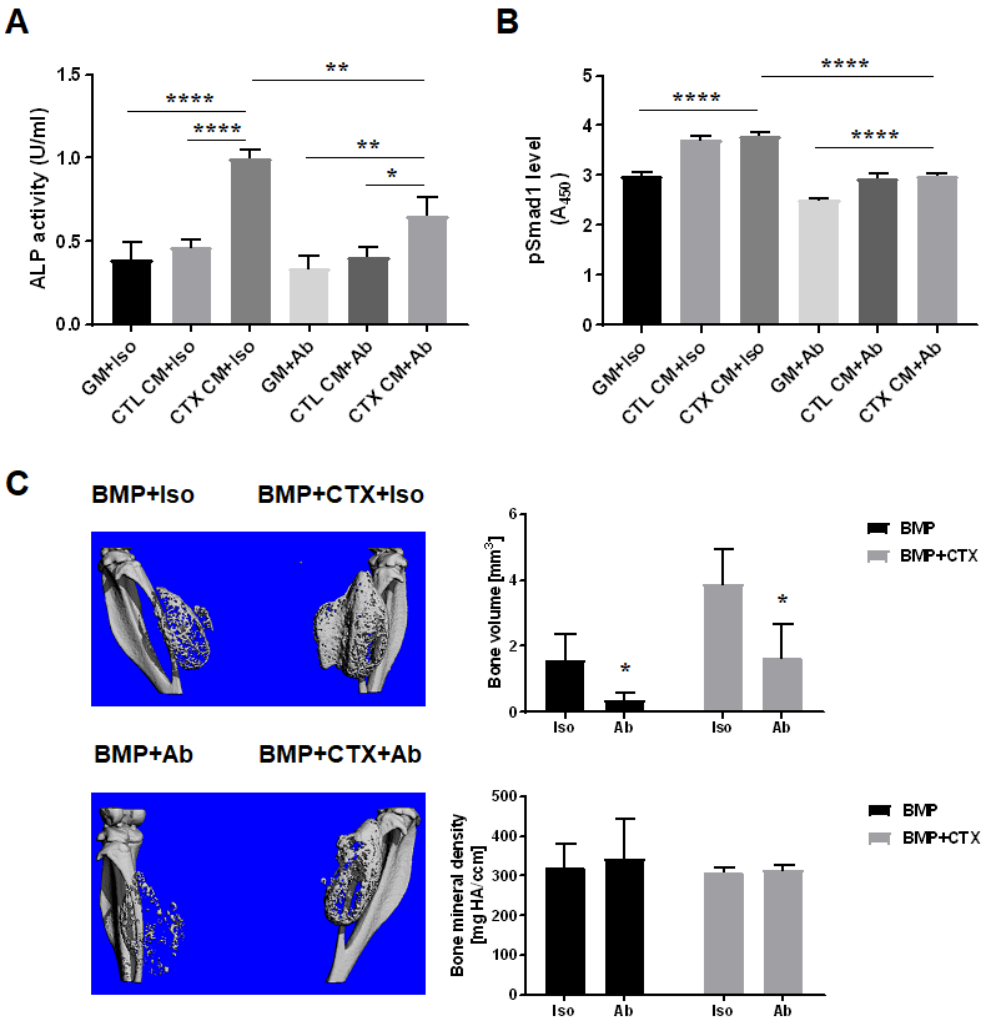

Figure 12. Inhibition of BMP-7 activity suppressed osteogenesis *in vitro* and reduced HO formation *in vivo* **(A)** Osteogenesis of MDSCs *in vitro*. ALP activity measured in different groups of cell lysates showed that treatment with BMP-7 neutralizing antibody suppressed the osteogenesis-promoting effect of CTX CM (*, $p < 0.05$; **, $p < 0.01$; ****, $p < 0.0001$; $n = 3$). Iso: isotype control antibody treatment group; Ab: BMP-7 neutralizing antibody treatment group. **(B)** BMP signaling *in vitro*. Phosphorylated Smad1 level in cell lysates measured by pSMAD1 ELISA showed that activation of BMP signaling was inhibited with addition of BMP-7 neutralizing antibody (****, $p < 0.0001$; $n = 3$). (C) HO formation *in vivo*. microCT imaging and analysis showed significant reduction in HO volume upon BMP-7 neutralizing antibody treatment, compared with isotype control antibody treatment (*, $p < 0.05$; $n = 4$). No significant difference in bone mineral density was found between BMP-7 neutralizing antibody and isotype control antibody treatment groups.

3.3.6 Suppression of inflammation reduced HO volume with concomitant reduction of BMP-7 production in CTX-injured muscle

To assess the involvement of inflammation in HO formation, the anti-inflammatory drug, dexamethasone, was administered to the animals for 7 days to suppress the inflammatory response induced by muscle injury. microCT imaging and analysis at two weeks showed significantly reduced bone volume in both legs (left leg: 0.0803 ± 0.119 mm^3; right leg: 0.717 ± 0.396 mm^3) (Figure 13A), compared to animals that did not receive anti-inflammatory drug treatment (left leg: 1.573 ± 0.577 mm^3; right leg: 3.458 ± 0.994 mm^3) (Figure 9A). Histological observation showed that, with dexamethasone administration, severe inflammatory cell infiltration into damaged muscle tissue was no longer evident in CTX-injured legs at the early time points (Figure 13B). In addition, the HO formed was less mineralized in both legs after dexamethasone treatment (left leg: 219.2 ± 44.94 mg HA/ccm; right leg: 296.8 ± 8.453 mg HA/ccm) (Figure 13A), compared to animals that did not receive anti-inflammatory drug treatment (left leg: 348.1 ± 10.45 mg HA/ccm; right leg: 370 ± 8.133 mg HA/ccm) (Figure 9A).

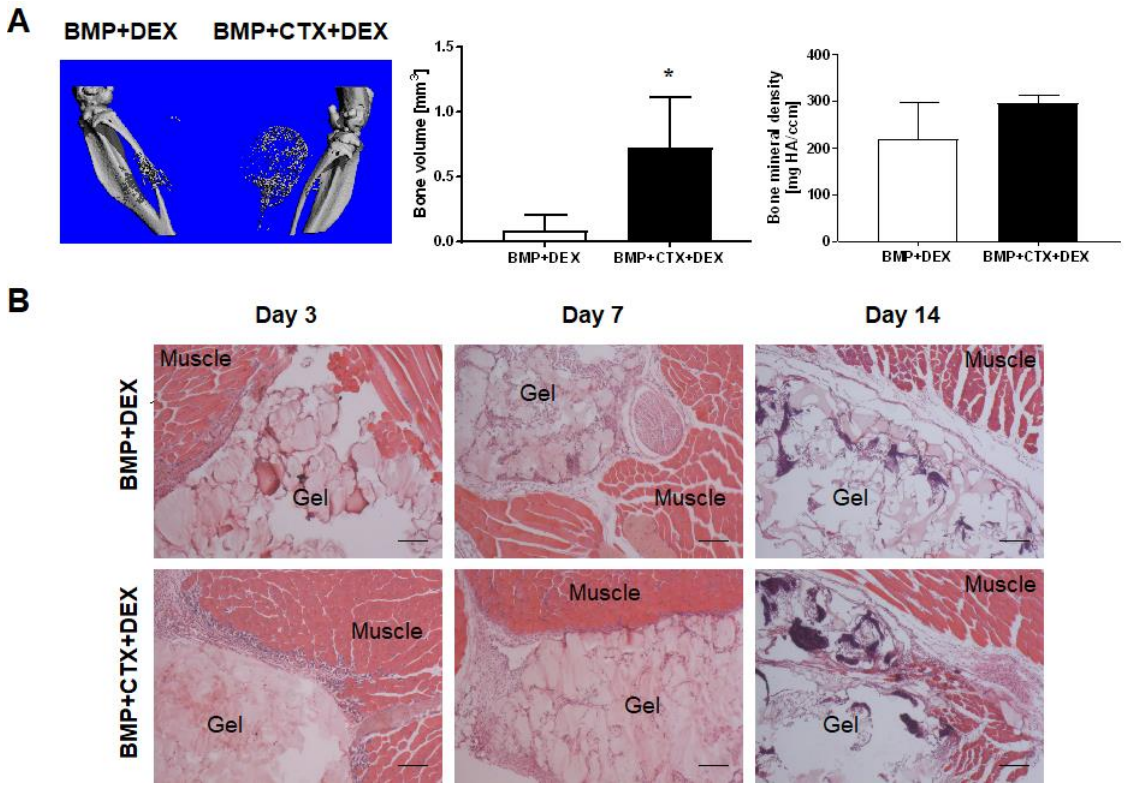

Figure 13. Suppression of inflammation reduced HO volume *in vivo*

(A) microCT imaging and analysis. Reduction of HO volume and bone mineral density was observed in animals treated with the anti-inflammatory drug, dexamethasone (DEX) (*, $p < 0.05$; $n = 4$). **(B)** H&E staining illustrating a time course of HO progression in animals treated with anti-inflammatory drug. A diminished inflammatory response was found in CTX-injured muscle. Bar = 200 μm.

Immunofluorescence staining showed decreased CD68 positive macrophage numbers in CTX-injured muscle of dexamethasone-treated animals, compared to animals without dexamethasone treatment, at both the day 3 and day 7 time points (Figure 14). Importantly, in addition to decreased macrophage number in dexamethasone-treated group, BMP-7 level in CTX-injured muscle tissue was also greatly reduced at the day 3 time point (Figure 14A&B). BMP-7 expression was only detectable within 3 days following CTX injury, and was undetectable beyond the acute inflammatory phase (Figure 14A&C).

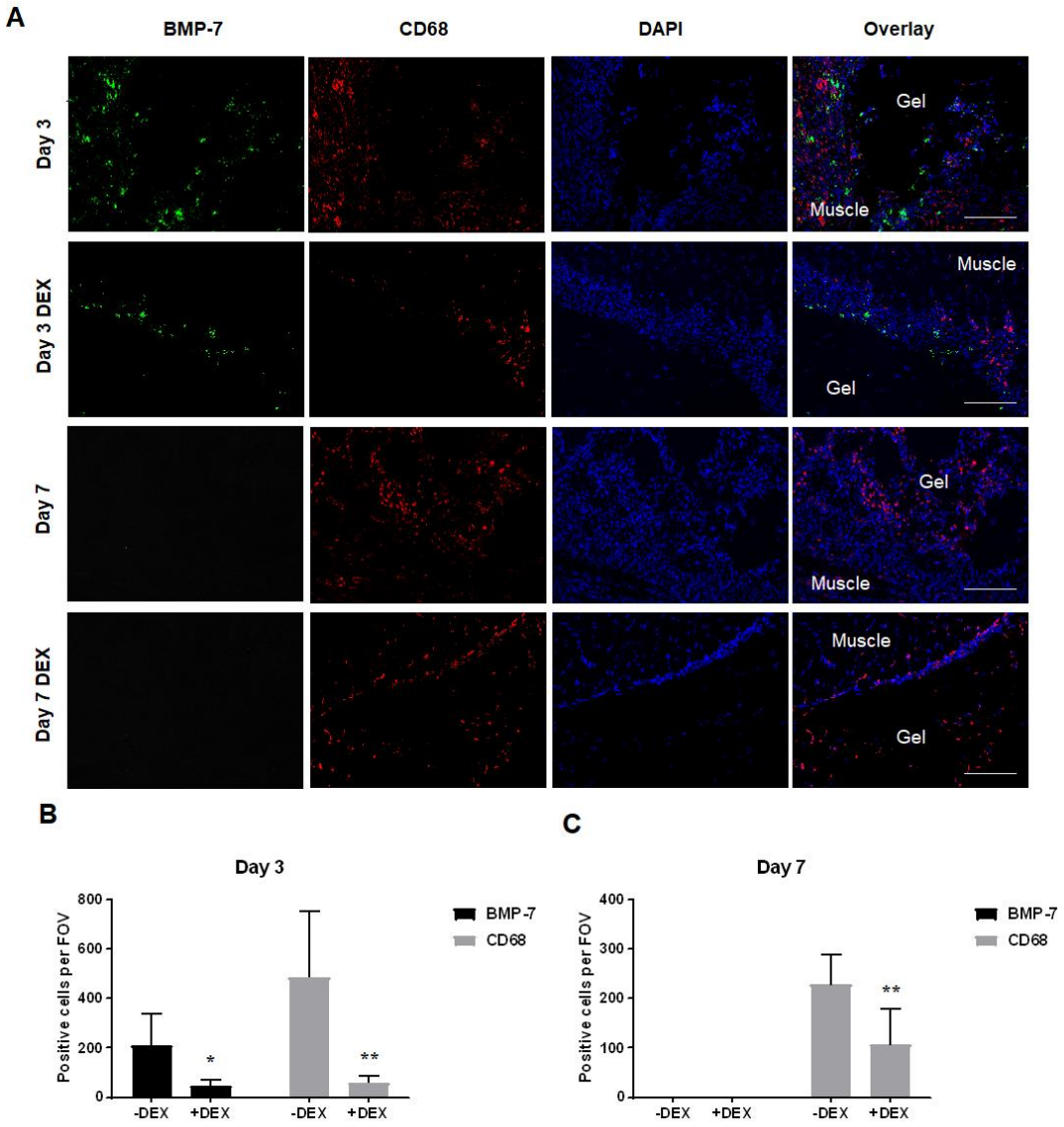

Figure 14. Suppression of inflammation *in vivo* reduced BMP-7 level in CTX-injured muscle

(A) Immunofluorescence staining showing decreased macrophage number (CD68, red) and reduced BMP-7 level (green) in CTX-injured muscle in animals treated with the anti-inflammatory drug, dexamethasone (DEX). Bar = 200 μm. **(B&C)** Quantitative analysis of BMP-7+ and CD68+ cells at the interface of hydrogel scaffold and muscle. Cell counts of BMP-7+ and CD68+ cells were done on 6 independent fields of view (FOV, 20× magnification). **(B)** On day 3, significant decrease in the number of BMP-7+ and CD68+ cells was observed in dexamethasone-treated animals (*, $p < 0.05$; **, $p < 0.01$). **(C)** On day 7, significant decrease in the number of CD68+ cells was observed in dexamethasone-treated animals (**, $p < 0.01$), while BMP-7+ cells were not detected.

3.4 DISCUSSION AND CONCLUSION

In this study, we first set out to determine the role of muscle injury in HO formation by using CTX to induce muscle injury in a BMP-2-induced HO mouse model. Our results showed that CTX-induced muscle injury significantly increased the volume of BMP-2-induced HO (Figure 9A) together with increased osteogenic marker gene expression (Figure 10B) and increased level of phosphorylated Smad1 (Figure 10A), suggesting the generation of a pro-osteogenesis environment after CTX treatment.

Next, we sought to explore by which mechanism muscle injury facilitates HO formation. To test the possibility that soluble factors present in damaged muscle tissue have an osteogenesis-promoting effect, we compared the effect of exposing MDSCs to culture medium conditioned by explanted control muscle tissue (CTL CM) *versus* that conditioned by explanted CTX-injured muscle tissue (CTX CM). MDSC is likely the same cell type identified as the muscle interstitial resident FAPs previously found to mediate BMP-2-induced HO *in vivo* [19, 24]. The MDSCs used in this study are positive for the surface markers Sca-1 and PDGFRα, have strong osteogenic potential, and are highly responsive to BMP signal in vitro (Supplemental Figure 2). Our data showed that CTX CM is capable of promoting osteogenesis by upregulating osteogenic marker gene and BMP receptor gene expression in MDSCs (Figure 10D) along with BMP signaling activation (Figure 10C), suggesting that certain BMP family proteins are present in the damaged muscle milieu and are capable of exerting an osteogenesis-promoting effect on MDSCs. Notably, we also found that CTL CM is also capable of promoting MDSCs osteogenesis and activates BMP signaling compared with GM, but to a lesser extent than CTX CM. We speculate that this is either because certain pro-osteogenesis factors are present at basal level in uninjured muscle tissue or muscle tissue was unavoidably injured during its collection

process resulting from incision and cutting. In summary, our findings suggest a general mechanism by which muscle injury facilitates HO formation via the soluble factors present in injured muscle that induce MDSC osteogenesis through BMP signaling pathway.

To identify which soluble factor is responsible for BMP signaling activation following muscle injury, Western blotting was performed against selected BMP subtypes that have been reported with great osteoinductive potential. We found that BMP-7 expression was highly upregulated at early time points following muscle injury, and that its expression was localized only to inflamed areas of muscle tissue highly populated by CD68 positive macrophages (Figure 11). We did not observe the change in expression of other BMP subtypes in injured muscle tissue. As ligand specificity of BMP signaling is mainly dictated by BMP type I receptor, with BMP-2/4 having a higher affinity for BMPRIA and BMP-6/7 for BMPRIB [117], the upregulation of BMP-7 was consistent with our *in vitro* finding that among the BMP type I receptors only *BMPRIB* expression was significantly upregulated in MDSCs after being exposed to muscle tissue CM (Figure 10D). To confirm the functional involvement of BMP-7, we performed BMP-7 inhibition experiment both *in vitro* and *in vivo*. Treatment with BMP-7 neutralizing antibody significantly inhibited the osteogenesis-promoting effect of CTX CM *in vitro* and reduced HO volume *in vivo* (Figure 12), strongly implicating the role of BMP-7 as a key osteoinductive factor responsible for the osteogenesis-promoting effect of muscle injury.

BMP-7, also known as osteogenic protein-1, is an FDA-approved osteoinductive adjuvant in orthopedic surgery known for its role in triggering stem cell osteogenic differentiation [118]. However, the physiological role of BMP-7 following muscle injury and its cellular origin is not clear at this point. Previous studies have shown that BMP signaling is normally active in muscle and important in maintaining muscle mass, and that inhibition of BMP signaling leads to muscle

antrophy [9, 119]. Studies have also shown that BMP signaling is indispensable for muscle regeneration following injury, and BMP signaling activation coincides with the period of satellite cell proliferation [10]. Therefore, BMP-7 may function to promote satellite cell proliferation in injured muscle [120, 121]. Recently, it has become clear that BMP-7 is a highly pleiotropic factor [122]. For example, it has been reported that BMP-7 inhibits inflammation by inducing M2 macrophage differentiation [123]. It can also act as an anti-fibrotic cytokine by antagonizing TGF-β1 [124-126]. Given the close spatial proximity of BMP-7 signal and macrophage signal observed by immunofluorescence staining, the upregulation of BMP-7 in injured muscle may also be a mechanism to counteract muscle injury-induced inflammation and fibrosis. However, in pathological conditions, such as in our case with supraphysiological doses of BMP-2, this physiological BMP-7 signal may well turn into strong osteogenic signal to cause aberrant osteogenesis.

Lastly, we showed that anti-inflammatory drug treatment reduced the volume of HO formation *in vivo*, with evident decreases in inflammatory cell infiltration (Figure 13). In addition, we found decreased BMP-7 level in CTX-injured muscle tissue in dexamethasone-treated animals compared with those not receiving the drug (Figure 14). The positive correlation between BMP-7 levels and macrophage numbers suggests that the osteogenesis-promoting effect of muscle injury could be largely related to the injury-induced inflammatory response. Our results thus provide a possible rationale for using anti-inflammatory drugs as HO prevention. Interestingly, we also observed in our study that either inhibition of BMP-7 activity or suppression of inflammation reduced the volume of HO in the left legs subjected only to BMP-2 injection. This can be explained by the fact that recombinant BMP triggers dose-dependent inflammatory reactions *in vivo* [127], and hydrogel muscle injection may cause mild muscle

tissue injury. Indeed, we observed BMP-7 expression located at the interface of BMP-2 hydrogel and muscle in the BMP-2 injection alone group, which became even less evident in animals receiving anti-inflammatory drug treatment (data not shown).

In summary, our results demonstrate that locally produced BMP-7 following muscle injury could be a key factor in facilitating HO formation, and the osteogenesis-promoting effect is largely related to the muscle injury-induced inflammatory response. We also tested this postulation in our mouse blast-amputation model, and showed that BMP-7 level was highly upregulated 3 days following blast injury (Figure 15), suggesting that BMP-7 might play a universal role in different types of muscle injury. Our lab's previous study has demonstrated the presence of BMP-4 ligand in human blast traumatized skeletal muscle tissue [128]. However, we did not find upregulation of BMP-4 in our mouse blasted muscle tissue. This may be due to different injury mechanism, tissue harvest time, and differences between human and mouse.

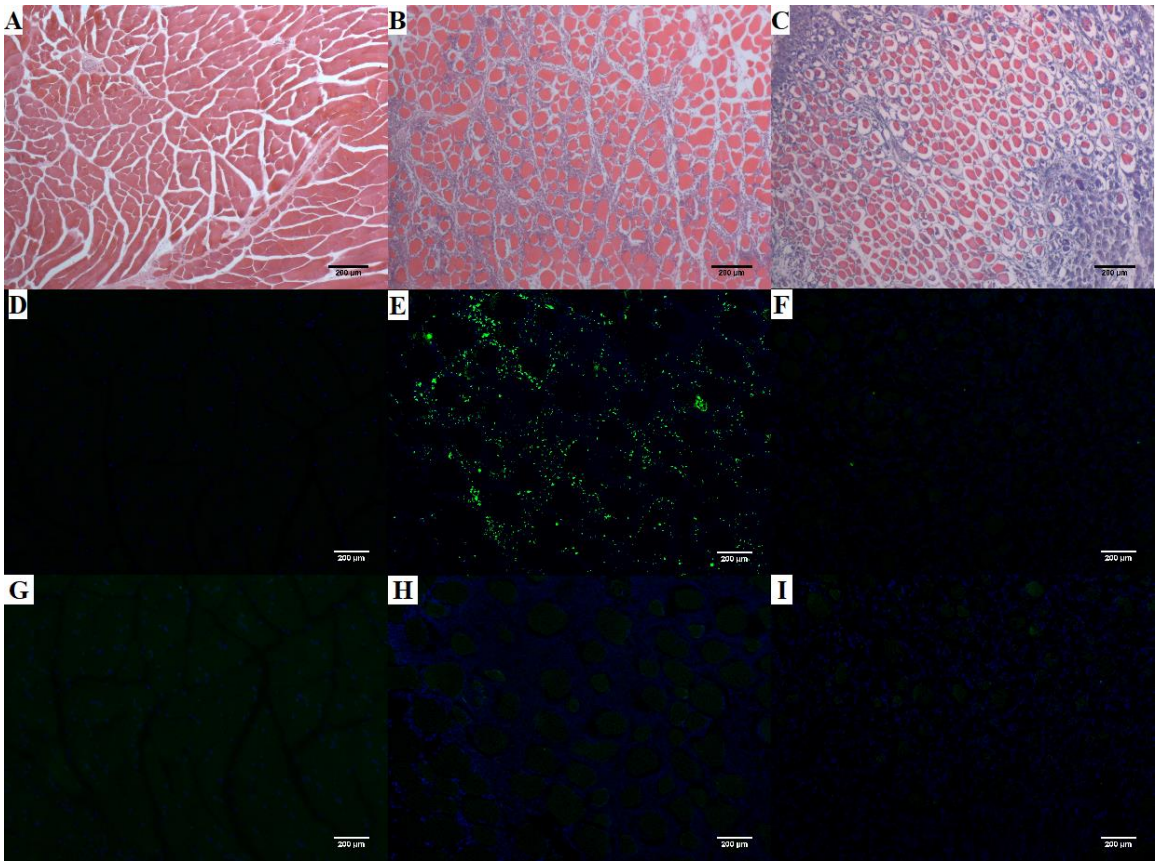

Figure 15. BMP-7 expression in mouse blast-traumatized muscle

(A-C) H&E staining illustrating muscle tissue morphology at different time points following blast injury: **(A)** uninjured muscle tissue; **(B)** 3 day post injury; **(C)** 7 day post injury. Scale bar = 200 μm **(D-F)** Immunofluorescence staining showing the expression of BMP-7 at different time points following blast injury: **(D)** uninjured muscle tissue; **(E)** 3 day post injury; **(F)** 7 day post injury. Scale bar = 200 μm **(G-I)** Immunofluorescence staining using isotype control antibody: **(G)** uninjured muscle tissue; **(H)** 3 day post injury; **(I)** 7 day post injury. Scale bar = 200 μm

4.0 ROLE OF CORTISOL STRESS RESPONSE IN HO PATHOGENESIS

Chapter 4 is adapted from a research article submitted to Journal of Bone and Mineral Research **Li L.**, Xiang S., Wang B., Lin H., Kihara S., Sun H., Alexander P.G., Tuan R.S.. *TGF-β1 plays a protective role in glucocorticoid-induced dystrophic calcification.* (submitted November 2019)

4.1 INTRODUCTION

As mentioned above, the pathogenesis of acquired HO is not well understood. However, it is noteworthy that acquired HO happens most frequently in severe trauma patients such as following blast injury, central nerve system injury, and burn injury, when the body is under great stress, a condition under which excessive endogenous glucocorticoid production has always been found [129]. Glucocorticoids are one type of stress hormones, which exert strong immunosuppressive effects to confine body immune responses being overactivated in life-threatening situations [130]. Endogenous cortisol production can rise to 240 mg per day under stress, whereas the normal daily production is about 10 mg per day [131], and the secretion level of glucocorticoids can reflect the severity of injury [132, 133]. Glucocorticoids have a big impact on bone and muscle: glucocorticoid excess, both pathological elevation and long-term therapeutic use, could result in osteoporosis and muscle atrophy [134]. It has also been reported that cortisol stress response is associated with pathological calcification in the cardiovascular

system [135, 136]. However, few studies have investigated the impact of glucocorticoids on DC/HO formation in the musculoskeletal system. Based on reported clinical observations, we hypothesized that high glucocorticoid level could result in an increased incidence of DC/HO. In this study, we administered a high dose of a synthetic glucocorticoid, dexamethasone (DEX), to animals with muscle injury induced by cardiotoxin (CTX) injection to mimic a glucocorticoid excess state following severe muscle trauma, in order to determine the role of glucocorticoids in DC/HO pathogenesis and the possible underlying mechanism.

It has recently been demonstrated that decreased plasmin level is associated with DC/HO formation [112, 137]. In these studies, the authors claimed that perturbation in the fibrinolytic system could be the underlying mechanism for traumatic HO, since hypofibrinolysis is a common occurrence upon traumatic injury. Interestingly, glucocorticoids also play a role in the fibrinolytic system, namely it increases plasminogen activator inhibitor-1 (PAI-1) level, which in turn decreases plasmin level, therefore leading to a state of hypercoagulation [138]. Increased PAI-1 level has been reported to be associated with pathological calcification in the cardiovascular system [139, 140]. In the musculoskeletal system, PAI-1 expression is negatively correlated with muscle regeneration [141, 142]. Since DC/HO could be regarded as a result of impaired tissue regeneration [143], we hypothesized that glucocorticoid excess could impair muscle regeneration and promote DC/HO through alterations in PAI-1 and plasmin levels.

The plasmin substrate that is responsible for DC/HO formation is unknown. A well-known plasmin target is transforming growth factor-beta 1 (TGF-β1), an inducer of PAI-1 and also a key factor involved in muscle regeneration and pathological calcification [99, 144]. However, there is no existing, conclusive evidence regarding the role of TGF-β1 in DC/HO formation. TGF-β appears to inhibit stem cell osteogenesis [145-148], whereas when its effects

on the immune and other systems are taken into consideration, its role can be pro-osteogenic [99, 149-152]. In this study, we have sought to evaluate the functional involvement of TGF-β1 in glucocorticoid-induced DC, and the results reported here show a protective role of TGF-β1 in glucocorticoid-induced DC.

4.2 METHODS

4.2.1 *In vivo* induction of DC/HO

Using a protocol approved by the Institutional Animal Care and Use Committee (Protocol No. 18032493), the calf muscle of 8-week-old male C57BL/6J mice (Jackson Laboratory, Bar Harbor, ME, USA) were injected once with 50 μL of 10 μM CTX (Calbiochem, San Diego, CA, USA) to induce muscle injury [153]. Mice were also subcutaneously injected with 10 mg/kg DEX (Henry Schein, Dublin, OH, USA) daily until the day of sacrifice. CTX injection alone or DEX injection alone served as control. Mice were then euthanized at different time points for imaging by microCT (Scanco Medical vivaCT 40, Brüttisellen, Switzerland) to detect ectopic mineralization. Scans were acquired at 45 kVp, 88 μA, 300 ms integration time and at an isotropic voxel size of 35 μm. Bone volume was calculated by selecting region of interest that was drawn to include the opaque area of DC/HO at each 2D slices but to exclude the tibia and fibula area. Bone mineral density was calculated as mg hydroxyapatite (HA)/volume (cubic centimeter, ccm).

For administration of corticosterone (R&D Systems, Minneapolis, MN, USA), corticosterone was dissolved in DMSO and subcutaneously injected daily, with corn oil vehicle containing 5% DMSO. Mice were also injected with CTX. Mice were euthanized at Day 7 time

point for imaging by microCT. Mice injected daily with corn oil vehicle containing 5% DMSO combined with CTX treatment served as control.

4.2.2 Histology

Following microCT analysis, muscle tissues were isolated and fixed in methanol and paraffin embedded. For histology, sections (9 μm thick) were collected on ColorFrost Plus microscope slides (ThermoFisher Scientific, Waltham, MA, USA) and dried overnight. Hematoxylin and Eosin (H&E), Alizarin Red, and Safranin-O staining were performed according to routine protocols. Images were taken using a CKX41 microscope (Olympus, Tokyo, Japan) equipped with a DFC 3200 camera (Leica, Wetzlar, Germany).

For immunofluorescence staining, tissue sections were decalcified in 0.5 M ethylenediaminetetraacetic acid (EDTA) for 1 hour and blocked in 10% bovine serum albumin for 10 min. Sections were incubated in primary antibodies against platelet-derived growth factor receptor α (PDGFRα) (AF1062, R&D Systems, Minneapolis, MN, USA) and bone morphogenetic protein-7 (BMP-7) (ab56023; abcam, Cambridge, MA, USA) overnight at 4 °C. On the second day, sections were incubated with secondary antibodies against goat IgG (ab150130; abcam) and rabbit IgG (ab150077; abcam) at room temperature for 1 h. After washing, the slides were mounted with 4′,6-diamidino-2-phenylindole (DAPI)-containing mounting medium (Vector Laboratories Inc., Burlingame, CA, USA). Slides were viewed using an inverted IX81 microscope (Olympus) equipped with a Retiga EXi cooled CCD camera (Qimaging, Surrey, BC, Canada) and MetaMorph software (Molecular Devices, San Jose, CA, USA).

4.2.3 Blood sample and muscle tissue collection

Blood sample was collected by cardiac puncture at the time of animal sacrifice. Mice were sacrificed at Day 3, 7, and 14 time points in (1) CTX+DEX co-treatment group; (2) CTX treatment alone group; and (3) DEX treatment alone group. In each group, untreated mice served as Day 0 control, and all data in one group were normalized to its Day 0 control. Blood was collected into an EDTA anticoagulant tube and centrifuged. Supernatant was collected for plasma protein analysis using commercial enzyme-linked immunosorbent assay (ELISA) kits purchased from abcam.

Following blood sample collection, muscle tissue samples were also collected at Day 3, 7, and 14 time points in the above-mentioned groups, with untreated mice serving as Day 0 control. Briefly, calf muscles from left and right sides were isolated and immediately snap-frozen in liquid nitrogen for later tissue RNA and protein extraction. Muscle tissue gene expression was determined by quantitative real-time reverse-transcription polymerase chain reaction (qRT-PCR) analysis and protein analysis by ELISA.

4.2.4 qRT-PCR analysis

Muscle tissues or cells were lysed in QIAzol Lysis Reagent and isolated using the RNeasy Mini Kit according to the manufacturer's instructions (QIAGEN, Hilden, Germany). RNA was then converted to cDNA using the SuperScript™ IV First-Strand Synthesis System (Invitrogen, Carlsbad, CA, USA). Quantitative real-time PCR was performed with a StepOne Plus Realtime PCR system using PowerUp™ SYBR® Green Master Mix (Applied Biosystems, Foster City, CA, USA). The relative level of gene expression was calculated using the 2-delta delta Ct

method. Primer sequences for actin, runt-related transcription factor 2 (*Runx2*), bone sialoprotein I (*Bsp1*), osterix (*Osx)*, PAI-1 (*Pai1)*, TGF-β1 (*Tgfb1)*, alkaline phosphatase (*Alp*), osteocalcin (*Ocn*) are listed in Table 1.

4.2.5 *In vivo* supplementation of TGF-β1

CTX and DEX treatments were the same as described above. For *in vivo* supplementation of TGF-β1, mice were subcutaneously injected with 100 μg/kg mouse TGF-β1 recombinant protein (ThermoFisher Scientific) daily for 7 days. Mice injected with saline served as control. At Day 7 and Day 14, mice were euthanized for microCT analysis of ectopic mineralization. Identical scan setting as described above was employed. Blood samples and muscle tissue samples were also collected for protein and gene expression analysis.

4.2.6 *In vitro* osteogenesis induction in muscle-derived stromal cells

To determine the effect of TGF-β1 on osteogenic differentiation of muscle-derived stromal cells (MDSCs) *in vitro*, MDSCs were harvested from another cohort of mice according to a previously described protocol [115]. MDSCs at passage 3 were used to perform the experiment. Briefly, 0.2 million cells were seeded into each well in a 6-well plate, and were maintained in high-glucose Dulbecco's Modified Eagle's Medium (GIBCO, Gaithersburg, MD, USA) supplemented with 20% fetal bovine serum (Gemini Bio Products, West Sacramento, CA, USA) and 1% penicillin/streptomycin (GIBCO). On the following day, cells were treated with either 50 ng/ml BMP-7 (R&D Systems) or 50 ng/ml BMP-7 plus 20 ng/ml TGF-β1 (R&D Systems) for three days. On culture Day 4, MDSCs were collected for PCR analysis of osteogenic marker gene

expression. MDSCs cultured in growth medium without BMP-7 and TGF-β1 treatment served as control.

4.2.7 Statistical analysis

All data were expressed as mean ± SD. N $\geqslant$ 4 for each group of *in vivo* animal experiments. Student's *t*-test was used to make comparisons between two groups, and one-way or two-way ANOVA followed by the Tukey's multiple comparisons test was used for comparisons of three or more groups. Statistical significance (*) was considered at $p < 0.05$. Statistical analyses were performed using GraphPad Prism 7.0 software (GraphPad Software Inc., LaJolla, CA, USA).

4.3 RESULTS

4.3.1 Glucocorticoid treatment stimulated ectopic mineralization

To determine the role of glucocorticoids in DC/HO pathogenesis, DEX was administered following muscle injury induced by CTX. microCT imaging and analysis showed that combined CTX and DEX treatment caused a significant amount of mineralization in the calf muscles of the animal, while either of the treatment alone could not result in ectopic mineralization (Figure 16A-C). Ectopic mineralization was found evident at Day 7 time point post muscle injury, and there was no significant change in bone volume until Day 21 (Figure 16D). However, there was a significant increase in bone mineral density, suggesting an active remodeling process progressing over the intervening time period (Figure 16D). We initially used a lower 1 mg/kg DEX dose and

found that ectopic mineralization could only be observed in about 40% of the treated animals, whereas 10 mg/kg DEX treatment stimulated ectopic mineralization in ~90% of the animals. Among all the animals with ectopic mineralization, an obvious trend of larger bone volume was found in higher DEX dose group compared with lower DEX dose group, and the lower DEX dose group appeared to show a more rapid clearance of mineralization, as decreased bone volume and bone mineral density was found at Day 21 time point in the 1 mg/kg DEX dose group (Figure 16D). Mice were monitored daily for reactivity and body weight. There were no signs of discomfort in mice with DEX treatment at our current doses and body weight was not affected by the treatment (Supplemental Figure 3).

We also tested another more physiological relevant glucocorticoid, corticosterone, which is the major glucocorticoid in rodents [154]. We demonstrated that combined CTX and corticosterone treatment elicited the same effect as combined CTX and DEX treatment (Supplemental Figure 4). There was no significant difference between the lower 20 mg/kg and the higher 40 mg/kg corticosterone dose treatment groups at Day 7 in terms of bone volume and density (Supplemental Figure 4). Treatment with corticosterone seemed to achieve a higher positive rate compared with DEX treatment. However, since there is no commercial available corticosterone solution for injection and given the low solubility of corticosterone, a considerable amount of corn oil vehicle needed to be used, which could accumulate subcutaneously with repeated daily injection, thus compromising the long-term administration of corticosterone. Therefore, we chose to use DEX injection for the following study. We also demonstrated that repeated daily subcutaneously injection was not likely to cause sufficient stress in itself to induce ectopic mineralization, given that daily vehicle injection combined with CTX treatment did not result in ectopic mineralization (Supplemental Figure 4).

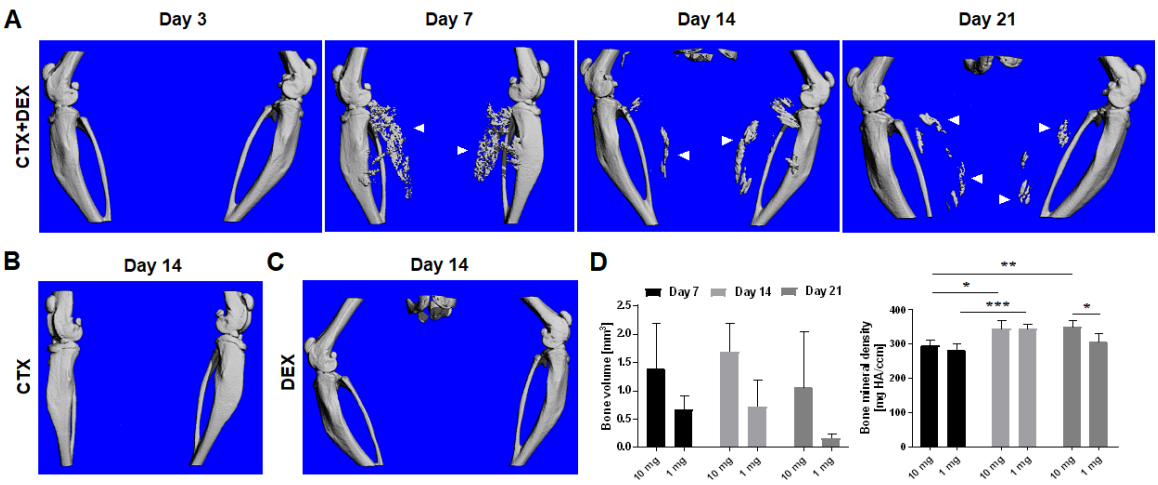

Figure 16. Glucocorticoid treatment stimulated ectopic mineralization

(A) microCT imaging illustrating the time course of ectopic mineralization formed in CTX+DEX co-treatment group. Arrowheads indicate ectopic mineralization. **(B)** microCT imaging demonstrating that CTX treatment alone did not result in ectopic mineralization. **(C)** microCT imaging demonstrating that DEX treatment alone did not result in ectopic mineralization. **(D)** microCT analysis of bone volume and bone mineral density in 10 mg/kg and 1 mg/kg CTX+DEX co-treatment groups. (*, $p < 0.05$; **, $p < 0.01$; ***, $p < 0.001$; $n = 4$)

4.3.2 Glucocorticoid treatment caused impaired muscle regeneration and enhanced osteogenesis

Histology revealed severe inflammatory cell infiltration into the CTX-injured muscle tissue at the Day 3 time point. In the CTX administration alone group, inflammatory response was efficiently resolved in two weeks as regenerated muscle fibers with centrally located nuclei were found as early as Day 7 (Figure 17A). However, such process was not found in the CTX+DEX co-treatment group. Instead, massive calcification deposits were found in the degenerating muscle fibers and inflammatory cells were still present at the Day 14 time point (Figure 17A&B). Increased expression of osteogenic marker genes, including *Runx2*, *Bsp1*, and *Osx*, was also observed in CTX+DEX co-treatment group, suggesting enhanced osteogenesis accompanying

impaired muscle regeneration (Figure 17C). In rare cases, DC can progress into HO within 2 weeks through an endochondral ossification process as demonstrated by positive Safranin-O staining (Supplemental Figure 5). In comparison, DEX treatment alone did not appear to affect muscle morphology nor the expression of osteogenic marker genes during the 14-day time course (Figure 17A-C).

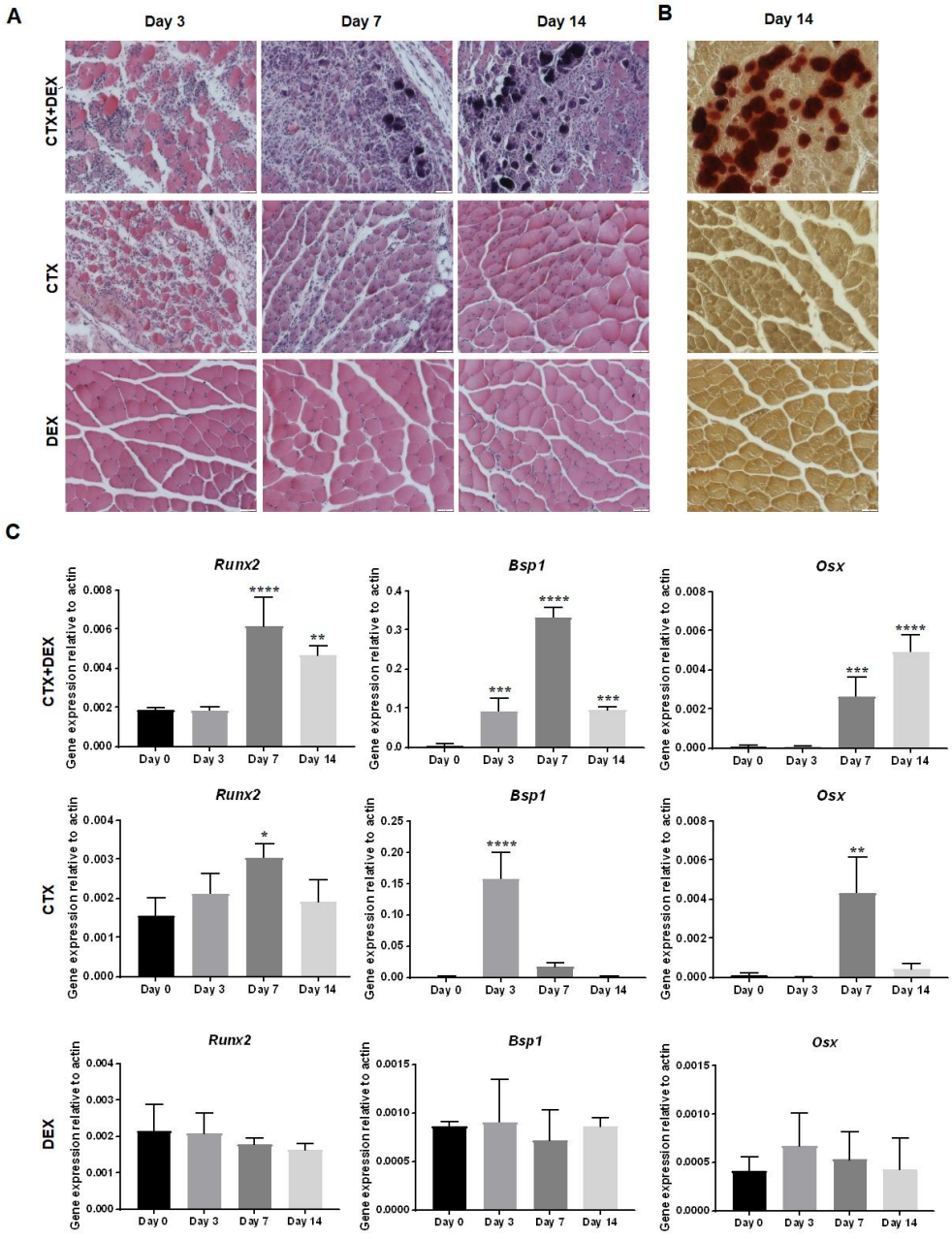

Figure 17. Glucocorticoid treatment caused impaired muscle regeneration and enhanced osteogenesis

(A) H&E staining showing the muscle regeneration processes, in which impaired muscle regeneration was observed in CTX+DEX co-treatment group. Bar = 50 μm. **(B)** Alizarin Red staining showing massive calcium depositions found in CTX+DEX co-treatment group. Bar = 50 μm. **(C)** PCR analysis of osteogenic marker gene expression in muscle tissue. Significant upregulation of expression of osteogenic marker genes (*Runx2*, *Bsp1*, *Osx*) was found in CTX+DEX co-treatment group over the 14-day time course. Gene expression levels are normalized to that of *Actin.* (*, $p < 0.05$; **, $p < 0.01$; ***, $p < 0.001$; ****, $p < 0.0001$; $n = 4$).

Increased PAI-1 level, an indicator of impaired muscle regeneration, was observed in CTX+DEX co-treatment group compared with CTX treatment alone group, both systemically (plasma) and locally (muscle tissue lysates) (Figure 18A&B). In addition, muscle production of PAI-1 was increased in CTX+DEX co-treatment group compared with CTX treatment alone group (Figure 18C). DEX treatment alone did not affect plasma or muscle tissue PAI-1 level (Figure 18A-C).

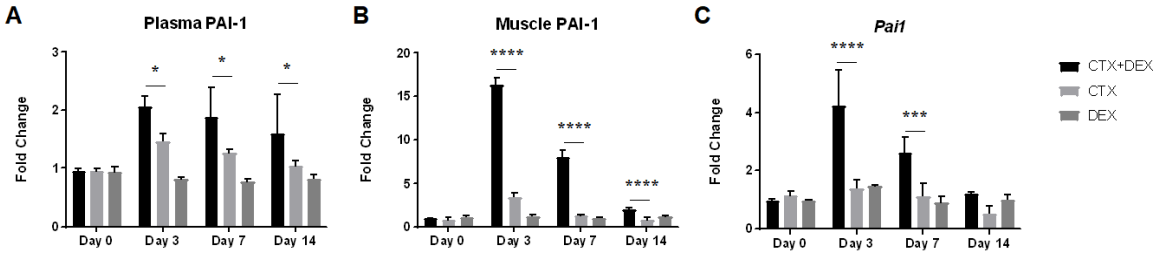

Figure 18. Glucocorticoid treatment caused increased PAI-1 level in CTX-injured muscle

(A) Blood sample analysis of PAI-1 level. CTX+DEX co-treatment increased plasma PAI-1 level. (*, $p < 0.05$; $n = 4$) **(B)** Muscle tissue sample analysis of PAI-1 level. CTX+DEX co-treatment increased muscle PAI-1 level. (****, $p < 0.0001$; $n = 4$). **(C)** PCR analysis of *Pai1* expression in muscle tissue. CTX+DEX co-treatment increased muscle *Pai1* expression. (***, $p < 0.001$; ****, $p < 0.0001$; $n = 4$). In each analysis, PAI-1 levels are normalized to Day 0 untreated control.

4.3.3 Lowered circulating TGF-β1 level correlated with DC formation

The above findings prompted us to next examine the circulating level of plasmin, the downstream target of PAI-1. ELISA results showed that plasmin level decreased over time in the CTX+DEX co-treatment group, while remaining relatively constant in the CTX treatment alone or the DEX treatment alone groups (Figure 19A). Accompanying the decreased plasmin level, muscle fibrin level was found to be significantly increased in the CTX+DEX co-treatment group (Figure 19B). At Day 3, a slight decrease in fibrin level was observed in the DEX treatment

alone group, and a significant increase in fibrin level was observed in the CTX treatment alone group (Figure 19B). However, muscle fibrin level in these two groups returned to baseline after 7 days (Figure 19B).

To explore the functional relationship between lowered plasmin level and DC/HO formation, we checked the expression of TGF-β1, a downstream target of plasmin. Our results showed that DEX treatment in the course of CTX-induced muscle injury resulted in a significant reduction in circulating TGF-β1 level, as well as reduced *Tgfb1* gene expression in muscle tissue as demonstrated by PCR analysis (Figure 19C&D). In comparison, CTX treatment alone did not affect plasma TGF-β1 level nor muscle *Tgfb1* gene expression, while DEX treatment alone decreased TGF-β1 level as well as muscle *Tgfb1* gene expression, although not in a statistically significant manner (Figure 19C&D).

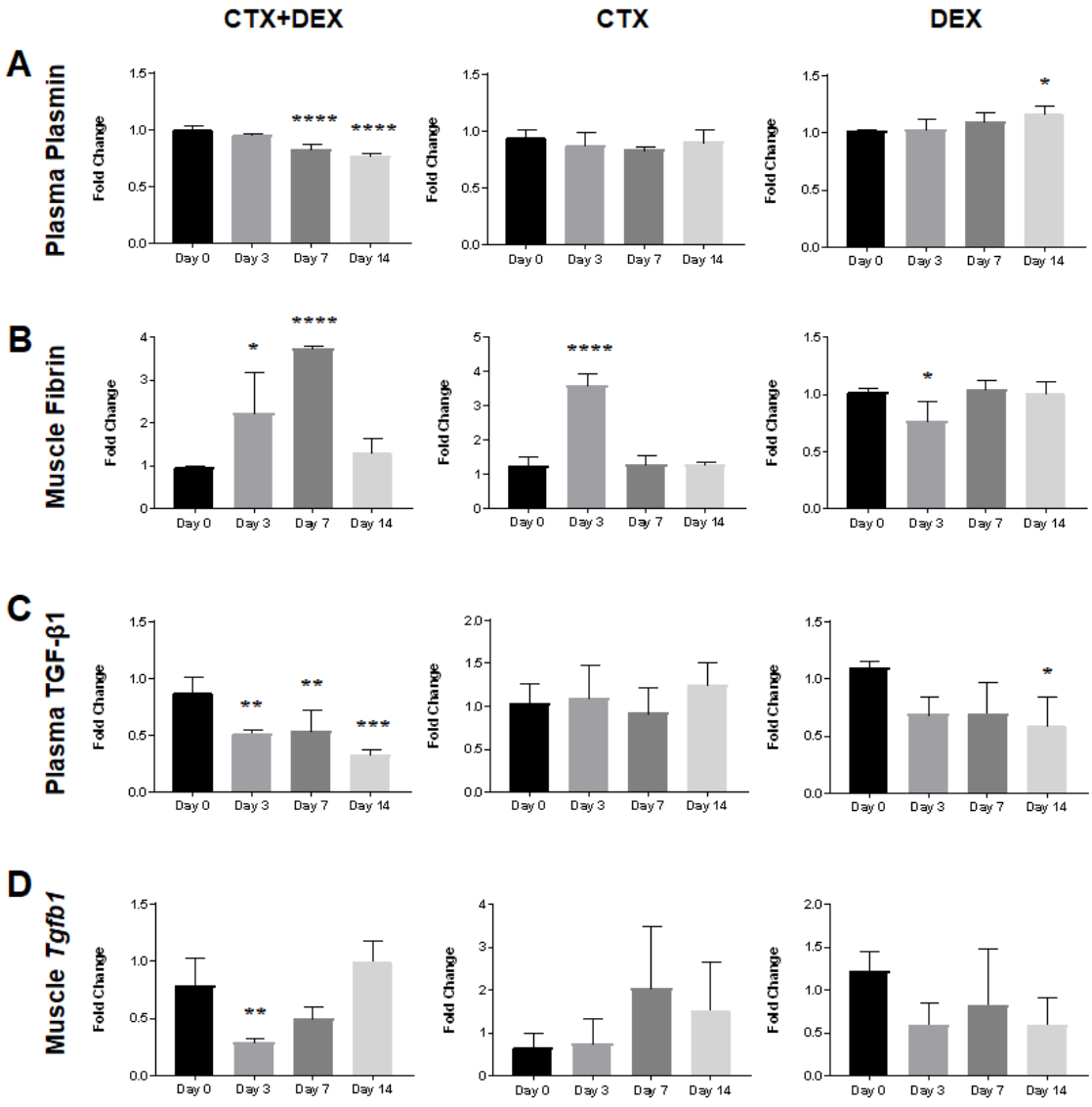

Figure 19. Glucocorticoid treatment caused decreased circulating TGF-β1 level

(A) Plasma levels of plasmin. CTX+DEX co-treatment caused a significant decrease in plasma plasmin level. (*, $p < 0.05$; ****, $p < 0.0001$; $n = 4$). **(B)** Fibrin levels in muscle tissue. CTX+DEX co-treatment caused a significant increase in muscle fibrin level. (*, $p < 0.05$; ****, $p < 0.0001$; $n = 4$). **(C)** TGF-β1 levels in plasma. CTX+DEX co-treatment caused a significant decrease in plasma TGF-β1 level. (*, $p < 0.05$; **, $p < 0.01$; ***, $p < 0.001$; $n = 4$). **(D)** PCR analysis of *Tgfb1* gene expression in muscle tissue. CTX+DEX co-treatment caused a significant decrease in muscle *Tgfb1* expression. (**, $p < 0.01$; $n = 4$).

4.3.4 TGF-β1 supplementation inhibited DC formation

To assess the functional involvement of TGF-β1 in DC/HO pathogenesis, recombinant mouse TGF-β1 protein was systemically administered for 7 days in addition to CTX+DEX co-treatments. Compared to saline treatment, TGF-β1 treatment significantly reduced bone volume (Saline: 1.385 ± 0.3251 mm^3; TGF-β1: 0.3377 ± 0.1832 mm^3) at Day 7 (Figure 20A&B). No qualitative differences in bone mineral density were found between saline treatment group and TGF-β1 treatment group (Saline: 297.3 ± 5.699 mg HA/ccm; TGF-β1: 285.1 ± 12.78 mg HA/ccm) at Day 7 (Figure 20A&B). Decreased osteogenic marker gene expression was also observed upon TGF-β1 treatment, suggesting suppression of osteogenesis (Figure 20C). Interestingly, the effect of 7-day TGF-β1 treatment persisted, as significantly reduced bone volume (Saline: 2.568 ± 1.052 mm^3; TGF-β1: 0.2757 ± 0.09123 mm^3) as well as reduced bone mineral density (Saline: 330.6 ± 9.395 mg HA/ccm; TGF-β1: 297.3 ± 8.944 mg HA/ccm) (Supplemental Figure 6) were seen at least until Day 14.

Given the known upregulation of PAI-1 production by TGF-β1, we examined the influence of TGF-β1 supplementation on plasma and muscle PAI-1 level. TGF-β1 supplementation significantly increased plasma and muscle tissue PAI-1 levels (Figure 20D&E), possibly correlated with increased DC formation. However, eventually reduced bone volume was observed with TGF-β1 supplementation (Figure 20A&B), suggesting that TGF-β1 could be the effector of the fibrinolytic system to regulate DC formation (Figure 20F).

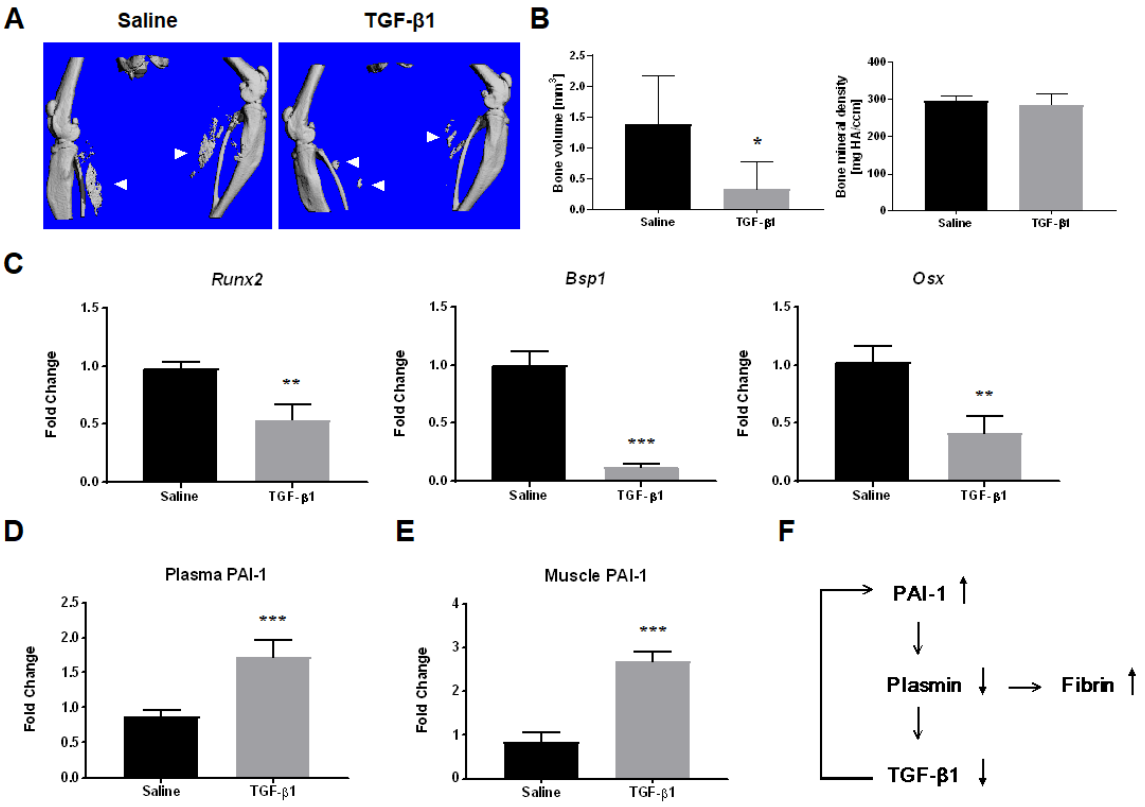

Figure 20. TGF-β1 supplementation inhibited DC formation

(A) microCT imaging demonstrating reduced bone volume with TGF-β1 supplementation. Arrowheads indicate ectopic mineralization. **(B)** microCT analysis of bone volume and bone mineral density with and without TGF-β1 supplementation (*, $p < 0.05$; $n = 6$). **(C)** PCR analysis of osteogenic marker gene expression in muscle tissue with and without TGF-β1 supplementation. Significant downregulation of osteogenic marker gene expression was found with TGF-β1 supplementation. (**, $p < 0.01$; ***, $p < 0.001$; $n = 3$). **(D)** *In vivo* TGF-β1 supplementation significantly increased plasma PAI-1 level. (***, $p < 0.001$; $n = 3$). **(E)** *In vivo* TGF-β1 supplementation significantly increased muscle tissue PAI-1 level. (***, $p < 0.001$; $n = 3$). **(F)** Schematic of negative feedback loop between PAI-1 and TGF-β1.

4.3.5 Possible mechanism of TGF-β1 in regulating DC formation

We have recently shown that muscle injury promotes HO by stimulating local BMP-7 production [155]. As TGF-β1 could act to antagonize BMP-7 activity by competing for their downstream co-Smad4 signaling component for nuclear signal transduction, we hypothesized that the reduction in circulating TGF-β1 level would attenuate the inhibitory effect of TGF-β1 on BMP-7, thereby promoting BMP-7-induced osteogenesis. Interestingly, we observed high cell density in the local tissue surrounding the calcium deposits, suggesting active tissue remodeling (Figure 21A). In addition, a great number of cells positive for PDGFRα, a marker of mesenchymal stem cells, were observed near the calcium deposits, suggesting the participation of muscle resident stem cells in DC formation and remodeling (Figure 21B). Furthermore, we also detected strong BMP-7 immunostaining surrounding the calcium deposits, suggesting that the muscle resident stem cell population could be under the regulation of BMP-7 signal (Figure 21B). This possible mechanism was tested *in vitro* using cultured MDSCs treated with BMP-7 and TGF-β1. Our results showed that *in vitro* supplementation of TGF-β1, at a concentration similar to that in plasma, almost completely blocked BMP-7-induced osteogenesis, evidenced by the marked downregulation of osteogenic marker gene expression (Figure 21C), suggesting that TGF-β1 could negatively regulate osteogenesis, specifically that induced by BMP-7.

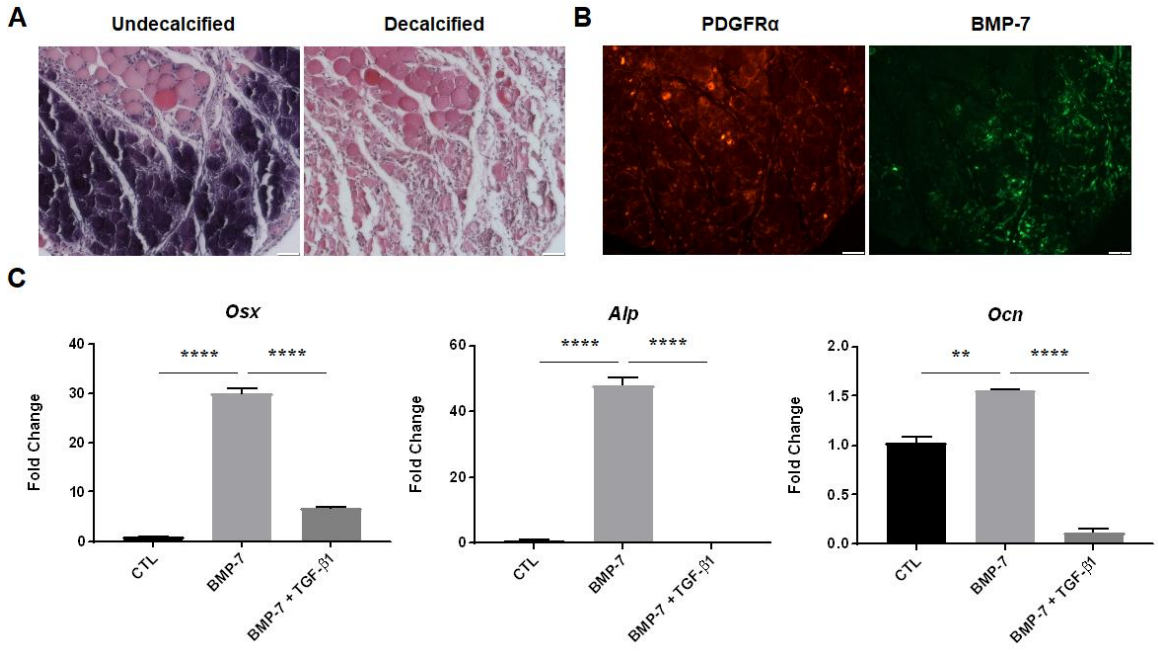

Figure 21. Cellular effects of TGF-β1 supplementation on glucocorticoid mediated osteogenesis *in vivo* and *in vitro*

(A) H&E staining of undecalcified and decalcified muscle tissue obtained 7 days following CTX+DEX co-treatment. High cell density was found surrounding the calcium deposits. Bar = 50 μm. **(B)** Immunofluorescence staining showing the PDGFRα (red) positive cells and BMP-7 (green) positive cells surrounding the calcium deposits. Bar = 50 μm. **(C)** PCR analysis of osteogenic marker gene expression in MDSCs treated with BMP-7 alone or with BMP-7 and TGF-β1. *In vitro* TGF-β1 supplementation almost completely blocked BMP-7-induced osteogenesis in MDSCs. (**, $p < 0.01$; ****, $p < 0.0001$; $n = 3$).

4.4 DISCUSSION AND CONCLUSION

In this study, we sought to determine the role of glucocorticoids in DC/HO formation following muscle injury. We have previously shown in a BMP-2-induced HO mouse model that BMP-7 production by resident cells following muscle injury promotes HO [155]. However, muscle

injury alone, although generating a pro-osteogenesis environment, seldom led to HO formation [155]. This suggests that other factors are required for ectopic mineralization [108]. In our previous study, a strong osteoinductive signal, i.e., supraphysiological dose of BMP-2, was present for inducing bone formation. However, under most physiological conditions, such strong osteoinductive signals are usually not present. Recently, a novel notion has been proposed for the mechanism of ectopic mineralization, namely instead of the presence of a strong osteoinductive signal, protective factors may be removed under pathophysiological conditions, allowing calcium deposition to take place [112]. In this study, we set out to explore, in addition to muscle injury, what the other factors are that may affect DC/HO formation.

We have chosen to focus on glucocorticoids as excessive endogenous glucocorticoid production has always been found following severe trauma, which coincides with increased HO incidence. In this study, we treated animals with high dose DEX following muscle injury, and our results showed that DEX treatment together with CTX-induced muscle injury resulted in a significant amount of DC in muscle (Figure 16A), while neither of the treatment alone could cause DC formation (Figure 16B&C). This DEX-induced response is dose-dependent response, evidenced by the higher positive rate and larger bone volume in the higher dose, 10 mg/kg DEX group compared to the lower dose 1 mg/kg DEX group (Figure 16D). In addition, the higher DEX dose presented sustained calcification, while in the lower DEX dose group, DC quickly diminishes over time (Figure 16D). Histologically, CTX+DEX co-treatment leads to impaired muscle regeneration (Figure 17A), which appears to lead to DC and enhanced osteogenesis (Figure 17B&C). PAI-1 level, as an indicator of impaired muscle regeneration, was found increased in CTX+DEX co-treatment group as well (Figure 18A-C). Taken together, these data

suggest that glucocorticoids stimulate DC formation, possibly by interfering with muscle regeneration.

We next sought to explore the mechanism responsible for glucocorticoid-mediated promotion of DC/HO formation. The fibrinolytic system has recently been reported to be associated with DC/HO formation, in which plasmin protects against muscle injury-induced DC [112]. We observed that PAI-1, a key regulatory component in the fibrinolytic system, is significantly upregulated upon CTX+DEX co-treatment, i.e., the group with DC formation (Figure 18A-C). The action of PAI-1, a serine protease inhibitor which inhibits tissue plasminogen activator and urokinase plasminogen activator, results in decreased plasmin level and thus increased fibrin accumulation (Figure 20F). Interestingly, decreased circulating plasmin level and increased muscle fibrin accumulation are also found in the CTX+DEX co-treatment group (Figure 19A&B), suggesting that glucocorticoids may indeed play a role as an upstream regulator of the fibrinolytic system in facilitating DC/HO formation. The plasmin substrate that is responsible for DC/HO formation needs to be identified. Recent reports by Schoenecker's group show that although delayed fibrin clearance has been associated with impeded macrophages invasion and subsequent enhanced osteogenesis, knocking down fibrinogen has failed to rescue low plasmin level-induced DC/HO formation [108, 112]. These authors suggest a number of plasmin substrates, including parathyroid hormone, fibroblast growth factor 23 and vitamin D, which are important hormones in regulating calcium and phosphate metabolism. However, given the definition of DC, which is calcium deposition under physiologically normal serum calcium and phosphate conditions, we are more inclined to believe that the plasmin substrate should be more of an injury-related factor.

TGF-β1 is a well-known target of plasmin, which releases active TGF-β1 from its latency-associated peptide [156]. TGF-β1 is also the strongest inducer of PAI-1 [157]. When active TGF-β1 level increases, elevated PAI-1 level prevents further increase in TGF-β1 level. This negative feedback mechanism maintains homeostasis of the fibrinolytic system, although it may exhibit certain level of hysteresis [158]. In this study, we demonstrated that increased PAI-1 level in the CTX+DEX co-treatment group is associated with decreased plasmin and TGF-β1 level (Figure 19A&C). Since TGF-β1 is also a key factor involved in muscle regeneration and pathological calcification, we hypothesize that TGF-β1 could be the downstream effector of the fibrinolytic system to regulate DC formation. We tested our hypothesis by *in vivo* supplementation of recombinant TGF-β1 protein, which led to significantly reduced bone volume as well as decreased osteogenic marker gene expression (Figure 20A-C). We also showed that TGF-β1 supplementation significantly increased plasma and muscle tissue PAI-1 level, suggesting that the treatment is effective (Figure 20D&E). However, increased PAI-1 level did not correlate with increased bone volume, further suggesting that this negative feedback loop may be initiated from PAI-1, with TGF-β1 as the effector (Figure 20F). Glucocorticoids might directly affect TGF-β1 production independent of PAI-1 regulation as we and others have demonstrated [159], but the net effect of glucocorticoids on TGF-β1 is still downregulation of its expression (Figure 19D).

To explore the underlying mechanism by which lowered TGF-β1 level correlates with enhanced osteogenesis, we performed *in vitro* TGF-β1 supplementation experiment using MDSCs, resident progenitor cells in muscle found both in mice and human [56, 81, 115]. Our results show that *in vitro* TGF-β1 supplementation to MDSC cell culture almost completely blocks BMP-7-induced osteogenesis, suggesting that TGF-β1 may play an inhibitory role on

MDSC osteogenesis (Figure 21C). MDSCs are the putative cell source responsible for HO formation [56, 82], and we have demonstrated here that a large number of PDGFRα positive cells, likely MDSCs, are present near the calcium deposits (Figure 21B), and participating in the process. We speculate that TGF-β1 at physiological level could be the protective factor that inhibits osteogenic differentiation of MDSCs. However, when TGF-β1 level is lowered under pathological conditions, muscle injury-induced BMP-7 upregulation could promote MDSC osteogenesis given that the protective factor(s) has been removed. In this study, we have demonstrated that glucocorticoid excess could be one of the reasons for lowered circulating TGF-β1 level. There have also been some controversies regarding the role of TGF-β1 in DC/HO formation [99]. We speculate that this is due to the different pathways leading to bone formation, namely endochondral ossification and intramembranous ossification. Endochondral ossification progresses through a cartilaginous precursor stage which requires TGF-β signaling for chondrogenesis, whereas in cases of intramembranous ossification, TGF-β signaling exerts a direct inhibitory effect on stem cell osteogenesis [160]. It is also well known that TGF-β1 is a highly pleiotropic factor and has a paracrine effect in immune modulation [161]. The limitation of this study is that we have not tested the effect of lowered circulating TGF-β1 level on the immune system, which will be our future research direction.

In summary, our study demonstrates that glucocorticoid excess impairs muscle regeneration and promotes DC/HO, and that TGF-β1 could be a key factor in modulating this process. We also tested this postulation in a mouse amputation model, where we did below-knee amputation to right leg of the animal and gave CTX injection to the calf muscle of left unamputated leg. We showed that under a stress condition, i.e. an amputation, CTX-induced muscle injury could easily result in DC/HO formation (3 out of 4 animals) within 2 weeks

(Figure 22). Plasma analysis of corticosterone, PAI-1, plasmin, and TGF-β1 at different time points will be the next step to test our hypothesis. These findings shed light on the understating of the pathogenesis of trauma-induced DC/HO.

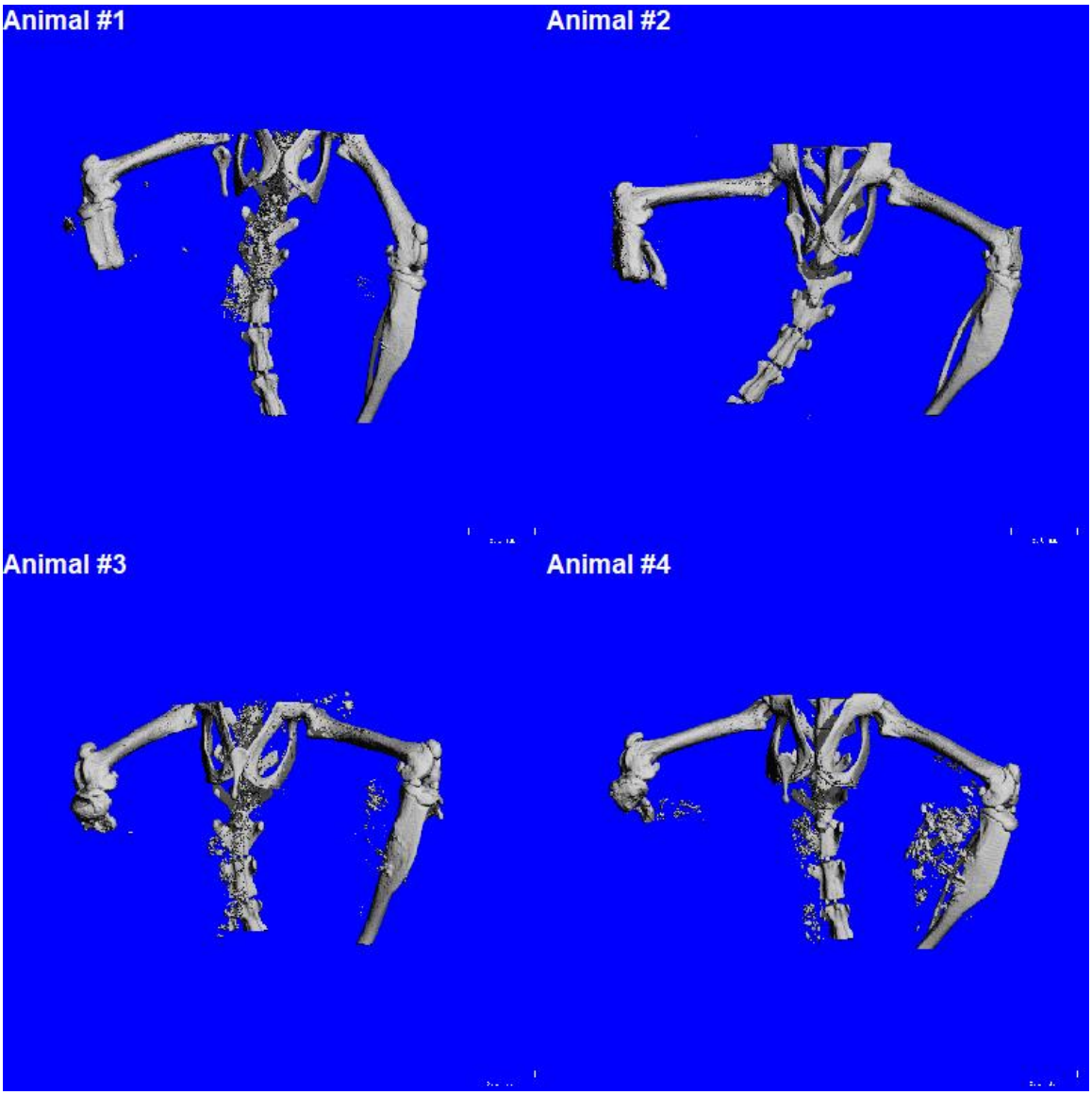

Figure 22. DC/HO formation in an amputation plus muscle injury mouse model

Representative microCT images showing DC/HO formation in #1,3,4 animals.

5.0 ROLE OF MUSLCE TISSUE DEATH IN HO PATHOGENESIS

5.1 INTRODUCTION

In order to preserve the residual limb function in blast-injured patients, the aggressive limb salvage strategy has been adopted [73]. This strategy generally advocates that amputation should be viewed as a reconstructive approach instead of an ablative one, and that residual limb length should be maintained as well as functional joint level. It has therefore often led to a final amputation level within zone of injury to preserve as much tissue as possible [106]. However, it has been noted that there is a significantly higher prevalence of HO in the residual limbs of combat-injured patients if a final amputation was performed within zone of injury compared to that was proximal to zone of injury [73]. This aggressive limb salvage strategy on one hand maximizes the function of residual limb, while on the other hand may increase the possibility of retaining nonviable tissue within the body [162]. Nonviable tissue may cause local inflammatory response that would trigger HO development. Indeed, it has been previously demonstrated that debridement of nonviable tissues diminishes HO formation [163]. In support of this notion, we have also found in our mouse blast-amputation model that minimized debridement led to a higher incidence of HO. However, the exact underlying mechanism for this observation is still unclear. Given that HO is always located distant from the injury zone/amputation site in our

mouse blast-amputation model, we hypothesized that dead muscle tissue elicits a systemic effect that facilitates HO formation.

This current study aims to elucidate the role of dead muscle tissue in HO pathogenesis by implanting devitalized muscle tissue into healthy recipient mouse. Our laboratory has previously characterized the cytokine expression in human blast-traumatized skeletal muscle tissue obtained during the debridement of high-energy wartime extremity wounds, and found that dead muscle tissue elicited an strong immune response with increased cytokine expression related to fibrosis, especially elevated TGF-β1 signal [164]. In this study, we hypothesized that immune response towards dead muscle tissue consumes TGF-β1 locally resulting in lowered circulating TGF-β1 level, which will facilitate muscle injury-induced DC/HO formation.

5.2 METHODS

5.2.1 Devitalized muscle tissue muscle pouch implantation

Muscle tissue was harvested from C57BL/6J mouse background and freeze-thawed for three times to achieve devitalization. Muscle pouch implantation was performed according to a previous described surgical procedure [165]. Briefly, animal was first anesthetized by Isoflurane inhalation, the inner thigh area was removed of hair and was sterilized broadly with ethanol. Then mouse was positioned onto the operative field facing up and a 0.5-cm longitudinal incision was made beneath the femoral artery. Muscle pouch was created by blunt dissection of muscle fibers in gracilis muscle. Next, a piece of 50 mg devitalized muscle tissue was placed into the exposed muscle pouch. Muscle fibers were then closed by tension, and skin was closed with 4-0

nylon sutures. Animal received a 3-day course of buprenorphine (0.05 mg/kg administered subcutaneously twice a day) for pain management. For muscle pouch implantation with CTX injection group, 100 μL 10 μM CTX was injected into biceps femoris muscle one day before devitalized muscle tissue muscle pouch implantation. Sham surgery was performed by cutting open the skin and exposing the muscle pouch but without devitalized muscle tissue implantation.

5.2.2 Blood sample collection and analysis

Blood sample was collected by cardiac puncture at the time of animal sacrifice. Mice were sacrificed at Day 3, Day 7, Day 14 time points with 4 mice in each of the following groups: untreated control group; CTX injection alone group; tissue implantation alone group; and CTX injection plus tissue implantation group. Blood was collected into the EDTA anticoagulant tube and centrifuged. Then, supernatant was collected and aliquoted for storage. Total TGF-β1 level and total plasmin (PLG) level were determined using commercial ELISA kits purchased from abcam biotechnology company.

5.2.3 Muscle tissue sample collection and analysis

Muscle tissues were collected at Day 3, Day 7, Day 14 time points as described above. Specifically, gracilis muscle with the devitalized muscle tissue implant was collected together as the inner thigh muscle group which reflects the local response induced by the dead muscle tissue; whereas biceps femoris muscle was collected as the outer thigh muscle group which reflects the systemic response induced by the dead muscle tissue. Muscle tissue phosphorylated Smad3 level

and fibrinogen level were determined using commercial ELISA kits purchased from abcam biotechnology company.

5.2.4 *In vitro* suppression of TGF-β signaling

To test the effect of suppressed TGF-β signaling on MDSCs osteogenesis *in vitro*, MDSCs were maintained for three days in CTX-injured muscle tissue derived CM with or without the supplementation of 10 μM TGF-β type I receptor inhibitor SB431542 (abcam). On culture Day 3, MDSCs were collected for the measurement of TGF-β signaling inhibition using a phosphorylated Smad3 ELISA kit as well as osteogenic marker gene expression by PCR.

5.2.5 Histology and immunohistochemistry

Muscle tissues were fixed in methanol and paraffin embedded, and routine H&E and Alizarin Red staining was performed on the tissue sections. Immunohistochemistry (IHC) was performed according to protocols described for the Vectastain Elite ABC Kit (Vector Laboratories, Burlingame, CA, USA). Primary antibody against PDGFRα was purchased from abcam biotechnology company.

5.3 RESULTS

5.3.1 Dead muscle tissue promoted DC formation

microCT imaging showed that combined devitalized muscle tissue implantation and CTX injection caused a significant amount of DC in 2 weeks while neither of them alone showed DC at implantation/injection sites (Figure 23). We also ruled out the effect of surgery on DC formation by showing that CTX injection plus sham surgery could not cause DC formation. Histology revealed that DC was always formed distant from the implant (Figure 24), indicating that dead muscle tissue did not calcify by itself but rather elicited a systemic effect that facilitates muscle injury-induced DC formation.

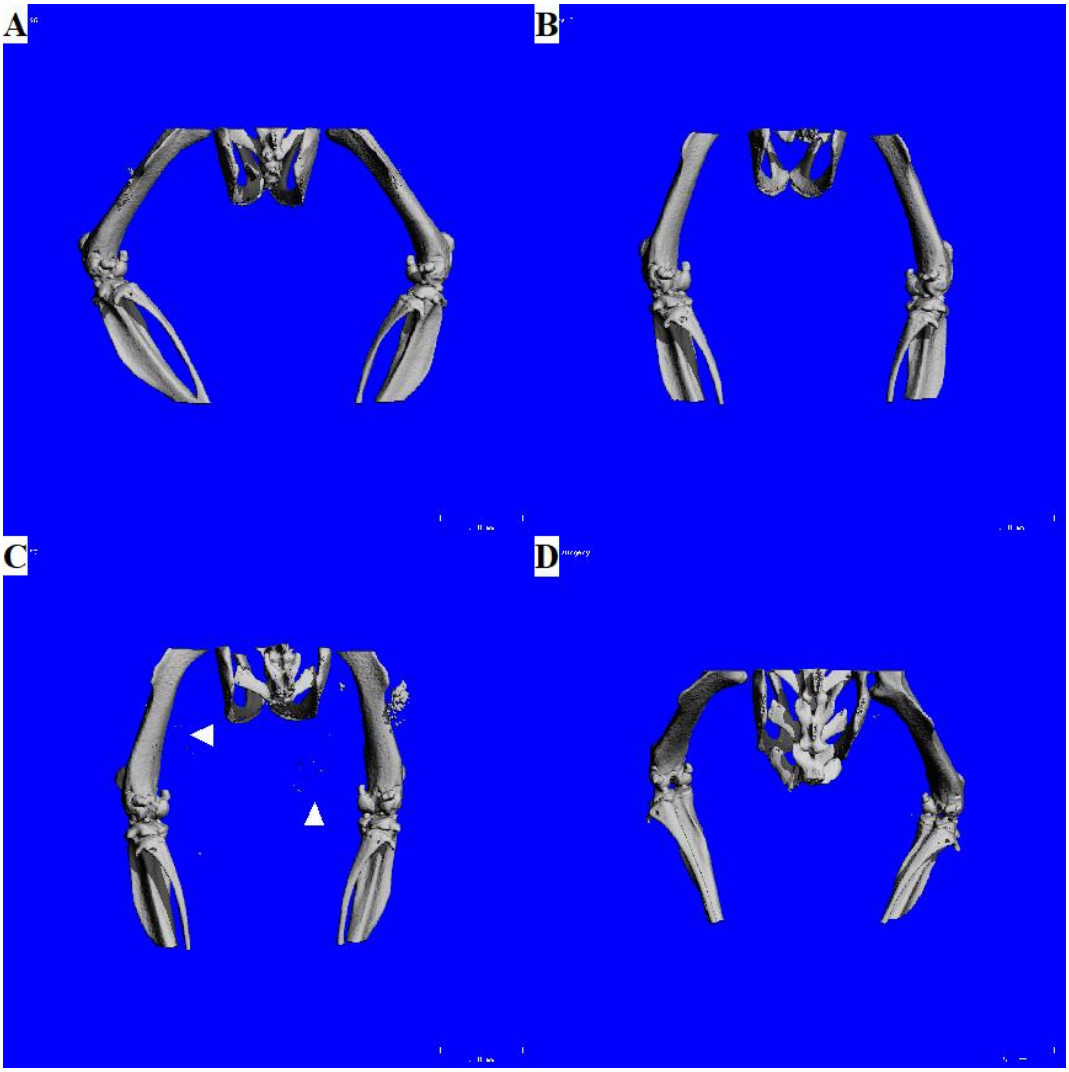

Figure 23. Dead muscle tissue promoted DC formation

microCT image showed DC formation in **(A)** CTX injection group; **(B)** tissue implantation alone group; **(C)** CTX injection plus tissue implantation group; **(D)** CTX injection plus sham surgery group. Arrowheads indicate ectopic mineralization.

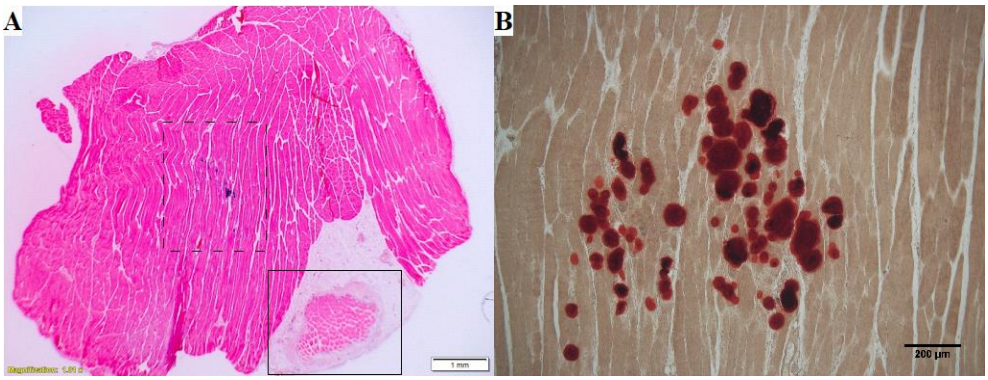

Figure 24. Location of DC relative to the implant

(A) H&E staining showing the location of the implant (black square) relative to the DC (dashed black square). **(B)** Alizarin Red staining demonstrating the calcium deposition. Scale bar = 200 µm

5.3.2 Implantation of dead muscle tissue caused a decrease in circulating TGF-β1 level

To determine how dead muscle tissue would affect DC formation, we collected blood sample from mice with or without devitalized muscle tissue implantation, and measured the total TGF-β1 level and total plasmin level at Day 3, Day 7, Day 14 time points after implantation. Significantly decreased plasma levels of TGF-β1 and plasmin were seen in mice with devitalized muscle tissue implant at later time points (Figure 25), which coincides with DC formation. We also confirmed the effect of the changes in circulating plasma protein levels of these proteins on muscle tissue by checking TGF-β1 and plasmin target protein expression on outer thigh muscle. We showed that starting from Day 7 time point onwards, decreased phosphorylated Smad3 level and increased fibrinogen level were seen in mice with devitalized muscle tissue implant in outer thigh muscle (Figure 26). This change in plasma and tissue protein level was not observed in sham operated animals (Supplemental Figure 7&8).

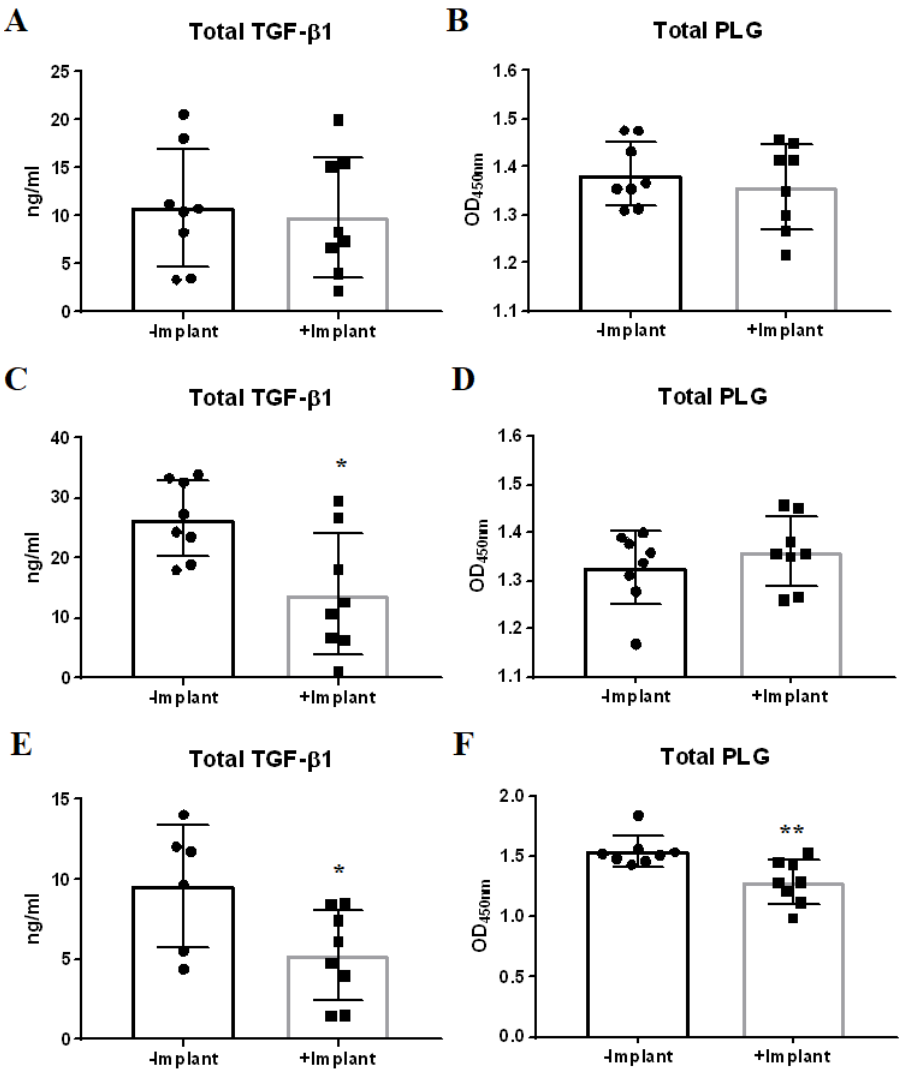

Figure 25. Implantation of dead muscle tissue caused a decrease in circulating TGF-β1 level

Blood sample analysis of total TGF-β1 and total PLG level in animal with or without dead muscle tissue implantation. **(A&B)** Day 3 time point. **(C&D)** Day 7 time point. **(E&F)** Day 14 time point.

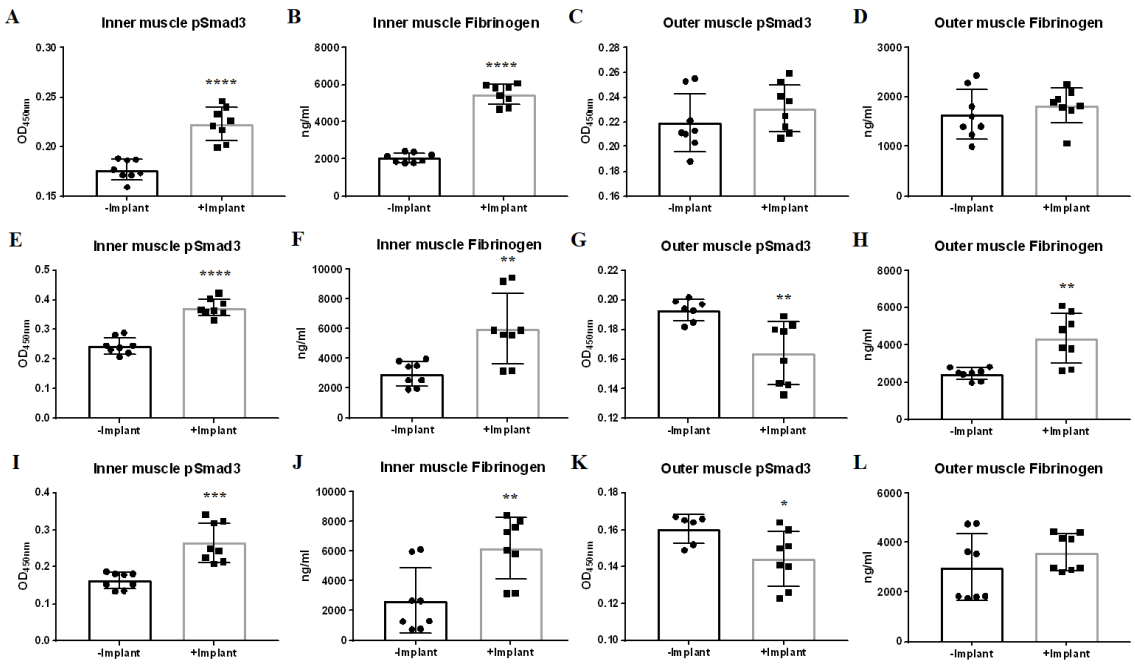

Figure 26. Effect of implantation of dead muscle tissue on muscle protein expression

Muscle tissue sample analysis of phosphorylated Smad3 level and fibrinogen level in animal with or without dead muscle tissue implantation. **(A-D)** Day 3 time point. **(E-H)** Day 7 time point. **(I-L)** Day 14 time point.

5.3.3 Local fibrotic response towards dead muscle tissue

We also collected muscle tissue sample from the inner thigh which reflects the local response induced by the dead muscle tissue. We found significant higher phosphorylated Smad3 level and fibrinogen level in mice with devitalized muscle tissue implant in the inner thigh muscle starting from Day 3 time point onwards (Figure 26). Histology confirmed this finding by showing the positive staining of phosphorylated Smad2 and fibrin(ogen) surrounding the implant, as well as collagen deposition typical of a fibrotic response (Figure 27). PCR analysis of the inner thigh muscle tissue demonstrated increased collagen type I expression as well as decreased *ALK5* expression but not increased TGF-β1 production (Figure 28A&B&C), suggesting that circulating

TGF-β1 is consumed locally. In addition, slightly decreased TGF-β1 production was found systemically (Figure 28E).

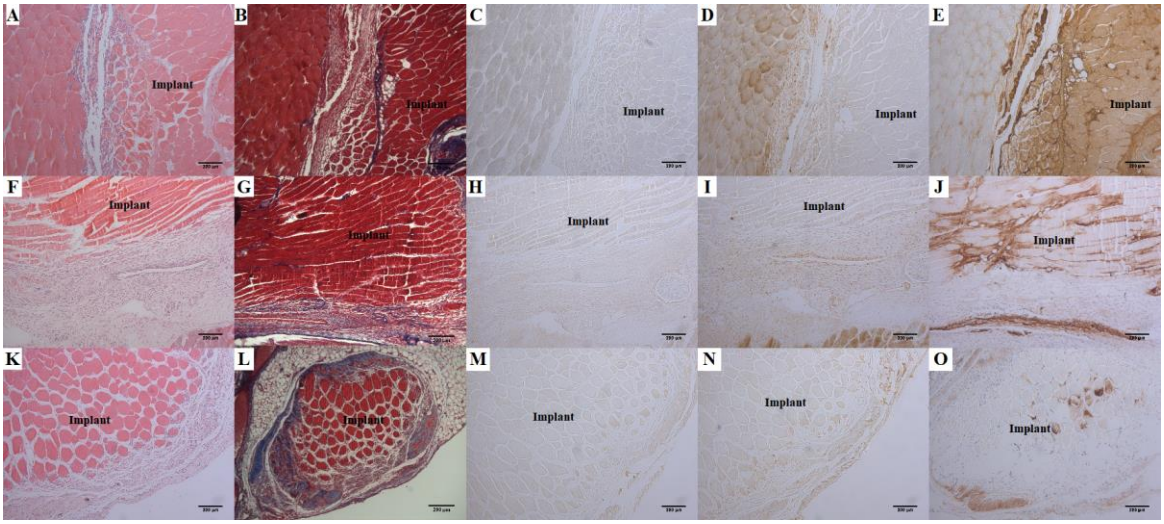

Figure 27. Local fibrotic response towards the dead muscle tissue

(A-E) Day 3 time point. **(F-J)** Day 7 time point. **(K-O)** Day 14 time point. H&E staining **(A)(F)(K)**. Trichrome staining **(B)(G)(L)**. IHC staining using isotype control antibody **(C)(H)(M)**. IHC staining showing the expression of phosphorylated Smad2 **(D)(I)(N)**. IHC staining showing the expression of fibrin(ogen) **(E)(J)(O)**.

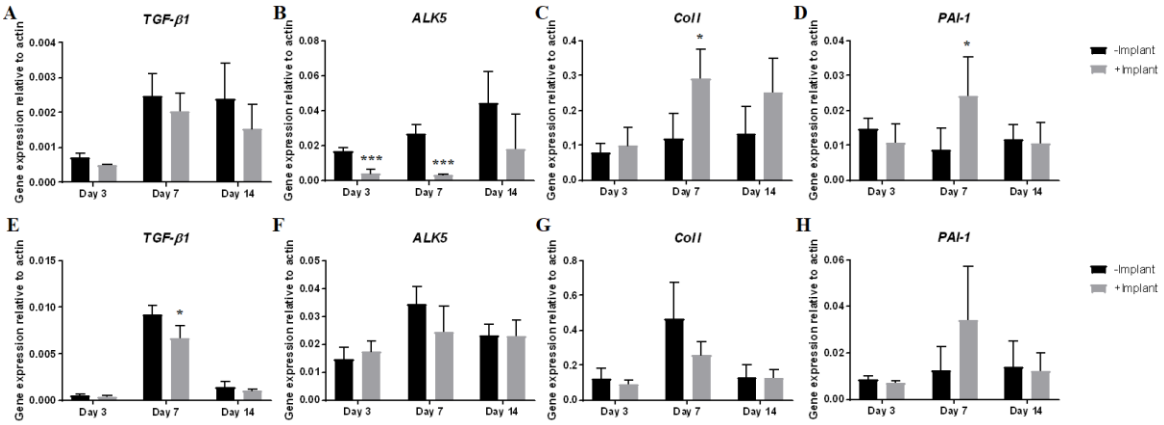

Figure 28. PCR analysis of TGF-β1 production

PCR analysis of gene expression level of different genes related to TGF-β1 signaling pathway at different time points. **(A-D)** Inner thigh muscle tissue. **(E-H)** Outer thigh muscle tissue.

5.3.4 Suppression of TGF-β signaling potentiated MDSCs osteogenesis *in vitro*

To test the effect of suppressed TGF-β signaling on MDSCs osteogenesis *in vitro*, we performed *in vitro* TGF-β signaling suppression experiment with a specific small molecular inhibitor of TGF-β type I receptor SB431542. Our results first demonstrated that, inhibition of TGF-β signaling by SB431542, although it did not affect Smad1 phosphorylation level (Figure 29A), significantly reduced Smad3 phosphorylation in MDSCs (Figure 29B). Accompanying the decreased phosphorylated Smad3 level, significant decrease in TGF-β1 target gene *PAI-1* expression was observed (Figure 29C). At the same time, greatly enhanced osteogenic marker gene expression was found in the treated MDSCs (Figure 29D). These data collectively suggest that suppressed TGF-β signaling potentiated MDSCs osteogenesis. Lastly, we demonstrated that PDGFRα positive MDSCs are present near the calcium deposits, suggesting the possibility that they are responsible for DC formation (Figure 30).

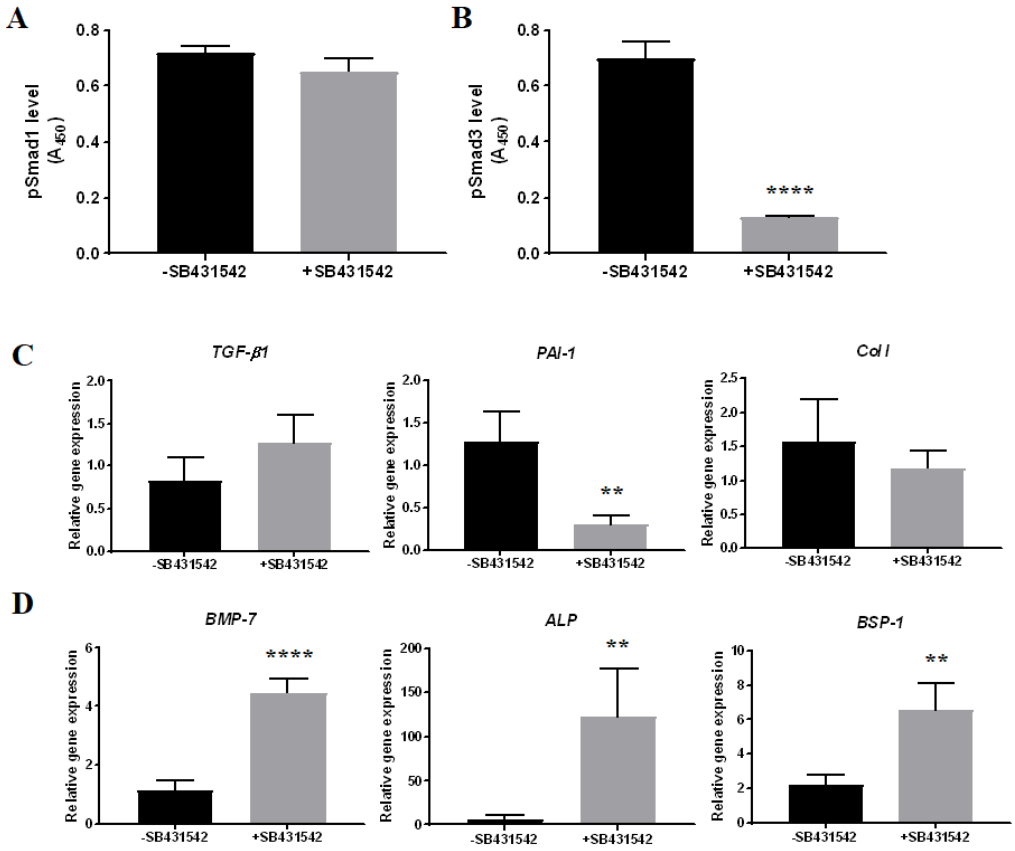

Figure 29. Suppressed TGF-β signaling potentiated MDSCs osteogenesis *in vitro*

(A) Phosphorylated Smad1 level measured by ELISA. **(B)** Phosphorylated Smad3 level measured by ELISA. **(C)** PCR analysis of TGF-β target gene expression. **(D)** PCR analysis of osteogenic marker gene expression.

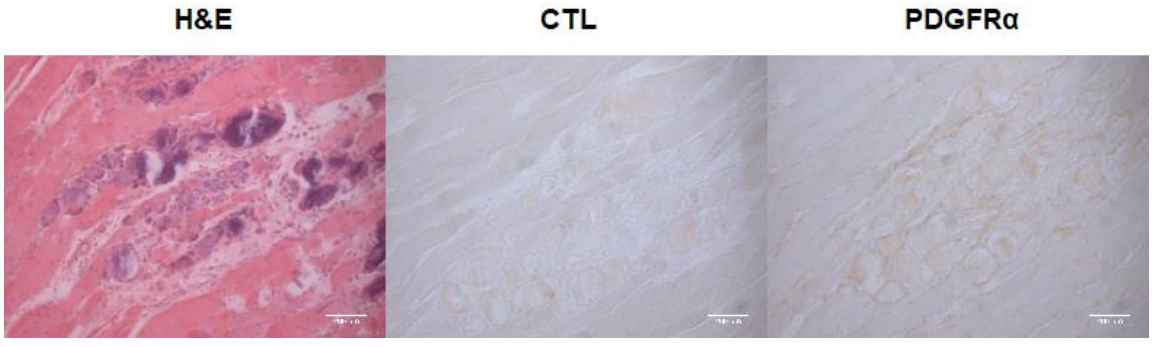

Figure 30. MDSCs participated in DC formation

IHC staining of PDGFRα positive MDSCs near the calcium deposits. CTL: without primary antibody.

Scale bar = 200 μm

5.4 DISCUSSION AND CONCLUSION

In this study, we have attempted to address why different amputation levels would affect HO incidence. We hypothesized that dead muscle tissue not removed in zone of injury could promote HO formation. Our results support this hypothesis by showing that dead muscle tissue promotes DC formation in CTX-injured muscle tissue via a systemic effect, i.e., decreased levels of circulating TGF-β1 and plasmin. We have previously shown that supplementation of TGF-β inhibits osteogenesis *in vivo* and *in vitro* (Part 4). Here, we demonstrated that inhibition of TGF-β signaling *in vitro* potentiated MDSCs osteogenesis, further confirming that TGF-β1 may negatively regulate osteogenesis. Therefore, TGF-β1 may act as a protective factor *in vivo* preventing pathological ectopic mineralization.

We also demonstrated that implantation of dead muscle tissue induces a local fibrotic response, resulting in increased fibrin accumulation and increased TGF-β signaling. Fibrin accumulation usually leads to subsequent fibrosis via TGF-β1 signaling [166]. We speculate that reduced circulating TGF-β1 level could be due to TGF-β1 being consumed locally, given the constant rate of production we have demonstrated above (Figure 29). Fibrin accumulation may also cause local hyperfibrinolysis, therefore exhausting circulating plasmin. Decreased plasmin level is associated with DC/HO formation [112, 137], and is also associated with decreased circulating TGF-β1 level as we have previously demonstrated (Part 4). Therefore, reduced circulating TGF-β1 level could also be due to decreased plasmin level.

The results reporting here could partially explain our previous finding that DC/HO in our blast-amputation model is always formed away from the amputation site. We speculate that local fibrosis caused by dead muscle tissue at the amputation site consumes circulating TGF-β1 and

plasmin, therefore leading to systemically decreased TGF-β1 and plasmin level, which will facilitate DC/HO formation in places distant from the zone of injury.

6.0 STUDY SUMMARY AND FUTURE DIRECTIONS

This dissertation research aims to explore the mechanism for blast-trauma induced HO. We first showed that in a live animal blast trauma model that muscle trauma resulted from blast wave exposure is associated with HO formation. We largely ruled out the effects of other risk factors and showed that muscle trauma may be a major determinant of HO formation. We therefore next investigated the role of muscle injury in HO pathogenesis and demonstrated that BMP-7 is a key osteoinductive factor in injured muscle that facilitates HO formation. However, as it is well known that muscle injury alone cannot induce HO formation, the subsequent studies in the thesis work were focused on investigating the additional factors that could work in concert with muscle injury to cause HO formation.

Recently, a novel notion has been proposed for the mechanism of ectopic mineralization: instead of the gain-of-function mutation (as in case of FOP), a loss-of-function cellular machinery could account for abnormal calcium deposition [108], namely the removal of the protective factors that normally prevent injured tissue from calcifying. We have focused on TGF-β1 as the target of protective factor since TGF-β signaling usually antagonizes BMP signaling by competing for their down-stream co-Smad4 signaling component for nuclear signal transduction (Figure 31). We hypothesized that lowered circulating TGF-β1 level would attenuate its inhibitory effect on BMP-7, thereby enhancing osteogenesis by allowing the BMP-7 signaling to

prevail. We further hypothesized that any pathological condition resulting in decreased circulating TGF-β1 level may lead to DC/HO formation.

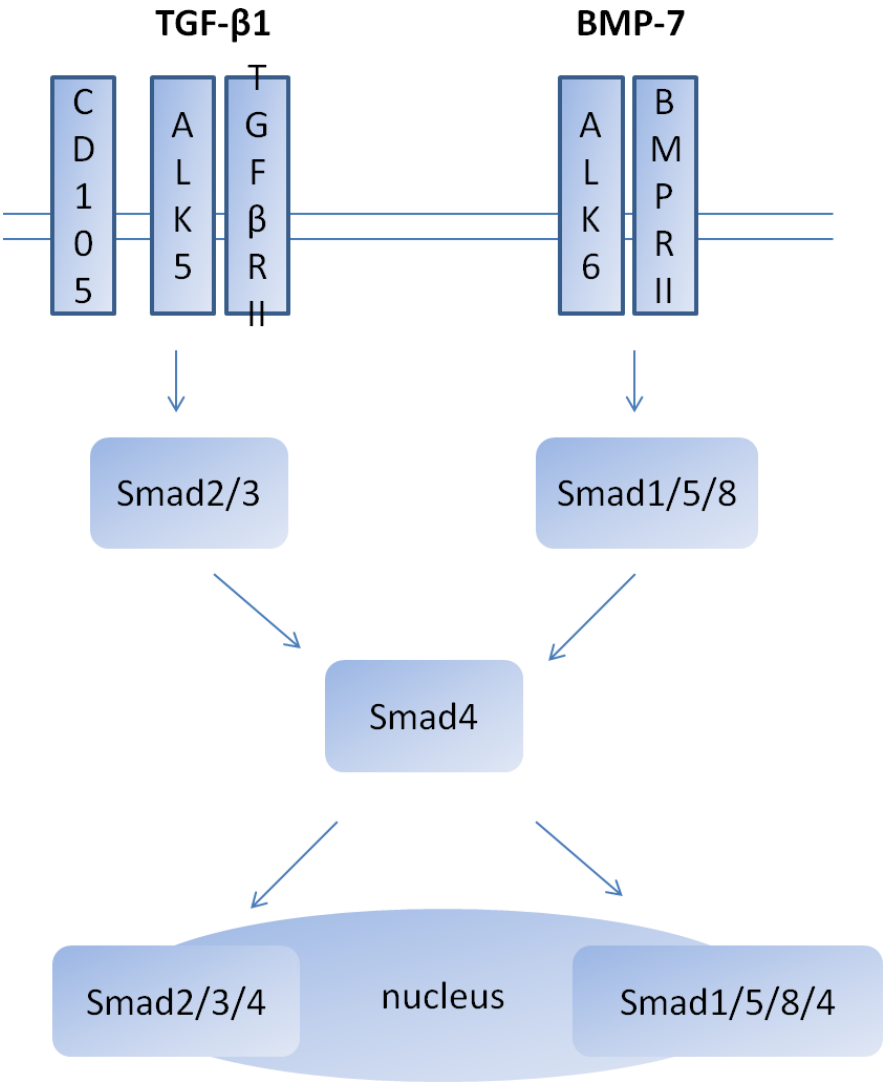

Figure 31. Schematic of BMP signaling and TGF-β signaling

Cortisol stress response is next studied because excessive endogenous glucocorticoid production has always been found following severe trauma, which coincides with increased HO incidence. We have shown that high level of glucocorticoids lowers circulating TGF-β1 level through alterations of protein level in the fibrinolytic system, which is relevant to the recent

finding that decreased plasmin level is associated with DC/HO formation [112]. Our results suggest that TGF-β1 could be the plasmin target in regulating DC/HO formation via its influence on MDSCs, a possible cellular source for DC/HO.

In the last part of the thesis work, we have demonstrated that the presence of dead muscle tissue promoted DC and also caused a decrease in circulating TGF-β1 level, further supporting our hypothesis that any pathological condition resulting in decreased circulating TGF-β1 level may lead to DC/HO formation. The effect reported here might be mediated via alterations of protein level in the fibrinolytic system, and might also be due to a direct fibrin-TGF-β1 binding mechanism which depletes TGF-β1 from circulation [167].

Decreased circulating TGF-β1 level has been reported to be associated with calcification in the cardiovascular system, i.e., severely depressed serum TGF-β1 level was found in advanced atherosclerosis featuring prominent calcification and ossification [168]. The pathogenesis of vascular calcification/ossification actually shares great similarity with muscle DC, in which tissue injury, inflammatory cell infiltration, progenitor cell osteogenic differentiation etc. are all integral parts of the disease [169, 170]. Interestingly, in atherosclerosis, BMP signaling also promotes vascular calcification, whereas TGF-β1 protects against disease progression [171-173]. These data collectively suggest a universal role of BMP and TGF-β signaling in pathological calcification/ossification.

We report here a two-hit model for of blast trauma-induced HO and trauma-induced HO in general: muscle injury-induced upregulated BMP-7 level combined with pathological condition-induced downregulation of circulating TGF-β1 level may result in DC/HO formation (Figure 32).

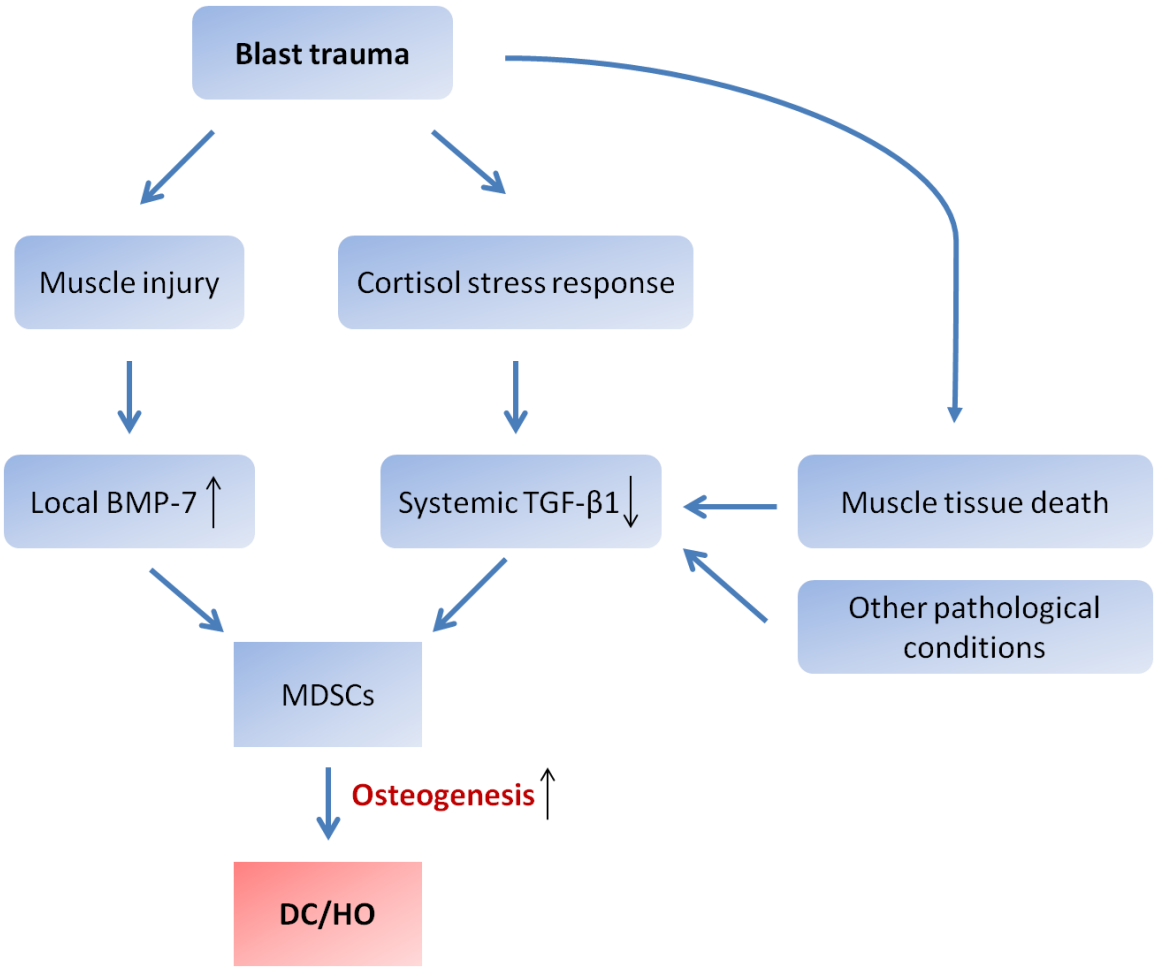

Figure 32. A schematic represents a two-hit model for blast trauma-induced HO

The limitation of this study is that we did not delve deep into the immune system in regulating DC/HO formation, especially the role of macrophages in DC/HO pathogenesis. Macrophages were initially thought to be the source of the osteogenic factors, that are indispensable for initiating osteogenic process [28, 29, 56]. However, recently some studies pointed out that depletion of macrophages actually promotes DC/HO formation [108, 174]. We also discovered these discrepancies in this dissertation research. We showed that treatment with DEX (as an anti-inflammatory drug used to reduce macrophage number) treatment could either inhibit or promote ectopic mineralization (Part 3&4). The reason for these seemingly different

processes is still unclear. We speculate that this is due to the plasticity of the macrophage, namely the immunomodulatory activity from different macrophage subsets. Our preliminary data showed that DEX treatment greatly increased M2 macrophage number in CTX-injured muscle tissue, which coincided with increased BMP-7 expression (Figure 33). Therefore, we hypothesized that M2 macrophage could promote osteogenesis. Supplementation of TGF-β1 *in vivo*, instead of reducing M2 macrophage number and suppressing osteogenesis, greatly increased M2 macrophage number with suppressed osteogenesis, thus contradicting our initial hypothesis (Figure 34). BMP-7 plays a role in inducing M2 macrophage differentiation [123]. However, supplementation of TGF-β1 *in vivo* did not affect BMP-7 expression (Figure 33). Therefore, the inter-relationship between all these molecules still needs to be explored, which will be our future research directions.

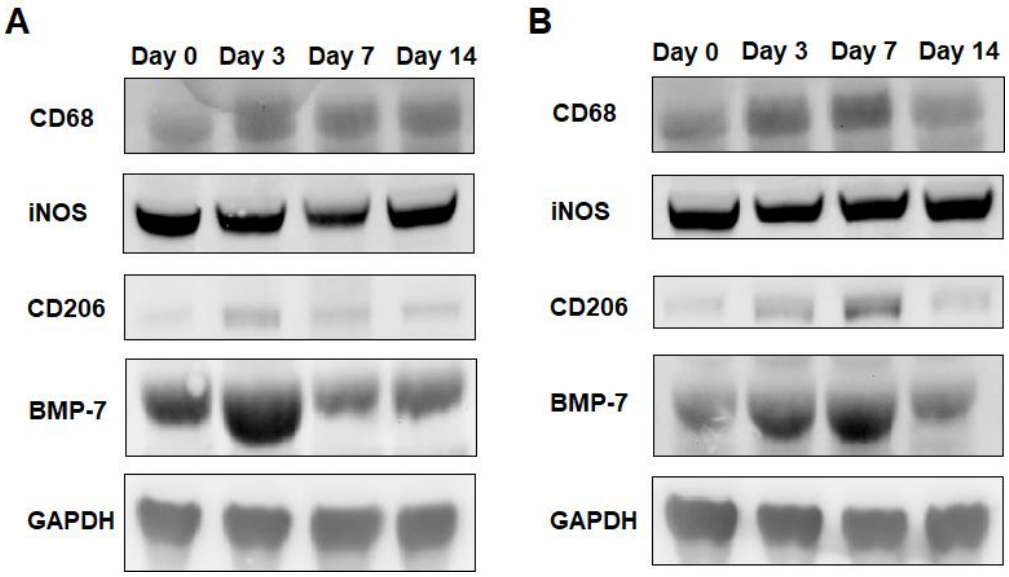

Figure 33. Participation of macrophage subsets in pathogenesis of DC/HO

Western blot analysis of macrophage marker expression at different time points. **(A)** CTX treatment alone. **(B)** CTX+DEX co-treatment. Increased M2 macrophage number coincided with increased BMP-7 expression. iNOS: M1 macrophage marker; CD206: M2 macrophage marker.

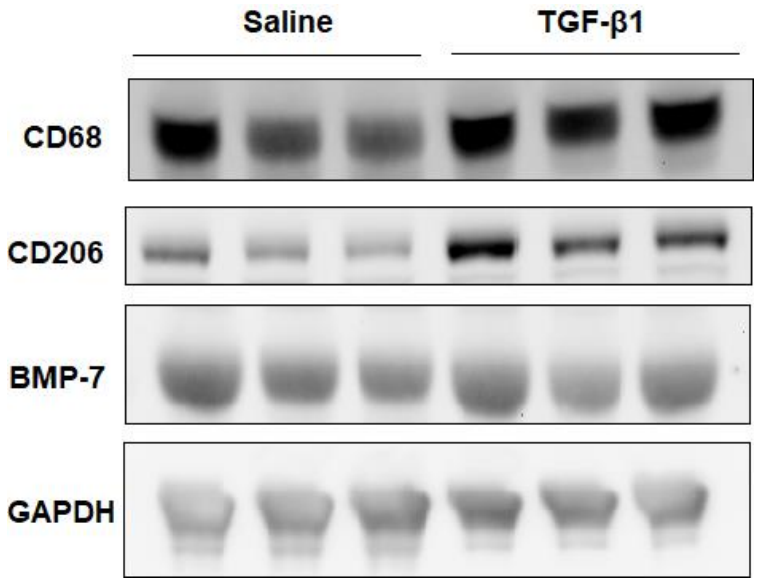

Figure 34. Effects of TGF-β1 supplementation *in vivo* on macrophages

Increased CD206 expression was observed with TGF-β1 supplementation upon CTX+DEX co-treatment. (n=3)

APPENDIX A

SUPPLEMENTAL FIGURES

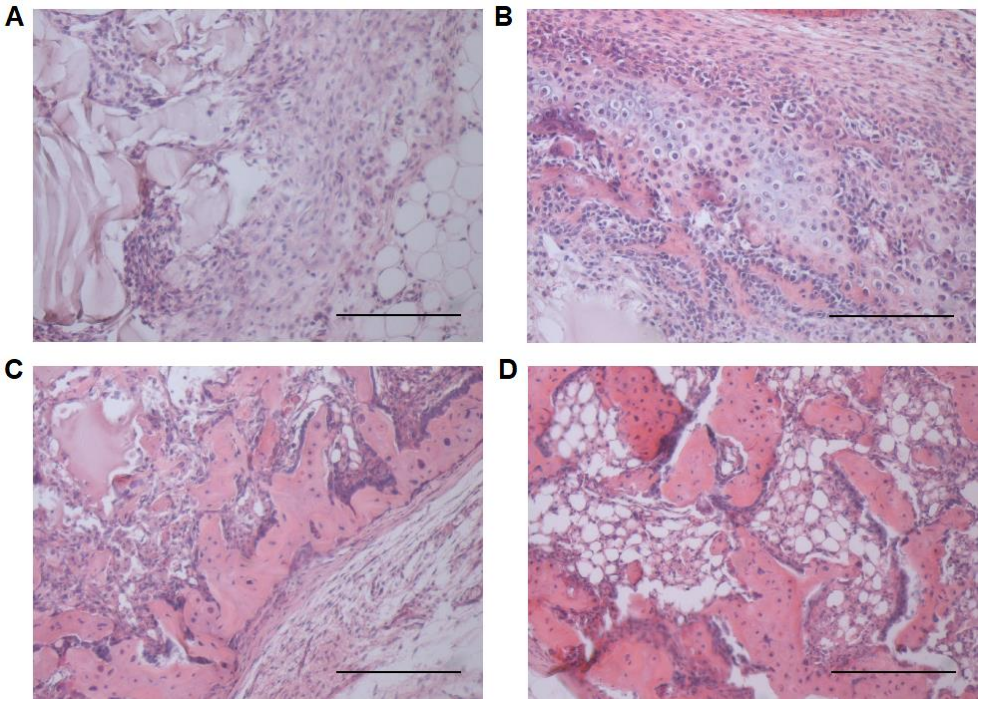

Figure 35. Supplemental figure 1. Morphology of bone formed in BMP-2 injection alone group and BMP-2/CTX co-injection group

(A&B) H&E staining showing the presence of cartilage morphology at the day 7 time point in BMP-2-induced HO. **(A)** BMP-2 injection alone group. **(B)** BMP-2/CTX co-injection group. **(C&D)** H&E staining of decalcified tissue showing the bone morphology at the day 14 time point in BMP-2-induced HO. **(C)** BMP-2 injection alone group. **(D)** BMP-2/CTX co-injection group. Bar = 200 μm.

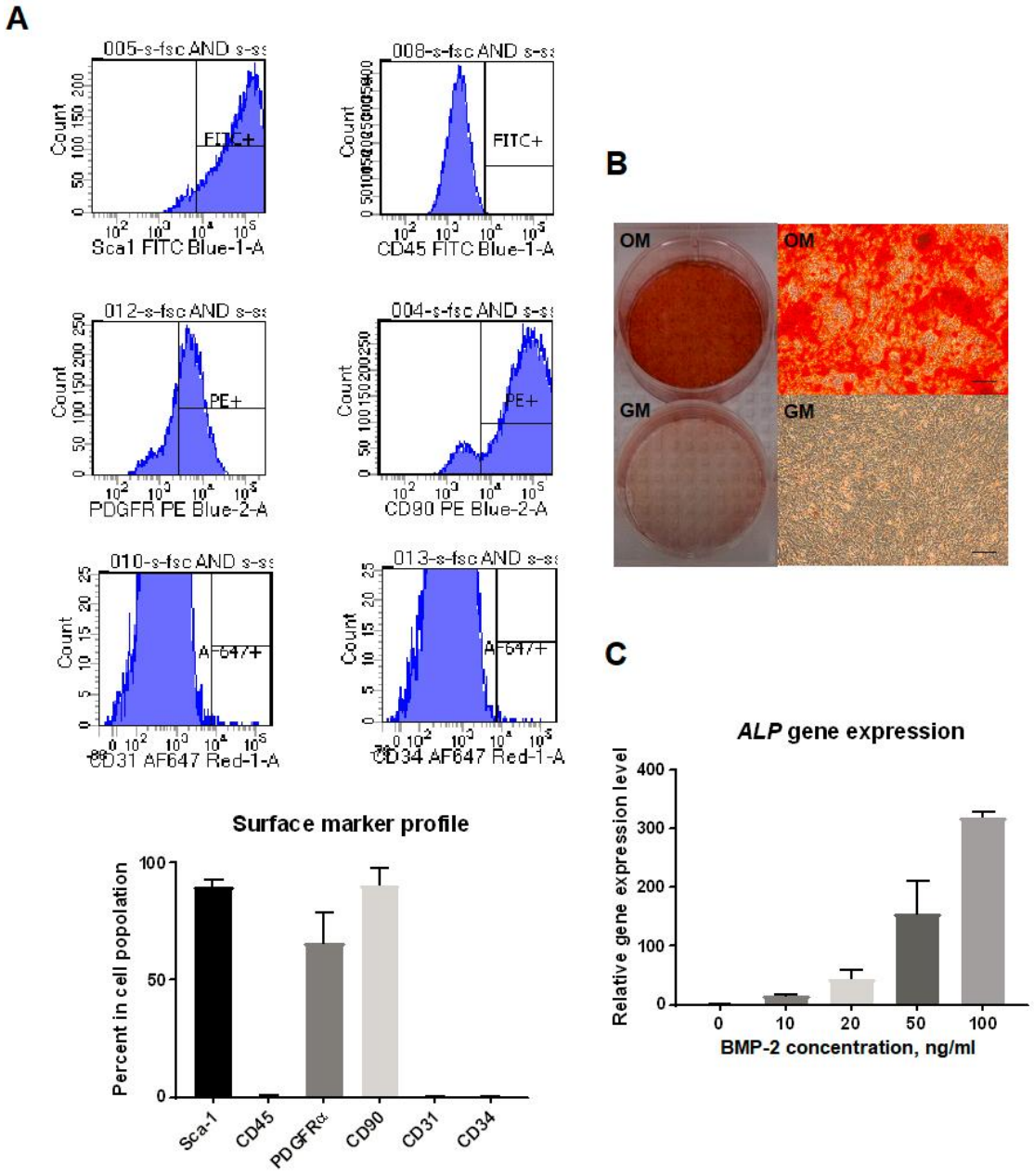

Figure 36. Supplemental figure 2. Characterization of MDSCs

(A) Surface marker profile of MDSCs analyzed by flow cytometry, including Sca-1, CD45, PDGFRα, CD90, CD31 and CD34. Percent of MDSCs positive for the respective surface markers in total cell population. **(B)** Alizarin Red staining of calcium deposits in MDSCs growing in osteogenic medium (OM) and growth medium (GM). Bar = 200 μm. **(C)** BMP-2-induced osteogenesis *in vitro*. ALP gene expression in MDSCs was upregulated upon treatment with different concentrations of BMP-2 recombinant protein for 3 days.

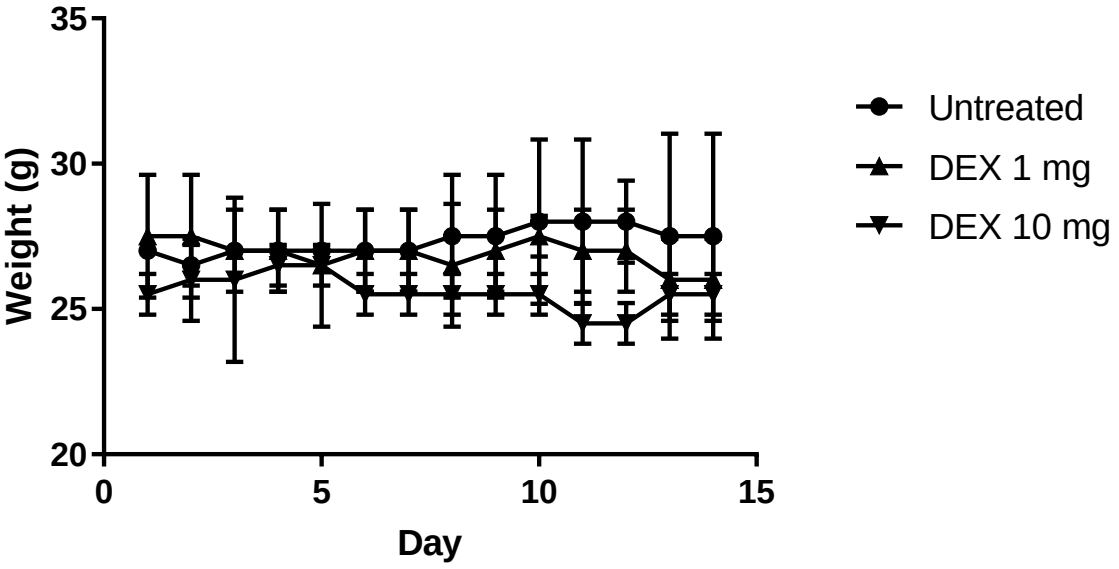

Figure 37. Supplemental figure 3. Effect of different doses of DEX treatments on animal body weight

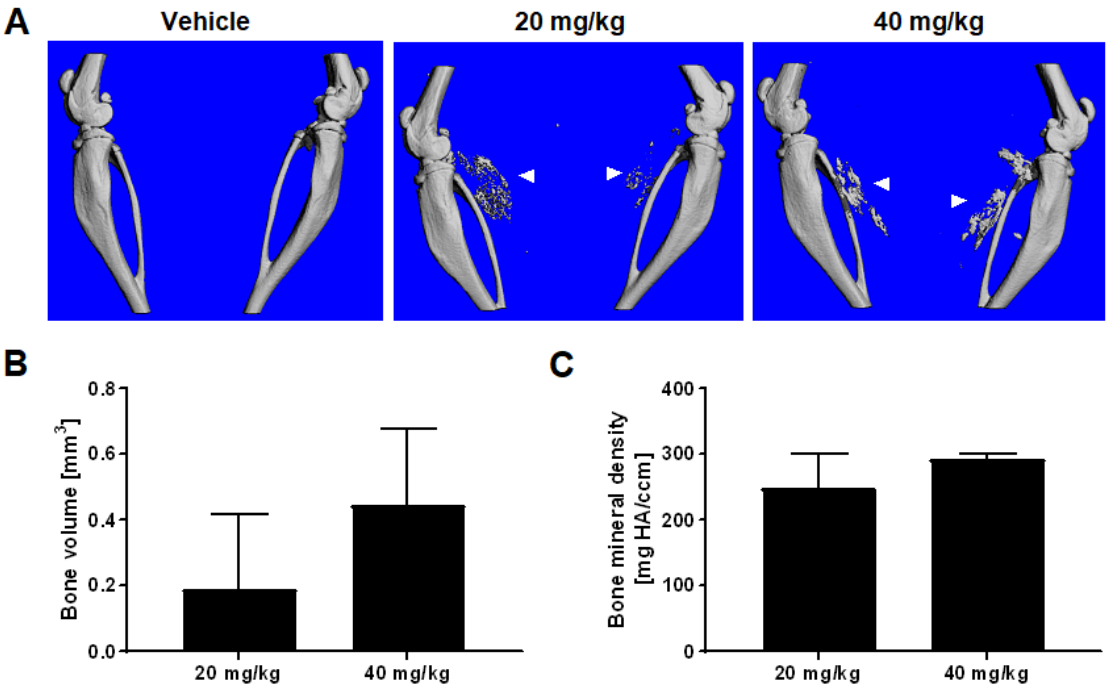

Figure 38. Supplemental figure 4. Corticosterone treatment stimulated ectopic mineralization

(A) microCT imaging illustrating ectopic mineralization formed in CTX+corticosterone co-treatment group at Day 7 time point. Arrowheads indicate ectopic mineralization. micoCT imaging demonstrating that vehicle treatment alone did not result in ectopic mineralization. **(B)** microCT analysis of bone volume in 20 mg/kg and 40 mg/kg CTX+corticosterone co-treatment group at Day 7. (n=4) **(C)** microCT analysis of bone mineral density in in 20 mg/kg and 40 mg/kg CTX+corticosterone co-treatment group at Day 7. (n=4)

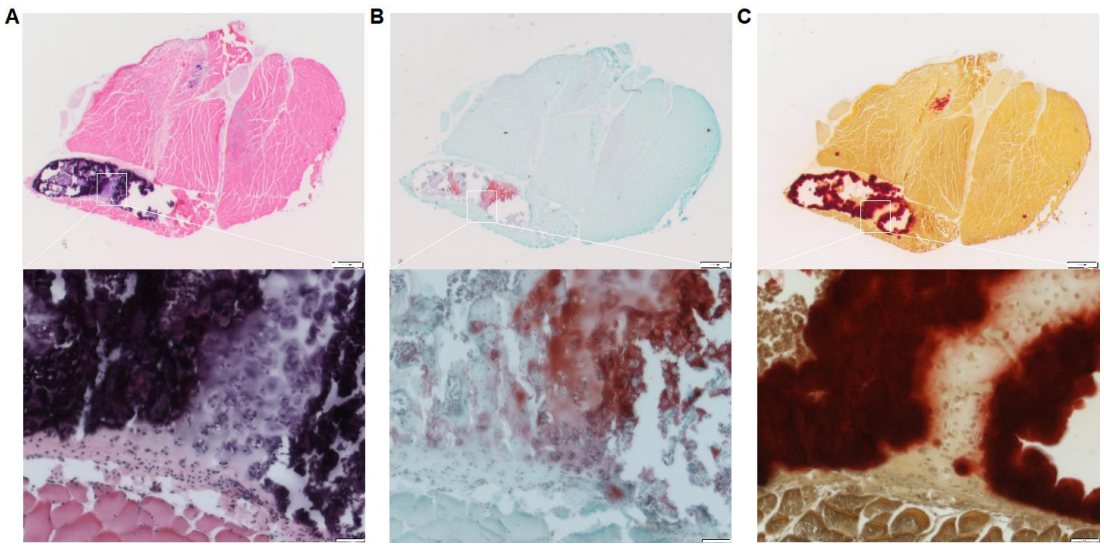

Figure 39. Supplemental figure 5. Characterization of HO formed in CTX+DEX co-treatment group

An endochondral ossification process was found in 2 weeks as demonstrated by **(A)** H&E staining. **(B)** Safranin-O staining. **(C)** Alizarin Red staining. Upper panels: Bar = 500 μm. Lower panels: Bar = 50 μm.

Figure 40. Supplemental figure 6. TGF-β1 supplementation inhibited DC formation at Day 14 time point **(A)** microCT imaging demonstrating reduced bone volume with TGF-β1 supplementation for 7 days. Arrowheads indicate ectopic mineralization. **(B)** microCT analysis of bone volume and bone mineral density with and without TGF-β1 supplementation (*, $p < 0.05$; $n = 9$).

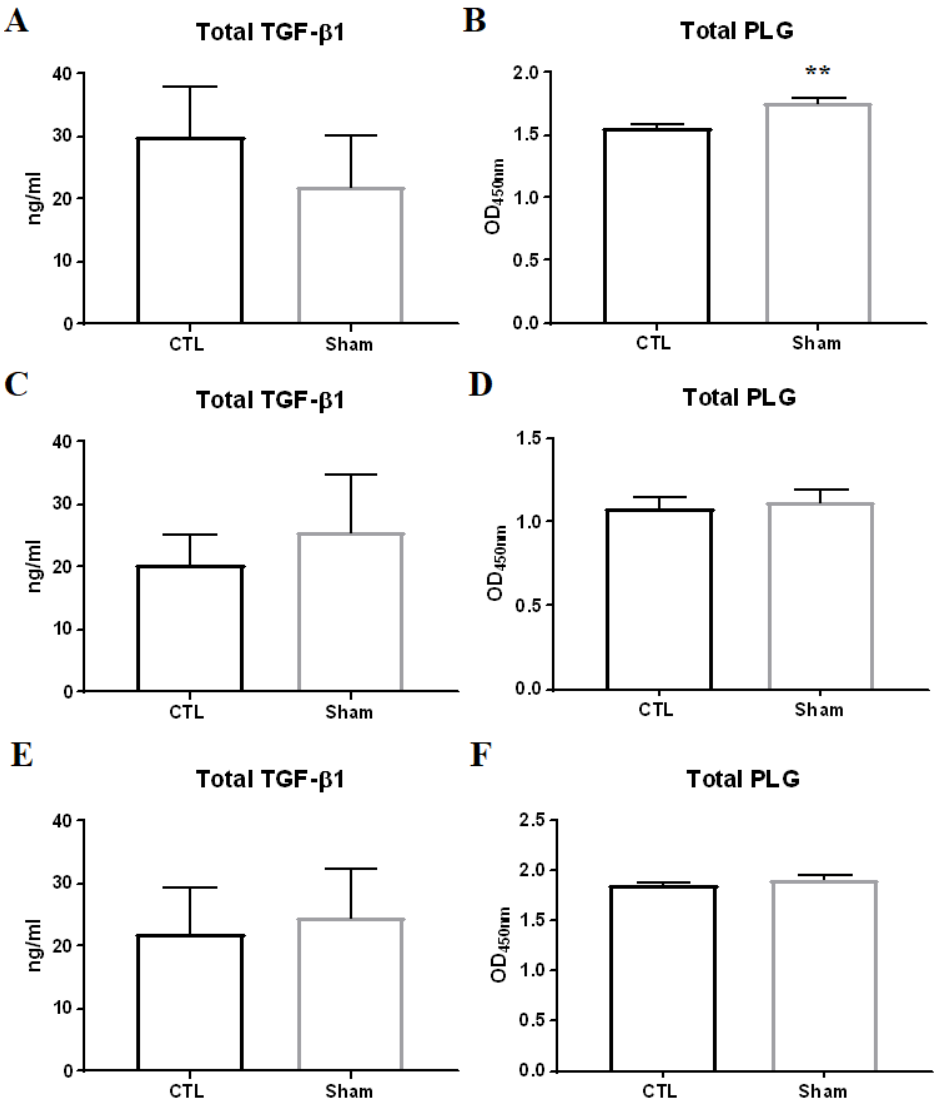

Figure 41. Supplemental figure 7. Sham surgery did not affect plasma TGF-β1 level

Blood sample analysis of total TGF-β1 and total PLG level in animal with CTX injection only (CTL) or CTX injection with sham surgery (Sham). **(A&B)** Day 3 time point. **(C&D)** Day 7 time point. **(E&F)** Day 14 time point.

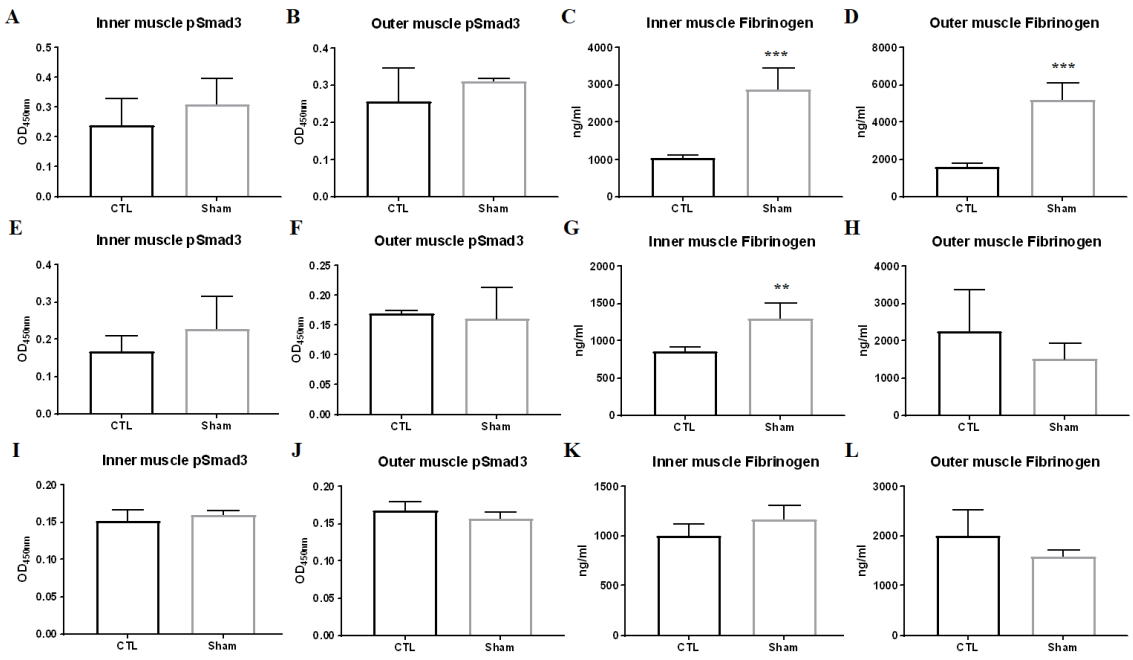

Figure 42. Supplemental figure 8. Sham surgery did not affect muscle phosphorylated Smad3 level

Muscle sample analysis of phosphorylated Smad3 level and fibrinogen level in animal with CTX injection only (CTL) or CTX injection with sham surgery (Sham). **(A-D)** Day 3 time point. **(E-H)** Day 7 time point. **(I-L)** Day 14 time point.

APPENDIX B

TABLES

Table 1. PCR primer sequences

	Forward (5’ to 3’)	Reverse (5’ to 3’)
Actin	GGCTGTATTCCCCTCCATCG	CCAGTTGGTAACAATGCCATGT
Runx2	ATGATGACACTGCCACCTCTGAC	ACTGCCTGGGGTCTGAAAAAGG
OSX	GATGGCGTCCTCTCTGCTT	CGTATGGCTTCTTTGTGCCT
ALP	ATCGGAACAACCTGACTGACCCTT	ACCCTCATGATGTCCGTGGTCAAT
BSP-1	TGCCCTCTGATCAGGACAAC	ATCCGACTGATCGGCACTCT
OCN	ACCATCTTTCTGCTCACTCTGCTG	TATTGCCCTCCTGCTTGGACATGA
BMPRIA	ACCAGACGGTGTTAATGCGT	CTCGATGAGCAATTGCAGGC
BMPRIB	CCCTCGGCCCAAGATCCTA	CAACAGGCATTCCAGAGTCATC
ACVR1	GTGGAAGATTACAAGCCACCA	GGGTCTGAGAACCATCTGTTAGG
TGF-β1	CACCTGCAAGACCATCGACA	CATAGTAGTCCGCTTCGGGC
ALK5	CCTCGAGACAGGCCATTTGT	GCCAGCTGACTGCTTTTCTG
Col I	TTCTCCTGGCAAAGACGGACTCAA	AGGAAGCTGAAGTCATAACCGCCA
PAI-1	TCTGGGAAAGGGTTCACTTTACC	GACACGCCATAGGGAGAGAAG

BIBLIOGRAPHY

1. Shehab, D., A.H. Elgazzar, and B.D. Collier, *Heterotopic ossification.* J Nucl Med, 2002. **43**(3): p. 346-53.
2. Eisenstein, N., S. Stapley, and L. Grover, *Post-Traumatic Heterotopic Ossification: An Old Problem in Need of New Solutions.* J Orthop Res, 2018. **36**(4): p. 1061-1068.
3. Shore, E.M., et al., *A recurrent mutation in the BMP type I receptor ACVR1 causes inherited and sporadic fibrodysplasia ossificans progressiva.* Nat Genet, 2006. **38**(5): p. 525-7.
4. Vanden Bossche, L. and G. Vanderstraeten, *Heterotopic ossification: a review.* J Rehabil Med, 2005. **37**(3): p. 129-36.
5. Alfieri, K.A., J.A. Forsberg, and B.K. Potter, *Blast injuries and heterotopic ossification.* Bone Joint Res, 2012. **1**(8): p. 192-7.
6. Chalmers, J., D.H. Gray, and J. Rush, *Observations on the induction of bone in soft tissues.* J Bone Joint Surg Br, 1975. **57**(1): p. 36-45.
7. Urist, M.R., *Bone: formation by autoinduction.* Science, 1965. **150**(3698): p. 893-9.
8. Urist, M.R. and B.S. Strates, *Bone morphogenetic protein.* J Dent Res, 1971. **50**(6): p. 1392-406.
9. Sartori, R., et al., *BMP signaling controls muscle mass.* Nat Genet, 2013. **45**(11): p. 1309-18.

10. Clever, J.L., et al., *Inefficient skeletal muscle repair in inhibitor of differentiation knockout mice suggests a crucial role for BMP signaling during adult muscle regeneration.* Am J Physiol Cell Physiol, 2010. **298**(5): p. C1087-99.

11. Pacifici, M., *Acquired and congenital forms of heterotopic ossification: new pathogenic insights and therapeutic opportunities.* Curr Opin Pharmacol, 2018. **40**: p. 51-58.

12. Pignolo, R.J., E.M. Shore, and F.S. Kaplan, *Fibrodysplasia ossificans progressiva: clinical and genetic aspects.* Orphanet J Rare Dis, 2011. **6**: p. 80.

13. Fukuda, T., et al., *Generation of a mouse with conditionally activated signaling through the BMP receptor, ALK2.* Genesis, 2006. **44**(4): p. 159-67.

14. Yu, P.B., et al., *BMP type I receptor inhibition reduces heterotopic [corrected] ossification.* Nat Med, 2008. **14**(12): p. 1363-9.

15. Agarwal, S., et al., *BMP signaling mediated by constitutively active Activin type 1 receptor (ACVR1) results in ectopic bone formation localized to distal extremity joints.* Dev Biol, 2015. **400**(2): p. 202-9.

16. Chakkalakal, S.A., et al., *An Acvr1 R206H knock-in mouse has fibrodysplasia ossificans progressiva.* J Bone Miner Res, 2012. **27**(8): p. 1746-56.

17. Lees-Shepard, J.B. and D.J. Goldhamer, *Stem cells and heterotopic ossification: Lessons from animal models.* Bone, 2018. **109**: p. 178-186.

18. Hatsell, S.J., et al., *ACVR1R206H receptor mutation causes fibrodysplasia ossificans progressiva by imparting responsiveness to activin A.* Sci Transl Med, 2015. **7**(303): p. 303ra137.

19. Wosczyna, M.N., et al., *Multipotent progenitors resident in the skeletal muscle interstitium exhibit robust BMP-dependent osteogenic activity and mediate heterotopic ossification.* J Bone Miner Res, 2012. **27**(5): p. 1004-17.

20. Kan, L., et al., *Transgenic mice overexpressing BMP4 develop a fibrodysplasia ossificans progressiva (FOP)-like phenotype.* Am J Pathol, 2004. **165**(4): p. 1107-15.

21. Lounev, V.Y., et al., *Identification of progenitor cells that contribute to heterotopic skeletogenesis.* J Bone Joint Surg Am, 2009. **91**(3): p. 652-63.

22. Medici, D., et al., *Conversion of vascular endothelial cells into multipotent stem-like cells.* Nat Med, 2010. **16**(12): p. 1400-6.

23. Agarwal, S., et al., *Local and Circulating Endothelial Cells Undergo Endothelial to Mesenchymal Transition (EndMT) in Response to Musculoskeletal Injury.* Sci Rep, 2016. **6**: p. 32514.

24. Joe, A.W., et al., *Muscle injury activates resident fibro/adipogenic progenitors that facilitate myogenesis.* Nat Cell Biol, 2010. **12**(2): p. 153-63.

25. Dey, D., et al., *Two tissue-resident progenitor lineages drive distinct phenotypes of heterotopic ossification.* Sci Transl Med, 2016. **8**(366): p. 366ra163.

26. Agarwal, S., et al., *Scleraxis-Lineage Cells Contribute to Ectopic Bone Formation in Muscle and Tendon.* Stem Cells, 2017. **35**(3): p. 705-710.

27. Lees-Shepard, J.B., et al., *Activin-dependent signaling in fibro/adipogenic progenitors causes fibrodysplasia ossificans progressiva.* Nat Commun, 2018. **9**(1): p. 471.

28. Kan, L., et al., *Dysregulation of local stem/progenitor cells as a common cellular mechanism for heterotopic ossification.* Stem Cells, 2009. **27**(1): p. 150-6.

29. Convente, M.R., et al., *Depletion of Mast Cells and Macrophages Impairs Heterotopic Ossification in an Acvr1(R206H) Mouse Model of Fibrodysplasia Ossificans Progressiva.* J Bone Miner Res, 2018. **33**(2): p. 269-282.

30. Convente, M.R., et al., *The immunological contribution to heterotopic ossification disorders.* Curr Osteoporos Rep, 2015. **13**(2): p. 116-24.

31. Barruet, E., et al., *NF-kappaB/MAPK activation underlies ACVR1-mediated inflammation in human heterotopic ossification.* JCI Insight, 2018. **3**(22).

32. Wang, H., et al., *ECSIT links TLR and BMP signaling in FOP connective tissue progenitor cells.* Bone, 2018. **109**: p. 201-209.

33. Hino, K., et al., *Neofunction of ACVR1 in fibrodysplasia ossificans progressiva.* Proc Natl Acad Sci U S A, 2015. **112**(50): p. 15438-43.

34. Alessi Wolken, D.M., et al., *The obligatory role of Activin A in the formation of heterotopic bone in Fibrodysplasia Ossificans Progressiva.* Bone, 2018. **109**: p. 210-217.

35. Hino, K., et al., *Activin-A enhances mTOR signaling to promote aberrant chondrogenesis in fibrodysplasia ossificans progressiva.* J Clin Invest, 2017. **127**(9): p. 3339-3352.

36. Micha, D., et al., *Inhibition of TGFbeta signaling decreases osteogenic differentiation of fibrodysplasia ossificans progressiva fibroblasts in a novel in vitro model of the disease.* Bone, 2016. **84**: p. 169-180.

37. Agarwal, S., et al., *Inhibition of Hif1alpha prevents both trauma-induced and genetic heterotopic ossification.* Proc Natl Acad Sci U S A, 2016. **113**(3): p. E338-47.

38. Wang, H., et al., *Cellular Hypoxia Promotes Heterotopic Ossification by Amplifying BMP Signaling.* J Bone Miner Res, 2016. **31**(9): p. 1652-65.

39. Uchibe, K., et al., *Genetic and pharmacological inhibition of retinoic acid receptor gamma function promotes endochondral bone formation.* J Orthop Res, 2017. **35**(5): p. 1096-1105.

40. Shimono, K., et al., *Potent inhibition of heterotopic ossification by nuclear retinoic acid receptor-gamma agonists.* Nat Med, 2011. **17**(4): p. 454-60.

41. Chakkalakal, S.A., et al., *Palovarotene Inhibits Heterotopic Ossification and Maintains Limb Mobility and Growth in Mice With the Human ACVR1(R206H) Fibrodysplasia Ossificans Progressiva (FOP) Mutation.* J Bone Miner Res, 2016. **31**(9): p. 1666-75.

42. Sakellariou, V.I., et al., *Heterotopic ossification following traumatic brain injury and spinal cord injury: insight into the etiology and pathophysiology.* J Musculoskelet Neuronal Interact, 2012. **12**(4): p. 230-40.

43. Balboni, T.A., R. Gobezie, and H.J. Mamon, *Heterotopic ossification: Pathophysiology, clinical features, and the role of radiotherapy for prophylaxis.* Int J Radiat Oncol Biol Phys, 2006. **65**(5): p. 1289-99.

44. McCarthy, E.F. and M. Sundaram, *Heterotopic ossification: a review.* Skeletal Radiol, 2005. **34**(10): p. 609-19.

45. Pape, H.C., et al., *Current concepts in the development of heterotopic ossification.* J Bone Joint Surg Br, 2004. **86**(6): p. 783-7.

46. Davis, E.L., et al., *Is heterotopic ossification getting nervous?: The role of the peripheral nervous system in heterotopic ossification.* Bone, 2018. **109**: p. 22-27.

47. van Kuijk, A.A., A.C. Geurts, and H.J. van Kuppevelt, *Neurogenic heterotopic ossification in spinal cord injury.* Spinal Cord, 2002. **40**(7): p. 313-26.

48. Sullivan, M.P., et al., *Heterotopic ossification after central nervous system trauma: A current review.* Bone Joint Res, 2013. **2**(3): p. 51-7.

49. Toffoli, A.M., et al., *From brain to bone: evidence for the release of osteogenic humoral factors after traumatic brain injury.* Brain Inj, 2008. **22**(7-8): p. 511-8.

50. Gautschi, O.P., et al., *Osteoinductive effect of cerebrospinal fluid from brain-injured patients.* J Neurotrauma, 2007. **24**(1): p. 154-62.

51. Cadosch, D., et al., *Serum after traumatic brain injury increases proliferation and supports expression of osteoblast markers in muscle cells.* J Bone Joint Surg Am, 2010. **92**(3): p. 645-53.

52. Gautschi, O.P., et al., *Serum-mediated osteogenic effect in traumatic brain-injured patients.* ANZ J Surg, 2009. **79**(6): p. 449-55.

53. Salisbury, E., et al., *Heterotopic ossification has some nerve.* Crit Rev Eukaryot Gene Expr, 2010. **20**(4): p. 313-24.

54. Xanthos, D.N. and J. Sandkuhler, *Neurogenic neuroinflammation: inflammatory CNS reactions in response to neuronal activity.* Nat Rev Neurosci, 2014. **15**(1): p. 43-53.

55. Kan, L., et al., *Substance P signaling mediates BMP-dependent heterotopic ossification.* J Cell Biochem, 2011. **112**(10): p. 2759-72.

56. Genet, F., et al., *Neurological heterotopic ossification following spinal cord injury is triggered by macrophage-mediated inflammation in muscle.* J Pathol, 2015. **236**(2): p. 229-40.

57. Torossian, F., et al., *Macrophage-derived oncostatin M contributes to human and mouse neurogenic heterotopic ossifications.* JCI Insight, 2017. **2**(21).

58. Debaud, C., et al., *Peripheral denervation participates in heterotopic ossification in a spinal cord injury model.* PLoS One, 2017. **12**(8): p. e0182454.

59. Lazard, Z.W., et al., *Osteoblasts Have a Neural Origin in Heterotopic Ossification.* Clin Orthop Relat Res, 2015. **473**(9): p. 2790-806.

60. Salisbury, E., et al., *Sensory nerve induced inflammation contributes to heterotopic ossification.* J Cell Biochem, 2011. **112**(10): p. 2748-58.

61. Olmsted-Davis, E.A., et al., *Progenitors in Peripheral Nerves Launch Heterotopic Ossification.* Stem Cells Transl Med, 2017. **6**(4): p. 1109-1119.

62. Tuzmen, C., et al., *Crosstalk between substance P and calcitonin gene-related peptide during heterotopic ossification in murine Achilles tendon.* J Orthop Res, 2018. **36**(5): p. 1444-1455.

63. Dey, D., et al., *The traumatic bone: trauma-induced heterotopic ossification.* Transl Res, 2017. **186**: p. 95-111.

64. Nauth, A., et al., *Heterotopic ossification in orthopaedic trauma.* J Orthop Trauma, 2012. **26**(12): p. 684-8.

65. Ranganathan, K., et al., *Heterotopic Ossification: Basic-Science Principles and Clinical Correlates.* J Bone Joint Surg Am, 2015. **97**(13): p. 1101-11.

66. Hug, K.T., T.B. Alton, and A.O. Gee, *Classifications in brief: Brooker classification of heterotopic ossification after total hip arthroplasty.* Clin Orthop Relat Res, 2015. **473**(6): p. 2154-7.

67. Amar, E., Z.T. Sharfman, and E. Rath, *Heterotopic ossification after hip arthroscopy.* J Hip Preserv Surg, 2015. **2**(4): p. 355-63.

68. Pavlou, G., et al., *Risk factors for heterotopic ossification in primary total hip arthroplasty.* Hip Int, 2012. **22**(1): p. 50-5.

69. Kornhaber, R., et al., *The development and impact of heterotopic ossification in burns: a review of four decades of research.* Scars Burn Heal, 2017. **3**: p. 2059513117695659.

70. Juarez, J.K., J.C. Wenke, and J.C. Rivera, *Treatments and Preventative Measures for Trauma-Induced Heterotopic Ossification: A Review.* Clin Transl Sci, 2018. **11**(4): p. 365-370.

71. Klein, G.L., *Disruption of bone and skeletal muscle in severe burns.* Bone Res, 2015. **3**: p. 15002.

72. Forsberg, J.A., et al., *Heterotopic ossification in high-energy wartime extremity injuries: prevalence and risk factors.* J Bone Joint Surg Am, 2009. **91**(5): p. 1084-91.

73. Potter, B.K., et al., *Heterotopic ossification following traumatic and combat-related amputations. Prevalence, risk factors, and preliminary results of excision.* J Bone Joint Surg Am, 2007. **89**(3): p. 476-86.

74. Potter, B.K., et al., *Heterotopic ossification following combat-related trauma.* J Bone Joint Surg Am, 2010. **92 Suppl 2**: p. 74-89.

75. Agarwal, S., et al., *Strategic Targeting of Multiple BMP Receptors Prevents Trauma-Induced Heterotopic Ossification.* Mol Ther, 2017. **25**(8): p. 1974-1987.

76. Kraft, C.T., et al., *Trauma-induced heterotopic bone formation and the role of the immune system: A review.* J Trauma Acute Care Surg, 2016. **80**(1): p. 156-65.

77. Evans, K.N., et al., *Inflammatory cytokine and chemokine expression is associated with heterotopic ossification in high-energy penetrating war injuries.* J Orthop Trauma, 2012. **26**(11): p. e204-13.

78. Forsberg, J.A., et al., *Do inflammatory markers portend heterotopic ossification and wound failure in combat wounds?* Clin Orthop Relat Res, 2014. **472**(9): p. 2845-54.

79. Martin, E.C., et al., *Trauma induced heterotopic ossification patient serum alters mitogen activated protein kinase signaling in adipose stem cells.* J Cell Physiol, 2018. **233**(9): p. 7035-7044.

80. Nesti, L.J., et al., *Differentiation potential of multipotent progenitor cells derived from war-traumatized muscle tissue.* J Bone Joint Surg Am, 2008. **90**(11): p. 2390-8.

81. Jackson, W.M., et al., *Mesenchymal progenitor cells derived from traumatized human muscle.* J Tissue Eng Regen Med, 2009. **3**(2): p. 129-38.

82. Jackson, W.M., et al., *Putative heterotopic ossification progenitor cells derived from traumatized muscle.* J Orthop Res, 2009. **27**(12): p. 1645-51.

83. Jackson, W.M., et al., *Differentiation and regeneration potential of mesenchymal progenitor cells derived from traumatized muscle tissue.* J Cell Mol Med, 2011. **15**(11): p. 2377-88.

84. Jackson, W.M., et al., *Mesenchymal progenitor cells derived from traumatized muscle enhance neurite growth.* J Tissue Eng Regen Med, 2013. **7**(6): p. 443-51.

85. Zupanc, H.R.H., P.G. Alexander, and R.S. Tuan, *Neurotrophic support by traumatized muscle-derived multipotent progenitor cells: Role of endothelial cells and Vascular Endothelial Growth Factor-A.* Stem Cell Res Ther, 2017. **8**(1): p. 226.

86. Supanc, H.R.H., S. Gorman, and R.S. Tuan, *Traumatized muscle-derived multipotent progenitor cells recruit endothelial cells through vascular endothelial growth factor-A action.* J Tissue Eng Regen Med, 2017. **11**(11): p. 3038-3047.

87. Davis, T.A., et al., *Heterotopic ossification in complex orthopaedic combat wounds: quantification and characterization of osteogenic precursor cell activity in traumatized muscle.* J Bone Joint Surg Am, 2011. **93**(12): p. 1122-31.

88. Evans, K.N., et al., *Osteogenic gene expression correlates with development of heterotopic ossification in war wounds.* Clin Orthop Relat Res, 2014. **472**(2): p. 396-404.

89. Peterson, J.R., et al., *Direct Mouse Trauma/Burn Model of Heterotopic Ossification.* J Vis Exp, 2015(102): p. e52880.

90. Hannallah, D., et al., *Retroviral delivery of Noggin inhibits the formation of heterotopic ossification induced by BMP-4, demineralized bone matrix, and trauma in an animal model.* J Bone Joint Surg Am, 2004. **86-A**(1): p. 80-91.

91. Peterson, J.R., et al., *Treatment of heterotopic ossification through remote ATP hydrolysis.* Sci Transl Med, 2014. **6**(255): p. 255ra132.

92. Peterson, J.R., et al., *Burn injury enhances bone formation in heterotopic ossification model.* Ann Surg, 2014. **259**(5): p. 993-8.

93. Ranganathan, K., et al., *The role of the adaptive immune system in burn-induced heterotopic ossification and mesenchymal cell osteogenic differentiation.* J Surg Res, 2016. **206**(1): p. 53-61.

94. Tannous, O., et al., *Heterotopic ossification after extremity blast amputation in a Sprague-Dawley rat animal model.* J Orthop Trauma, 2011. **25**(8): p. 506-10.

95. Jaffe, D.E., et al., *Does Blast Medium Affect Heterotopic Ossification in a Blast-amputation Model?* Clin Orthop Relat Res, 2015. **473**(8): p. 2680-7.

96. Polfer, E.M., et al., *The development of a rat model to investigate the formation of blast-related post-traumatic heterotopic ossification.* Bone Joint J, 2015. **97-B**(4): p. 572-6.

97. Pavey, G.J., et al., *Bioburden Increases Heterotopic Ossification Formation in an Established Rat Model.* Clin Orthop Relat Res, 2015. **473**(9): p. 2840-7.

98. Agarwal, S., et al., *mTOR inhibition and BMP signaling act synergistically to reduce muscle fibrosis and improve myofiber regeneration.* JCI Insight, 2016. **1**(20): p. e89805.

99. Wang, X., et al., *Inhibition of overactive TGF-beta attenuates progression of heterotopic ossification in mice.* Nat Commun, 2018. **9**(1): p. 551.

100. Qureshi, A.T., et al., *Early Characterization of Blast-related Heterotopic Ossification in a Rat Model.* Clin Orthop Relat Res, 2015. **473**(9): p. 2831-9.

101. Seavey, J.G., et al., *Early local delivery of vancomycin suppresses ectopic bone formation in a rat model of trauma-induced heterotopic ossification.* J Orthop Res, 2017. **35**(11): p. 2397-2406.

102. Pavey, G.J., et al., *Targeted stimulation of retinoic acid receptor-gamma mitigates the formation of heterotopic ossification in an established blast-related traumatic injury model.* Bone, 2016. **90**: p. 159-67.

103. Wheatley, B.M., et al., *Palovarotene inhibits connective tissue progenitor cell proliferation in a rat model of combat-related heterotopic ossification.* J Orthop Res, 2018. **36**(4): p. 1135-1144.

104. Qureshi, A.T., et al., *Inhibition of Mammalian Target of Rapamycin Signaling with Rapamycin Prevents Trauma-Induced Heterotopic Ossification.* Am J Pathol, 2017. **187**(11): p. 2536-2545.

105. Stuhmiller, J.H., et al., *Blast injury translating research into operational medicine*. 2008, U.S. Army Medical Research and Materiel Command,: Fort Detrick, Md. p. 35 p.

106. Forsberg, J.A. and B.K. Potter, *Heterotopic ossification in wartime wounds.* J Surg Orthop Adv, 2010. **19**(1): p. 54-61.

107. Jaffin, J.H., et al., *A laboratory model for studying blast overpressure injury.* J Trauma, 1987. **27**(4): p. 349-56.

108. Moore-Lotridge, S.N., et al., *Trauma-Induced Nanohydroxyapatite Deposition in Skeletal Muscle is Sufficient to Drive Heterotopic Ossification.* Calcif Tissue Int, 2018.

109. Anthonissen, J., et al., *The role of muscular trauma in the development of heterotopic ossification after hip surgery: An animal-model study in rats.* Injury, 2016. **47**(3): p. 613-6.

110. Kumar, T.K., et al., *Snake venom cardiotoxins-structure, dynamics, function and folding.* J Biomol Struct Dyn, 1997. **15**(3): p. 431-63.

111. Arnold, L., et al., *Inflammatory monocytes recruited after skeletal muscle injury switch into antiinflammatory macrophages to support myogenesis.* J Exp Med, 2007. **204**(5): p. 1057-69.

112. Mignemi, N.A., et al., *Plasmin Prevents Dystrophic Calcification After Muscle Injury.* J Bone Miner Res, 2017. **32**(2): p. 294-308.

113. Moore, S.N., et al., *Validation of a Radiography-Based Quantification Designed to Longitudinally Monitor Soft Tissue Calcification in Skeletal Muscle.* PLoS One, 2016. **11**(7): p. e0159624.

114. Lin, H., et al., *Cartilage tissue engineering application of injectable gelatin hydrogel with in situ visible-light-activated gelation capability in both air and aqueous solution.* Tissue Eng Part A, 2014. **20**(17-18): p. 2402-11.

115. Glass, G.E., et al., *TNF-alpha promotes fracture repair by augmenting the recruitment and differentiation of muscle-derived stromal cells.* Proc Natl Acad Sci U S A, 2011. **108**(4): p. 1585-90.

116. Luu, H.H., et al., *Distinct roles of bone morphogenetic proteins in osteogenic differentiation of mesenchymal stem cells.* J Orthop Res, 2007. **25**(5): p. 665-77.

117. ten Dijke, P., et al., *Identification of type I receptors for osteogenic protein-1 and bone morphogenetic protein-4.* J Biol Chem, 1994. **269**(25): p. 16985-8.

118. Cecchi, S., S.J. Bennet, and M. Arora, *Bone morphogenetic protein-7: Review of signalling and efficacy in fracture healing.* J Orthop Translat, 2016. **4**: p. 28-34.

119. Winbanks, C.E., et al., *The bone morphogenetic protein axis is a positive regulator of skeletal muscle mass.* J Cell Biol, 2013. **203**(2): p. 345-57.

120. Friedrichs, M., et al., *BMP signaling balances proliferation and differentiation of muscle satellite cell descendants.* BMC Cell Biol, 2011. **12**: p. 26.

121. Ono, Y., et al., *BMP signalling permits population expansion by preventing premature myogenic differentiation in muscle satellite cells.* Cell Death Differ, 2011. **18**(2): p. 222-34.

122. Boon, M.R., et al., *Bone morphogenetic protein 7: a broad-spectrum growth factor with multiple target therapeutic potency.* Cytokine Growth Factor Rev, 2011. **22**(4): p. 221-9.

123. Singla, D.K., R. Singla, and J. Wang, *BMP-7 Treatment Increases M2 Macrophage Differentiation and Reduces Inflammation and Plaque Formation in Apo E-/- Mice.* PLoS One, 2016. **11**(1): p. e0147897.

124. Zhong, L., et al., *The anti-fibrotic effect of bone morphogenic protein-7(BMP-7) on liver fibrosis.* Int J Med Sci, 2013. **10**(4): p. 441-50.

125. Midgley, A.C., et al., *Hyaluronan regulates bone morphogenetic protein-7-dependent prevention and reversal of myofibroblast phenotype.* J Biol Chem, 2015. **290**(18): p. 11218-34.

126. Scherner, O., et al., *Endoglin differentially modulates antagonistic transforming growth factor-beta1 and BMP-7 signaling.* J Biol Chem, 2007. **282**(19): p. 13934-43.

127. Lee, K.B., et al., *BMP induced inflammation: a comparison of rhBMP-7 and rhBMP-2.* J Orthop Res, 2012. **30**(12): p. 1985-94.

128. Kluk, M.W., et al., *Fibroregulation of mesenchymal progenitor cells by BMP-4 after traumatic muscle injury.* J Orthop Trauma, 2012. **26**(12): p. 693-8.

129. Klein, G.L., *The Effect of Glucocorticoids on Bone and Muscle.* Osteoporos Sarcopenia, 2015. **1**(1): p. 39-45.

130. Sapolsky, R.M., L.M. Romero, and A.U. Munck, *How do glucocorticoids influence stress responses? Integrating permissive, suppressive, stimulatory, and preparative actions.* Endocr Rev, 2000. **21**(1): p. 55-89.

131. Straub, R.H. and M. Cutolo, *Glucocorticoids and chronic inflammation.* Rheumatology (Oxford), 2016. **55**(suppl 2): p. ii6-ii14.

132. Pileri, D., et al., *Serum Levels of Cortisol, Immunoglobulin, and C-reactive Protein in Burn Patients.* Ann Burns Fire Disasters, 2009. **22**(1): p. 3-5.

133. Pandya, U., et al., *Increased total serum random cortisol levels predict mortality in critically ill trauma patients.* Am Surg, 2014. **80**(11): p. 1112-8.

134. Sato, A.Y., M. Peacock, and T. Bellido, *Glucocorticoid Excess in Bone and Muscle.* Clin Rev Bone Miner Metab, 2018. **16**(1): p. 33-47.

135. Hamer, M., et al., *Salivary cortisol responses to mental stress are associated with coronary artery calcification in healthy men and women.* Eur Heart J, 2010. **31**(4): p. 424-9.

136. Hamer, M., et al., *Cortisol responses to mental stress and the progression of coronary artery calcification in healthy men and women.* PLoS One, 2012. **7**(2): p. e31356.

137. Yuasa, M., et al., *Fibrinolysis is essential for fracture repair and prevention of heterotopic ossification.* J Clin Invest, 2015. **125**(9): p. 3723.

138. van Zaane, B., et al., *Systematic review on the effect of glucocorticoid use on procoagulant, anti-coagulant and fibrinolytic factors.* J Thromb Haemost, 2010. **8**(11): p. 2483-93.

139. Kochtebane, N., A.M. Alzahrani, and A. Bartegi, *Expression of uPA, tPA, and PAI-1 in Calcified Aortic Valves.* Biochem Res Int, 2014. **2014**: p. 658643.

140. Pratte, K.A., et al., *Plasminogen activator inhibitor-1 is associated with coronary artery calcium in Type 1 diabetes.* J Diabetes Complications, 2009. **23**(6): p. 387-93.

141. Koh, T.J., et al., *Mice deficient in plasminogen activator inhibitor-1 have improved skeletal muscle regeneration.* Am J Physiol Cell Physiol, 2005. **289**(1): p. C217-23.

142. Naderi, J., et al., *Plasminogen activator inhibitor type 1 up-regulation is associated with skeletal muscle atrophy and associated fibrosis.* Am J Pathol, 2009. **175**(2): p. 763-71.

143. Meyers, C., et al., *Heterotopic Ossification: A Comprehensive Review.* JBMR Plus, 2019. **3**(4): p. e10172.

144. Delaney, K., et al., *The role of TGF-beta1 during skeletal muscle regeneration.* Cell Biol Int, 2017. **41**(7): p. 706-715.

145. Guerrero, F., et al., *TGF-beta prevents phosphate-induced osteogenesis through inhibition of BMP and Wnt/beta-catenin pathways.* PLoS One, 2014. **9**(2): p. e89179.

146. Shi, A., et al., *Small molecule inhibitor of TGF-beta signaling enables robust osteogenesis of autologous GMSCs to successfully repair minipig severe maxillofacial bone defects.* Stem Cell Res Ther, 2019. **10**(1): p. 172.

147. Sun, X., et al., *TGF-beta inhibits osteogenesis by upregulating the expression of ubiquitin ligase SMURF1 via MAPK-ERK signaling.* J Cell Physiol, 2018. **233**(1): p. 596-606.

148. Xu, J., et al., *High-Dose TGF-beta1 Impairs Mesenchymal Stem Cell-Mediated Bone Regeneration via Bmp2 Inhibition.* J Bone Miner Res, 2019.

149. Li, Y., et al., *TGF-beta Stimulates Endochondral Differentiation after Denervation.* Int J Med Sci, 2017. **14**(4): p. 382-389.

150. Rosen, D., et al., *Systemic administration of recombinant transforming growth factor beta 2 (rTGF-beta 2) stimulates parameters of cancellous bone formation in juvenile and adult rats.* Bone, 1994. **15**(3): p. 355-9.

151. Gazit, D., et al., *Bone loss (osteopenia) in old male mice results from diminished activity and availability of TGF-beta.* J Cell Biochem, 1998. **70**(4): p. 478-88.

152. Tachi, K., et al., *Enhancement of bone morphogenetic protein-2-induced ectopic bone formation by transforming growth factor-beta1.* Tissue Eng Part A, 2011. **17**(5-6): p. 597-606.

153. Hardy, D., et al., *Comparative Study of Injury Models for Studying Muscle Regeneration in Mice.* PLoS One, 2016. **11**(1): p. e0147198.

154. Gong, S., et al., *Dynamics and correlation of serum cortisol and corticosterone under different physiological or stressful conditions in mice.* PLoS One, 2015. **10**(2): p. e0117503.

155. Makowski, G.S. and M.L. Ramsby, *Interaction of amorphous calcium phosphate with fibrin in vitro causes decreased fibrinolysis and altered protease profiles: implications for atherosclerotic disease.* Inflammation, 2001. **25**(5): p. 319-29.

156. Annes, J.P., J.S. Munger, and D.B. Rifkin, *Making sense of latent TGFbeta activation.* J Cell Sci, 2003. **116**(Pt 2): p. 217-24.

157. Omori, K., et al., *Inhibition of Plasminogen Activator Inhibitor-1 Attenuates Transforming Growth Factor-beta-Dependent Epithelial Mesenchymal Transition and Differentiation of Fibroblasts to Myofibroblasts.* PLoS One, 2016. **11**(2): p. e0148969.

158. Li, H., et al., *Computational analysis reveals the coupling between bistability and the sign of a feedback loop in a TGF-beta1 activation model.* BMC Syst Biol, 2017. **11**(Suppl 7): p. 136.

159. Li, Y., et al., *Transforming Growth Factor Beta is regulated by a Glucocorticoid-Dependent Mechanism in Denervation Mouse Bone.* Sci Rep, 2017. **7**(1): p. 9925.

160. Senarath-Yapa, K., et al., *Small Molecule Inhibition of Transforming Growth Factor Beta Signaling Enables the Endogenous Regenerative Potential of the Mammalian Calvarium.* Tissue Eng Part A, 2016. **22**(9-10): p. 707-20.

161. Chen, W. and P. Ten Dijke, *Immunoregulation by members of the TGFbeta superfamily.* Nat Rev Immunol, 2016. **16**(12): p. 723-740.

162. Brown, K.V., et al., *Comparison of development of heterotopic ossification in injured US and UK Armed Services personnel with combat-related amputations: preliminary findings and hypotheses regarding causality.* J Trauma, 2010. **69 Suppl 1**: p. S116-22.

163. Rath, E.M., et al., *Gluteus minimus necrotic muscle debridement diminishes heterotopic ossification after acetabular fracture fixation.* Injury, 2002. **33**(9): p. 751-6.

164. Jackson, W.M., et al., *Cytokine expression in muscle following traumatic injury.* J Orthop Res, 2011. **29**(10): p. 1613-20.

165. Asatrian, G., L. Chang, and A.W. James, *Muscle pouch implantation: an ectopic bone formation model.* Methods Mol Biol, 2014. **1213**: p. 185-91.

166. Vidal, B., et al., *Fibrinogen drives dystrophic muscle fibrosis via a TGFbeta/alternative macrophage activation pathway.* Genes Dev, 2008. **22**(13): p. 1747-52.

167. Martino, M.M., et al., *Heparin-binding domain of fibrin(ogen) binds growth factors and promotes tissue repair when incorporated within a synthetic matrix.* Proc Natl Acad Sci U S A, 2013. **110**(12): p. 4563-8.

168. Grainger, D.J., et al., *The serum concentration of active transforming growth factor-beta is severely depressed in advanced atherosclerosis.* Nat Med, 1995. **1**(1): p. 74-9.

169. Fuery, M.A., et al., *Vascular ossification: Pathology, mechanisms, and clinical implications.* Bone, 2018. **109**: p. 28-34.

170. Leszczynska, A. and J.M. Murphy, *Vascular Calcification: Is it rather a Stem/Progenitor Cells Driven Phenomenon?* Front Bioeng Biotechnol, 2018. **6**: p. 10.

171. Toma, I. and T.A. McCaffrey, *Transforming growth factor-beta and atherosclerosis: interwoven atherogenic and atheroprotective aspects.* Cell Tissue Res, 2012. **347**(1): p. 155-75.

172. Yao, Y., et al., *Inhibition of bone morphogenetic proteins protects against atherosclerosis and vascular calcification.* Circ Res, 2010. **107**(4): p. 485-94.

173. Reifenberg, K., et al., *Overexpression of TGF-ss1 in macrophages reduces and stabilizes atherosclerotic plaques in ApoE-deficient mice.* PLoS One, 2012. **7**(7): p. e40990.

174. Tirone, M., et al., *Severe Heterotopic Ossification in the Skeletal Muscle and Endothelial Cells Recruitment to Chondrogenesis Are Enhanced by Monocyte/Macrophage Depletion.* Front Immunol, 2019. **10**: p. 1640.